Adsorption and Grafting of Polyelectrolytes at Solid-Liquid Interfaces

DISSERTATION

zur Erlangung des Grades

Doktor der Naturwissenschaften

(Dr. rer. nat.)

vorgelegt

am Fachbereich Chemie

der Fakultät Mathematik und Naturwissenschaften

der Technischen Universität Dresden

von

Nikolay Houbenov

Geboren am 02 April 1971 in Sofia, Bulgarien

Gutachter: Prof. Dr. M. Stamm
                Prof. Dr. H.-J. Adler
                Prof. Dr. S. Minko

Eingereich am: 28.01.05.

Tag der Verteidigung: 29.08.05

Contents

Chapter 5

Experimental Techniques 21

Chapter 6

Synthesis of Polymer Brushes 45

Chapter 7

Mixed Amphiphilic Polymer Brush for Switching of Energetic state and Surface Charge in Aqueous Media   50

Chapter 8

Properties of Binary Polyelectrolyte Brush Composed of Oppositely Charged Polymers   59

Chapter 11

Regulation of Protein Adsorption by Switching of Surface Charge, Surface Energetic State and Chemical Composition of Binary Polymer Brushes

Chapter 12

Protein Adsorption onto Binary Polymer Brushes: Effect of Electrolyte Concentration, Surface Chemistry and Switching Layers Phenomenon

Chapter 13

Control of Protein Adsorption via Compositional Gradients

Chapter 1

Introduction.

Design of synthetic thin polymer films capable of smart response is a challenging task for creation of new coatings with a potential to adjust and improve surface characteristic of the materials. Recently many studies devote a special attention to surfaces, which performance is not fixed at variable environmental conditions [Bli98, Tsu98, Tsu00, Bir00]. Often it is of importance to combine antagonistic, mutually incompatible, properties, e.g. acid and base, hydrophobic and hydrophilic, conductive and not conductive, adsorbing and repelling and many others, on a single plane. Development of such sophisticated surface with a predictable response under different conditions is currently imposed from the requirements of nanotechnology, biomaterials and medicine.

Polymers, grafted with one end to a planar surface, represent a recently reported example of stimuli sensitive nanomaterials. Modification of surfaces via grafting of different polymers is well known and promising method for regulation of adsorption, adhesion, wetting, reactivity, micro/nanopatterning, swelling, friction, stabilization of colloids and other surface properties sensitive to the surface composition [Raph92, Man97, Hab99, Huss00, Russ02].

A novel strategy for fabrication of responsive functional polymer films is based on grafting of several different functional polymers onto a solid substrate at high grafting density, resulting in varied types of polymer brushes [Sid99, Min02a]. It is shown that grafting of two chemically different polymers on one substrate implies adaptive/switching properties of the thin polymer coating. This behavior is affected by a phase segregation mechanism in the thin polymer films [Lem03]. Such an arrangement suggests many interesting applications of the polymer brushes, regarding their versatile adaptive surfaces, capable for responding to changes of solvent polarity, pH, temperature, electromagnetic field and other stimuli, generally by reversible swelling [Luz04].

This thesis focuses on synthesis of binary polymer brushes chemically tethered to a solid substrate and investigation of their responsive/adaptive to external stimuli properties.

Recently the polymer brushes attract interest from academic and practical point of view, due to their well-defined surface properties and predictable environmental response [Min02a, Min02b, Pru98]. Large number of experimental and theoretical investigations is devoted to homopolymer brushes [Zhu91, Halp92, Sev96, Qua99, Coh99, Hab99, Bie99]. In contrast, binary polymer brushes were synthesized [Sid99] and studied intensively only in the last few years [Min99, Min02a, Min02b, Mül02, Lem03]. It was shown that the combination of polar and non-polar polymers in the layer results in an mixed amphiphilic polymer brush surface, able to switch from hydrophilic to hydrophobic (and vice versa) surface energetic states by appropriate tuning of the external conditions [Min02a, Min03b, Min03c, Mot03].

We synthesized and characterized mixed amphiphilic polymer brushes, as our results are in a good agreement with literature data. In the frame of this thesis, the amphiphilic brush was investigated in terms of its response to aqueous surrounding media. The ability to reversibly switch the properties of the material from water-repellent to hydrophilic was investigated in aqueous media, which is a new aspect in evaluation of its responsive behavior.

Features that are even more promising can be attributed to the mixed brushes if the polymers in the layer carry electrical charges. There are only a few theoretical approaches, predicting some particular properties of such novel material [Shu01a, Shu01b]. We performed the first attempt to synthesize and experimentally to investigate binary polyelectrolyte brush, composed of oppositely charged polymers. The larger variety of combinations of electrostatic and short-range interactions leads to much more complex response as compared to homopolyelectrolyte and binary amphiphilic brushes. In the latter case, a completely switching of the surface composition can be approached by the change of the solvent, while a layered segregation of two different polymers in the binary polyelectrolyte brush can be easily approached by a small change of pH.

The amphiphilic and binary polyelectrolyte brushes were further examined as adaptive tool for regulation of adsorption of different charged species from aqueous solutions. In terms of simplicity, first we performed adsorption of nanoparticles with fixed charges onto binary polyelectrolyte brushes. Tuning the surface response of the brush without

changing the behaviour of the adsorbate allows one to investigate the switching of acid/base properties of the layers via long-range electrostatic forces.

Adsorption of synthetic polyampholytes was performed onto amphiphilic and binary polyelectrolyte brushes. In this case the adsorbate molecules bear both acidic and basic groups as in the vicinity of isoelectric pH the net charge is zero. These properties of polyampholytes allow investigating the adsorption behaviour of both type polymer brushes at different charge asymmetries at the adsorbing interface.

Adsorption of proteins onto amphiphilic and binary polyelectrolyte brushes is the most complex case we consider here. The strong internal coherence of the protein molecules imply different adsorption behaviour compared to that of the polyampholytes. Different interactions may originate from redistribution of charged groups, changes in the hydration state and structural rearrangement, caused by the switching phenomenon, and exhibited by polymer brushes.

Chapter 2
Theory of polymer brushes.

2.1. Introduction.

Polymer brushes refer to an assembly of polymer chains, attached by one end to a surface at high grafting density. The chains are stretched away from the substrate due to excluded volume effect [de Gen76, de Gen80, Ale77, Mil91, Halp92, Fle93, Szle96, Zha00].

Mixed polymer brushes, constituted from two incompatible polymers and grafted to the same substrate, represent another example of responsive surfaces. In this case, the micro-phase segregation of the polymers in the mixed brush results in change of structure and surface chemical composition, influenced by external environment.

2.2. Theory of monocomponent polymer brushes.

The term polymer brush was derived and specified by Alexander [Ale77], who performed theoretical analysis, considering grafted by one end polymer chains to a planar surface. The theory of Alexander was further developed by de Gennes [Gen76, Gen80], who investigated polymer brushes by self consistent field (SCF) calculations.

To build the profile of a polymer chain, grafted to a planar surface, one needs to assume an interfacial limitation factor, influencing its behavior. Deformation (or expansion) of grafted layers is an expression of the energetic balance between the interaction and the free elastic energies. Sufficiently strong overlapping of the polymer chains themselves occurs at the interface, and it is initiated by the dense tethering factor. Hence, an increase of the inter-contact between monomer units, and therefore, also of related interaction energy, takes place in the system. Following that order, the chains are forced to expand away from the surface (Z direction), and that way, to minimize monomer units contact by increase the brush layer thickness, d. As result, the interaction energy per chain, F_{nt} tends to lower, on expense of the elastic one, F_{el}. The equilibrium thickness state for a brush-like layer can be determined, evaluating the balance between both energies.

The entire free energy finds an expression by both terms, discussed above:

$$F = F_{nt} + F_{el} \qquad (2.1)$$

To simplify the meaning of both parameters, one assumes a step-like statistical segments depth profile and equal distance between free ends and the surface, *d*, for all chains, i.e., the description of the layer assumes a single plane profile.

The concentration of single segments can be expressed as:

$$\varphi = Na^3/d_g^2 d \tag{2.2}$$

where *N* is the number of statistical segments along the chains, *a* is their diameter and d_g is the average distance between the anchoring points. The latest must be smaller than radius of gyration of an unperturbed chain.

Considering the findings above, one needs to obtain a more precise expression for the free energy. It is provided by the Flory approximation [Flo81], evaluating the configurational entropy loss. Considering an ideal chain, forced to expand the distance *d* and related to entropic "springs" with a spring constant kT/R_g^2, the free energy cost per chain is:

$$F \approx kT\left[\frac{3d^2}{2Na^2} + \nu N\left(\frac{N}{d}\right)\right] \tag{2.3}$$

where *k* is the Boltzmann constant, R_g-radius of gyration, T-temperature and ν is a dimensionless excluded volume parameter.

Minimization with respect to the brush height gives the equilibrium thickness:

$$d \approx N(\nu a^2)^{1/3} \tag{2.4}$$

then

$$F \approx kTN(\nu a^{-1})^{2/3} \tag{2.5}$$

The results for the simple model, first noted by Alexander, can be summarized as follows:

• Sequence of brushes with coverage and increasingly large *N*.

• Height *d* grows linearly with *N*, while unstretched chain dimension R_g only grows as $N^{1/2}$

• The properties of long enough chains, $d \gg R_g$ (chains are strongly stretched), may be expected to be quite different from unstretched chains in solution.

Properties well described by the simple model:

• Rough measurements of the brush height *d*.

• Rough measurements of the free energy per chain *F*.

• Rough measurements of the stretching-repulsion balance.

To conclude, one can state that Alexander approach does not attempt to examine in details the conformation of polymer chains or density profile of the chain units. The model describes the hydrodynamic thickness, permeability and force, required to compress the brush.

Dealing with this matter, simple results have been obtained for a wide range of brush properties. An uncomplicated hypothesis, that the free chain ends can be located at any distance from the interface [Mil91, Sem75, Mil88, Mill89] has been developed.

2.3. Theory of mixed binary polymer brushes and phase segregation.

Mixed brushes theoretical studies was started by Marko and Witten in year 1991, who successively showed a microphase separation between two chemically different polymers, grafted to a planar surface. It is important to note that the incompatibility between both types of chains should have a higher value as well. For studying any mixed polymer brush system, one have to apply the mean field theory for strong stretching limit, also successively applied for homopolymer brush.

Marko et al. extended the theory for case of mixed polymer brush [Mar91]. The basic idea in their study is that the incompatibility of both polymers increases the mixing free energy per chain, which is function of the monomer concentration.

$$\frac{E}{nkT} = \Lambda \int \frac{d^3r}{\Omega\sigma} \phi_A(\vec{r})\phi_B(\vec{r}) \qquad (2.6)$$

where ϕ is the volume fraction of polymers A and B, $n = \Omega\sigma$ is the total number of molecules in the layer, Ω is the surface of the layer, $\vec{r}$ is a radius-vector which points out monomer units and σ is the grafting density.

Λ [volume^{-1}] is calling coupling constant and is related to Flory-Huggins parameter χ, via:

$$\chi = \Lambda V/N \qquad (2.7)$$

A and B indexes in equation (2.6) represent two chemically different polymers

The incompressibility conditions one can state as $\phi_A = 1 - \phi_B$. When $\Lambda > 0$, the monomers of A and B will separate.

Recently the mixed brushes prepared from polymers of similar molecular weight but different chemical compositions were intensively investigated theoretically and experimentally [Zhu96, Min01, Min02a, Min02b, Sid99]. It was shown that the mixed brush morphology is affected by the interplay between lateral and phase segregation, governed by solvent quality. The lateral segregation of mixed brushes is dominant in nonselective solvent and results in ripple

morphology, while in selective solvent the unfavored polymer forms clusters embedded in the continuous phase (dimple morphology) of the second polymer. This mechanism introduces the adaptive and switching properties of the thin film, which can change morphology, surface energetic state, and functionality upon exposure to a controlled environment.

A binary polymer brush exhibits mainly two segregation routes. The first one is a lateral segregation (Figure 2.1.a) characterized by a homogeneity in perpendicular direction and the chains form so called ripples. The right scheme (2.1.b) represents the perpendicular case of segregation. One of the polymers enriches the top layer, while the other one collapses near to the surface. Typical morphology formed is

a **b**
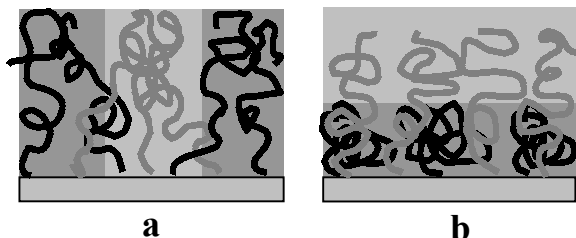
Figure 2.1. Phase segregation routes for a mixed polymer brush in melt.

dimple morphology. It is noteworthy to say that the ripple morphology (case 2.1.a) occurs by the block co-polymer melts as well. The difference is in two dimensional periodicity of the structure and also in the brush-like profile, perpendicular to the surface.

The theory of Milner, Marko and Witten predicts the main phenomena operating in the binary brushes, but it is limited only for very high grafting densities and /or long chains. By reason of that, a more general method has been developed by M. Müller [Müll02]. The basis of this approach lies on the self consisted field theory, initially using Matsen and Schick calculations [Mat94] for phase diagram of block-copolymers. The monomer densities and effective fields have been calculated, using Fourier approach. This method is useful to analyse the stable morphologies-lamellas, square, hexagonal, dimple phases. Varying the incompatibility of the polymers, total and relative grafting densities of A and B, as well as the solvent quality concerning different polymer components chemistry, one can build up phase diagram for mixed polymer brushes, regarding a first order phase transitions. The delicate interplay between both types phase segregations was shown to result in different morphologies as well [Min02a].

In the Figure 2.2, a phase diagram for a symmetrical binary brush as a function of solvent selectivity ζ is shown in order to outline the origin of responsive behavior of the mixed brush [Min02a]. The reversible microphase separation of the components occurs in the following order:

- Non selective solvent ($\zeta = 0$). Laterally homogeneous to ripple phase transition, upon increasing the incompatibility of A and B species.

- Decreased solvent quality for A ($\zeta<0$). Ripple phase convert in dimple structures, as

the A component segregates into clusters.

- Decreased solvent quality for B ($\zeta > 0$). Ripple phase convert in dimple structures, as the B component segregates into clusters.

(a)

(b)

(c)
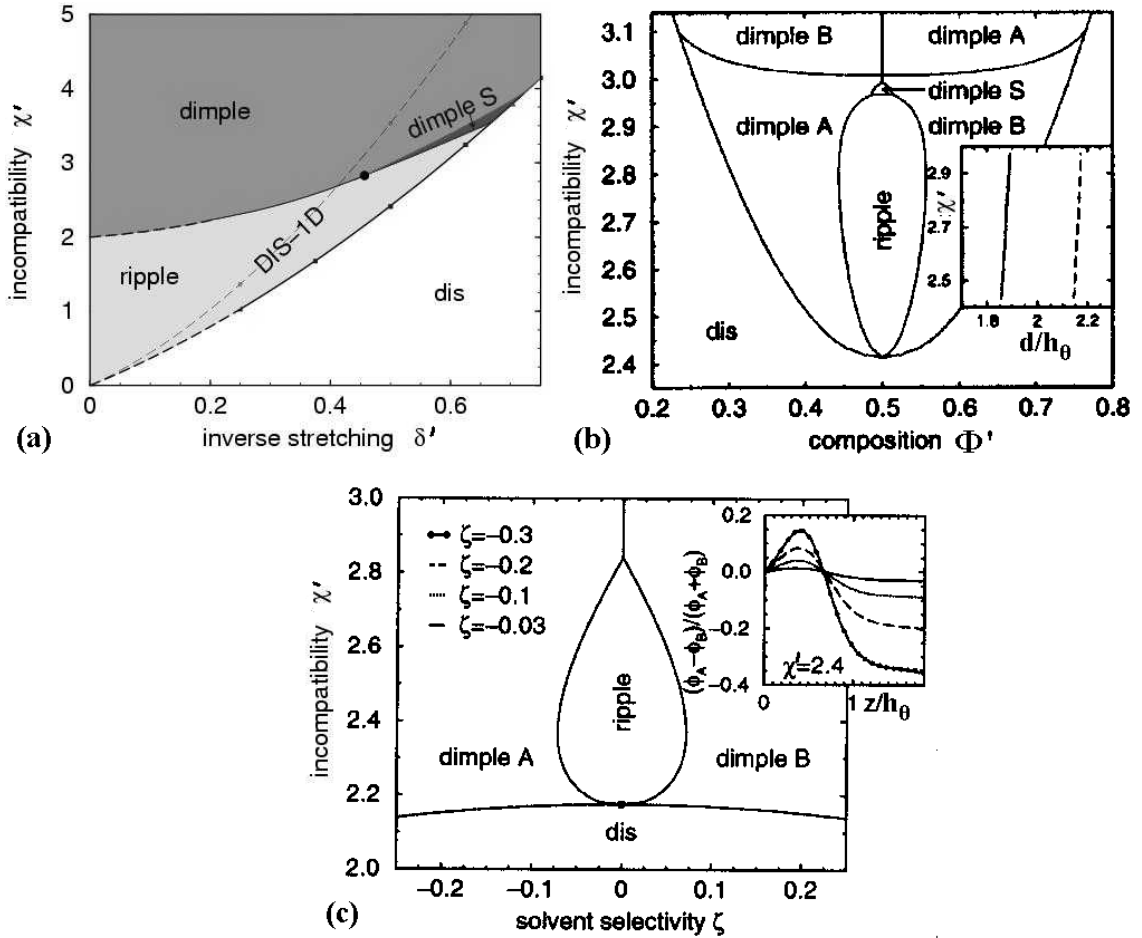
Figure 2.2. Phase diagrams adopted from [Mül02] and [Min02b].: (a) symmetric binary polymer brush as function of incompatibility χ' and inverse stretching δ', the layered 1D morphology was found to be not stable at $\delta' > 0.25$ and is pre-empted by the laterally segregated morphologies, however the hypothetical transition from the disordered phase to 1D phase is shown with the dashed line; (b) inverse stretching $\delta' = 0.5$ as function of incompatibility χ' and the brush composition Φ', the inset displays the variation of the lateral period d for the lamellar and checkerboard clusters (solid) and hexagonal cluster structures (dashed); (c) symmetric binary polymer brush as function of incompatibility χ' and solvent selectivity ξ, the inset presents the laterally averaged perpendicular composition profile at $\chi' = 2.4$ for various solvent selectivity.

2.4. Binary polyelectrolyte brushes.

A particular case of the polymer brushes are polyelectrolyte brushes, consisting of electrically charged polymers [Bie02a, Bie02b]. Recently polyelectrolytes attached to a surface and formed brush-like layers have attracted great interest because the structure and properties of the layers are strongly modified by electrostatic interactions of the charged chains and the osmotic pressure of counter ions. Swelling of polyelectrolyte brushes and chain conformation

strongly depends on external environment, ionic strength, valence of counter ions and pH [Pin91, Ross92, v.Goe94, Mis89], demonstrating tough responsive properties of the thin films.

Polymer brushes fabricated by oppositely charged polyelectrolytes grafted on the same planar substrate exhibit a complicated behavior [Shu01a, Shu01b]. In contrast equally charged homopolymer brush, when the intra- and interchain Coulomb repulsion leads to a stretching of the chains, the oppositely charged mixed brush has the possibilities to reduce the electrostatic repulsion depending on charge ratio. Consequently, the larger variety of combinations of electrostatic and short-range interactions leads to much more complex response.

Binary polyelectrolyte brushes were studied theoretically. However, in the frame of this thesis, the first attempt to synthesize such brushes is presented [Hou03]. Such materials are promising to tune behavior and surface charge of the film, which is important to regulate adsorption of proteins, cells and colloidal particles.

Chapter 3
Polyelectrolytes.

3.1. Introduction.

The term polyelectrolyte is employed for a wide field of macromolecules which contain dissociable subunits. Polymers with both positive and negative charges are referred to as polyelectrolytes, macroions or polyions. These polymers may be synthetic, natural or modified. The synthetic polyelectrolytes include polymers that can be prepared by several methods, the major one being chain growth polymerization. The distinctive behavior of polyelectrolytes in aqueous solutions is what separates this class of polymers from non-ionic polymers. In aqueous solution, the polymer coils are greatly expanded by the presence of charged groups. If the solution is free of added electrolytes, the polymer coil expands as the polymer concentration decreases. This is known as "polyelectrolyte effect". In presence of added electrolytes, the polyelectrolytes behave like non-ionic polymers and chain expansion is not observed.

A polymer system can be described via persistent length, L_p, i.e., the maximal length by which the system is still rigid [Barr95]. Particularly, for polyelectrolyte systems one introduces an additional electrostatic term:

$$L_p = L_0 + L_e,$$
(3.1)

where L_0 is the intrinsic persistence length, dependent on the structure of the chemical segments. The electrostatical part, L_e, depends on Debye length, k^{-1}, via $L_e \propto 1/k^y$ [Oi77, Wan88, Hol98]. Neglecting the excluded volume effects and the interactions between different polymer chains, and assuming low concentration counterions regime [Odi78, Sko77], one can state:

$$L_e = \frac{\alpha^2 e^2}{4 a^2 \kappa^2 \varepsilon k T}$$
(3.2)

Here α is the dissociation degree, e is the elementary charge, a- the length of a monomer unit, ε- the dielectric constant of the solution, k- the Boltzmann constant and T- the temperature. Debye length is given as function of ionic strength I of the solution by next equation [Foers95, Wang88]:

$$\kappa^2 = 8\pi l_B N_A I$$
(3.3)

where N_A is the Avogadro number. I can be expressed as a function of the ion charge z_i and the ion concentration c_i:

$$I = 0,5\sum_i z_i c_i \tag{3.4}$$

The Bjerrum length l_B indicates the distance, with which the coulomb reciprocal effect energy of two point charges straight corresponds to the thermal energy kT.

$$l_B = \frac{e^2}{4\pi\varepsilon\varepsilon_0 kT} \tag{3.5}$$

where ε_0 is the influence constant. In accordance to the equation 3.2, polyelectrolytes are stretched when I of the environment is reduced. With rising of I, the electrostatic contribution to the persistence length will decrease and the polymer chains become more flexible. The behavior is than more similar to uncharged polymers.

3.2. Acidic and basic polyelectrolytes.

A distinguishing property among polyelectrolytes is the basicity (acidity) of the monomers, building the polyelectrolyte chain. Usually, when polyelectrolytes are under study, it is performed in aqueous solution, where they can dissociate (polyacrylic acid -PAA) or associate ions from the solution (protonation of poly(2-vynilpyridine- P2VP). The annealed charge model describes an experimental system, where the monomers have weak acidic (basic) groups, and the pH of the solution controls the degree of association and dissociation of ions on the polymer chain.
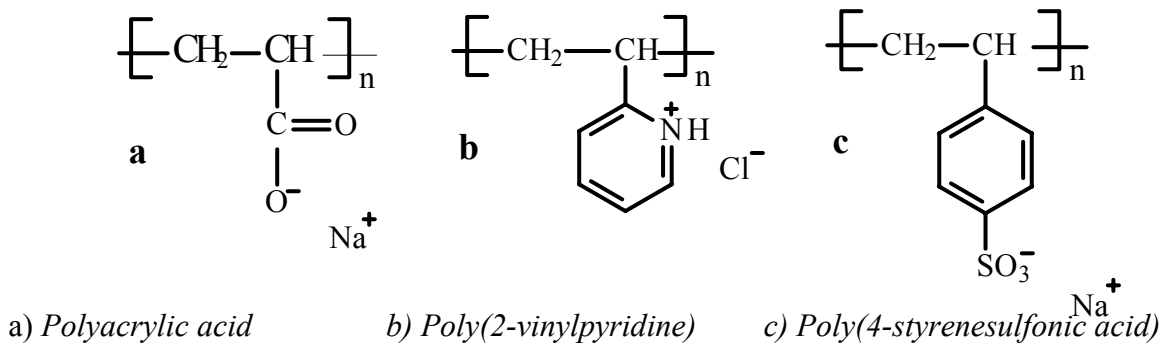

a) *Polyacrylic acid*   b) *Poly(2-vinylpyridine)*   c) *Poly(4-styrenesulfonic acid)*

Figure 3.1. Examples for anionic (a, c) and cationic (b) polyelectrolytes

A typical acidic polyelectrolyte is the sodium salt of polyacrylic acid, while poly(2-vinylpyridine) is an example for a basic polyelectrolyte.

3.3. Weak and strong polyelectrolytes.

With respect to different dissociation behavior one can distinguish between strong and weak, or between quenched and annealed polyelectrolytes [Barr95, Raph90]. So called strong polyelectrolytes, poly-salts, e.g., Na-polystyrene-sulfonate, dissociate completely in the total pH range accessible by experiment. The total charge as well as its specific distribution along the chain is solely imposed by chemistry, i.e., by polymer synthesis. That is why such polyelectrolytes are also called quenched.

On the other hand, weak polyelectrolytes (polyacids and polybases) dissociate only in a rather limited pH range. In this thesis are presented results mainly from weak polyelectrolytes properties and behavior. The total charge of the chain is not fixed but it can be tuned by changing the pH of the solution. Because of dissociation and recombination of ion pairs along the chain one can expect spatial and/or temporal fluctuations in the local degree of dissociation. Such titrating polyelectrolytes exhibit an annealed inhomogeneous charge distribution. A pronounced charge accumulation appears at chain ends because there are fewer neighbors for the charges to interact with and the penalty in energy is therefore reduced.

The charge inhomogeneity can have a strong impact on processes dominated by end-effects, such as the self-assembly of weakly charged linear micelles and adsorption on charged surfaces [Scho97, Fle93]. For end-grafted weak polyelectrolytes, a rather unusual regime has been obtained where the chain stretching (brush thickness) depends non-monotonously on salt concentration and grafting density [Isra94, Zhu95] . This is mainly due to the fact that the net charge of a chain as well as its distribution along the chain is not fixed but depends on its local environment [Zit02].

The dissociation of low molecular weight acid (HA $\rightleftharpoons$ H$^+$+A$^-$) can be described by well known relation between its degree of dissociation (α = [A$^-$]/[HA]+[A$^-$]) and pH of the solution.

$$pH = pK_a + \log_{10}\left(\frac{\alpha}{1-\alpha}\right) \qquad (3.6)$$

The dissociation behavior of polyacids can be described in a similar way, but the resulting pKa value is now an apparent one (in the physico-chemical literature denoted by pKapp) [Katch47]. In contrast to low-molecular-weight acids, the charged groups of polyacids are

linked together along the chain. Therefore, the dissociation of one acid group is correlated in a complex way to the position and the number of other charged groups of the chain, resulting in a masking of the intrinsic pK_0 a of a (polyelectrolyte) monomer. The corresponding relation [Man88, Raph90] can be written as:

$$pH = pK_a^0 + \log_{10}\left(\frac{\alpha}{1-\alpha}\right) + \frac{1}{NkT}\frac{\partial F_{el}}{\partial \alpha} \qquad (3.7)$$

with F_{el} being the electrostatic free energy of the polyelectrolyte chain and N is the chain length. Introducing the chemical potential by

$$\mu(\alpha) = kT \log_{10}\left(\frac{\alpha}{1-\alpha}\right) + \frac{1}{N}\frac{dF_{el}}{d\alpha} \qquad (3.8)$$

equation 3.7 can be rewritten

$$pH = pK_a^0 + \frac{1}{kT}\mu(\alpha) \qquad (3.9)$$

Clearly, the chemical potential has two contributions: 1) an entropic, related to the mixing of charged and noncharged groups along the chain and 2) an electrostatic, describing the interaction with charged groups forming the local charge environment of an ionizable site.

For good and θ solvents, the electrostatic contribution $\mu_{el}(\alpha) = N^{-1} \partial F_{el}/\partial \alpha$ is an increasing monotonic function of α. For poor solvents, Raphael and Joanny [Raph90] found a non-monotonic variation of $\mu_{el}(\alpha)$, and thus of $\mu(\alpha)$, with α, which results in a first-order phase transition from a collapsed weakly charged conformation to an extended strongly charged state.

3.4. Flexible and stiff polyelectrolytes.

Flexibility of the chain influences strongly the polymer conformation in different quality solvents, i.e. the polymer chains conformation depends on the environmental properties. In presence of poor solvent, the polymer chains tend to collapse toward compact states, in which polymer solvent contacts are minimized. The difference in phase behavior between flexible and stiff polymers can be easily understood. As a flexible polymer is cooled, the Boltzmann weight for polymer-polymer contacts increases and so the number of contacts increases, at a

cost in the entropy of the polymer. The entropy cost derives from the fact that the polymer must bend back on itself in order for the units to be in contact. The increase in the number of contacts is continuous and so the radius of gyration of the polymer varies continuously- coil-globule transition is of second order. However, bending a stiff polymer back on itself is more difficult, it costs both entropy and energy. This larger cost can be repaid if more than one pair of units is in contact, which is true if the two parts of the polymer run parallel to each other for several units. Of course, if the polymer is stiff the, the entropy cost for two parts of the polymer to run parallel for a number of units is small. The low energy configurations of a stiff polymer are those with long parts of the polymer parallel. The energy gain is even larger if a number of parts of the polymer form a pack, e.g. if four parts of the polymer which are running parallel form a square bundle, the energy is not twice but four times that of two parts running parallel. When the polymer is cooled below the point, where the energy gain of bundles outweighs their entropy cost, then these bundles multiply and the radius of gyration drops suddenly by coil-solid transition is first order.

3.5. Polyampholytes

Charged polymers, sometimes called electrolyte polymers, are roughly divided into two categories:

-polyelectrolytes, with monomers of the same charge sign,

and

-polyampholytes, with randomly arranged monomers of both signs.

This simple category works well and represents the typical characteristics of charged polymers.

Polyampholytes contain both acidic (anionic) and basic (cationic) functional groups. Often these polymers undergo aqueous dissolution only in the presence of salt and coil dimensions increase as the ionic strength of the solution increases. This is primarily due to the screening of attractive electrostatic interactions within the polymer coils.

For a polyampholyte composed of weak acidic and basic monomer units the net charge of the polymer depends on the pH value and can be described with the Henderson Hasselbalch equation. This equation gives the dissociation degree of a polyacid and/or the protonation

degree of a polybase, α, and thus, the charge portion of the particular monomer units in the polyampholyte [Ley64, Man70].

$$pH = pK_a + n \cdot \log\left(\frac{\alpha}{1-\alpha}\right) \tag{3.10}$$

$$pH = pK_b + n \cdot \log\left(\frac{1-\alpha}{\alpha}\right) \tag{3.11}$$

where pK_a and pK_b are the acid and base constants of the monomer units, respectively.

3.6. Proteins

Proteins are biopolymers (called polypeptides) of L-amino acids joined to each other via peptide bonds. Only L-amino acids are used to make proteins (rare exceptions of proteins in bacterial cell wall, which contain some D-amino acids).

The order or sequence of amino acids distinguishes different proteins from each other. This sequence determines the 3-dimensional shape of the protein. Alterations to the amino acid sequence of a protein change its 3D shape. The difference between a polypeptide and a protein is that the term polypeptide refers simply to a chain of amino acids [Stry91, Ebe93]. The term protein refers to the chain of amino acids after it folds properly and is (in some cases) modified. Proteins may consist of more than one polypeptide chain.

Proteins are sometimes described as the "workhorses" of the cell because they do so many things - catalyze reactions, provide structural integrity, transport molecules, supply movement, bind molecules, and others.

Chapter 4

Adsorption at Solid-Liquid Interfaces.

The behavior of macromolecules and nano-scaled materials at solid/liquid interfaces is recently an object of intensive investigations. In particular, the performance of proteins at solid-liquid interfaces is the key for understanding many fundamental and practical processes and different assemblies onto appropriate surfaces. For instance, it is thought that the adsorption of fibrinogen to many biomaterials is a direct cause of thrombosis [Fen95].

4.1. Adsorption modes.

There exist two different types of adsorption- physical adsorption (physisorption) and chemical adsorption (chemisorption). In physisorption the interaction are of physical nature, i.e., van der Waals forces between the molecules in the system. The interactions are long-ranged and weak, as the energy released by it is comparable to the condensation enthalpy. As result, there are no cleaved chemical bonds in the adsorbed molecules and only the accommodation process at the surface will change their conformation. In case of physisorption of polyelectrolytes, long-range electrostatic forces mainly contribute to the binding of the molecules. They are relatively stronger than the van der Waals interactions, but do not cause a cleavage of the chemical bonds of the adsorbed molecules.

Chemisorption is an exothermic process and involves formation of chemical bonds (mainly covalent) between adsorbate and adsorbent. The interactions in chemisorption are stronger than in physisorption, and the adsorption enthalpy is much greater, in order of $dH< -40$ kJ/mol. For physisorption this value tend to be $>- 25$ kJ/mol.

4.2. Driving forces: adsorbent-adsorbate interactions.

Adsorption from solution is a competitive process, i.e., for adsorption to occur, the interaction between the solute molecules and the sorbent material is preferred over the interaction between solvent and sorbent. In an adsorption process various driving forces may operate, depending of the nature of system components, presented in:

(a) Van der Waals interaction includes Debye, Keesom and London inter-forces. Dispersion interactions (London-van der Waals interactions) are always presented in a

system. Debye and Keesom-Van der Waals interactions (also defined as dipolar interactions) operate by polar and polarizable parts.

(b) Coulomb (charge-charge) interactions take place, when the components (adsorbent and adsorbate) bear electrical charges. Coulomb forces play a main role in the double electrical layer formation at a charged interface.

(c) Hydrophobic interactions occur due to dehydration of non-polar parts of the adsorbent and solute molecules. The fact, that these interactions appear only in aqueous environment, reserves to them a central role in this thesis. The contribution of hydrophobic interactions very often dominates over those from other type of physical adsorption. It is known before and it is additionally proved in this thesis that the adsorption affinity gradually increases with increasing the number of hydrophobic (hydrocarbon) moieties.

(d) Hydrogen bonding is effective at an interface, where hydroxyl, amino or other electron donating (or electron accepting) groups are present. In aqueous medium the adsorption is only weakly influenced by them, because of the compensation of adsorbent-adsorbate and water-water contributions on one hand, and adsorbent-water and adsorbate-water on the other.

4.3. Adsorption kinetics.

The adsorption rate comprises two steps-(a) transport of solute molecules towards the interface and (b) interaction with the adsorbent surface.

(a) The basic mechanisms are diffusion or convection by laminar or turbulent flow. In absence of convection, the flux J from the bulk to the surface is given by:

$$J = (c_b - c_s)\left(\frac{D}{\pi.t}\right)^{1/2}$$
(4.1)

where c_b and c_s are the solute concentration in the bulk and at the surface, D the diffusion coefficient and t the contact time between the solute and the surface.

If the transport processes take place under steady-state convective diffusion, driven by a concentration gradient, the result is:

$$J = k_{tr}(c_b - c_s) \tag{4.2}$$

where k_{tr} is the transport constant, dependent on D and hydrodynamic conditions.

(b) The molecules of an adsorbing substance can attach (+) to the surface and detach (-) from it. The processes can be described by the net flux (adsorption rate), which equals to:

$$\frac{dA}{dt} = \frac{dA}{dt}\Big|_+ - \frac{dA}{dt}\Big|_- \tag{4.3}$$

The forward and backward fluxes can be written separately.

$$\frac{d\theta}{dt}\Big|_+ = k_a(1-\theta)c_s; \quad \frac{d\theta}{dt}\Big|_- = k_d\theta \tag{4.4}$$

where the fraction of unoccupied sorbent surface area is $(1-\theta)$, c_s is the forward flux, k_a is the attachment rate constant, k_d is the detachment rate constant $\theta = A/A_{max}$, A_{max} being the adsorbed amount when the surface is saturated by adsorbent molecules. Hence $dA/dt|_+$ varies linearly with $d\theta/dt|_+$.

$$\frac{d\theta}{dt} = \frac{d\theta}{dt}\Big|_+ - \frac{d\theta}{dt}\Big|_- \tag{4.5}$$

The attachment rate constant k_a can vary with θ, and therefore with time. The reason is the repulsive barrier caused by electrostatics repulsion, solvation effects or a short residence time for attachment for a fraction of the molecules.

Reached equilibrium ($d\theta/dt = 0$) implies:

$$k_a(1-\theta)c_s = k_d\theta \tag{4.6}$$

where c_{eq} is the equilibrium concentration of the adsorbate, corresponding to equilibrium A ($c_b=c_s=c_{eq}$). The equilibrium adsorption constant can be stated as $K = k_a/k_d$. The "off"-equilibrium $dA/dt|_-$ can be given by $k_a(1-\theta)c_{eq}$, providing that $dA/dt|_-$ is determined by k_d and θ. Hence, the adsorption net rate becomes:

$$\frac{dA}{dt} = \frac{dA}{dt}\Big|_{+} - \frac{dA}{dt}\Big|_{-} = k_a(1-\theta)(c_s - c_{eq}) \qquad (4.7)$$

By combination of 4.2 and 4.7 with $J = dA/dt$, one derives:

$$\frac{dA}{dt} = \frac{c_b - c_{eq}(\theta)}{\dfrac{1}{k_{tr}} + \dfrac{1}{k_a(1-\theta)}} \qquad (4.8)$$

The relation 4.8 concerns molecules, which do not change their conformation during the adsorption process (usually small rigid molecules).

Polymers may suffer conformational changes, caused by interactions at an interface. The reason is, that when polymers adsorb onto a surface, they do so with a affinity (high conformational entropy), reflecting in a high value of the adsorption equilibrium constant- $K = k_a/k_d$. Then the relation between A and θ becomes more complicated. The complicity arises from the expansion of the polymer coil, determined by the χ parameter (discussed in Chapter 2).

In Fig. 4.1 a typical adsorption isotherm is shown. Below an adsorption saturation it can be derived that for adsorbed amount c_{eq} is extremely low. Since adsorption saturation is reached (expressed by semi- plateau in the isotherm), $c_{eq}(\theta)$ sharply increases and approaches c_b. The dA/dt value drops significantly near the saturation kink on the adsorption curve. Considering these findings, one can assume that away from saturation $c_{eq} \approx 0$, and equation 4.8 can be written in the form:
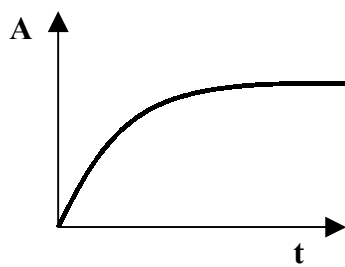
Figure 4.1. Adsorbed polymer amount v/s adsorption time.

$$\frac{c_b / A_{max}}{d\theta / dt} = \frac{1}{k_{tr}} + \frac{1}{k_a(1-\theta)} \qquad (4.9)$$

If $k_{tr} << k_a(1-\theta)$, than (considering 4.8) the net dA/dt (or for this matter $d\theta/dt$), is determined by the transport towards the interface, independent on θ. In case of $k_{tr} << k_a(1-\theta)$, a barrier for attacment at the interface and at high surface coverage dA/dt can be determined by the rate of adsorption, and therefore depends on θ.

Deriving the adsorption isotherm equation, one can express $c_{eq}(\theta)$ (from 5.8.) in an appropriate manner:

$$c_{eq} = \frac{k_d}{k_a} \frac{\theta}{1-\theta} = \frac{1}{K}\left(\frac{\theta}{1-\theta}\right) \tag{4.10}$$

The value of K (as it was state above) for polymer systems is extremely high, which presumes that k_a can not attain very high values, the value of k_d must be small, i.e., the rate of desorption is comparably insignificant to that of the adsorption.

4.4. Adsorption thermodynamics.

Thermodynamically an adsorption is possible, when the free enthalpy of the system decreases during the process. In case of adsorption, the free enthalpy of the system comprises the entropy and enthalpy of solid-state surface polymer and solution. The changes in free enthalpy ΔG can be expressed by changes in enthalpy ΔH and entropy ΔS of the system [Atk90, Eir77, Eve86].

$$\Delta G = \Delta H - T. \Delta S \tag{4.11}$$

In case of non-charged polymers with small affinity to the surface, the driving adsorption force is the system entropy increase. However, ΔH has a considerable influence on adsorption of highly charged polyelectrolytes onto charged substrate, revealing strong electrostatical interactions in the system [Coh91, Hoo94].

Chapter 5

Experimental Techniques.

5.1. Introduction.

To characterize the surface layers, one needs to apply different common or specific physical methods. In this chapter the theoretical basis of the techniques, as well as some additional modes, specified to investigate particular properties of the polymer layers will be extensively discussed.

According to the sequential order of layers investigation, one can sort the methods as follows:

Information for layer growth (ex- and in-situ) and optical properties of the sample was derived, using *null-ellipsometry* in different modes. The method is basic in the field of multi-step surface modification, swelling layer phenomenon at "in situ" conditions and adsorption monitoring.

Fourier Transform Infra-Red Spectroscopy in Attenuated Total Reflection mode (*FTIR-ATR*) was used for structural measurements to provide information about the chemical composition of different phases, building the polymer layer.

Surface charge variations with media quality were investigated in the frame of *electrokinetic method*, measuring *zeta potential* of the samples under specific conditions in electrolyte solution. A very important feature, the isoelectric points (*IEP*), of the different substrates and substances used in this study was detected by this method.

Contact angle method provides information concerning the surface energetic state and wettability of the modified substrates.

The morphology of the grafted (or adsorbed) polymer layers was investigated with *Atomic Force Microscopy* (*AFM*), recently developed in the field of polymer science.

An appropriate combination of all these methods provides a better understanding of processes and phenomena, occurred at interfaces, as well as complementary surface information about the systems, studied here.

5.2. Null Ellipsometry.

Ellipsometry is a non-destructive optical method for determining thickness and optical properties of thin films. It measures changes in the state of polarization of the light, reflected off the film's surface. Ellipsometry methods, single or multi wavelength, also have been

adopted for monitoring film growth in situ, allowing the precise control of a number adsorption and expansion processes.

5.2.1. Polarized light.

Relevant properties of various materials can be described by the complex dielectric function ε or by the corresponding refractive index n. An electromagnetic wave consists of an electric field $\vec{E}$ and a magnetic field $\vec{B}$. These vectors are mutually perpendicular and at the same time perpendicular to the direction of propagation, given by vector $\vec{k}$ (specified below). States of polarization can be classified as follows: The light adopts linear polarization state, when the electrical field vector oscillates within a plane. Elliptically polarized light means that the trace of the electric field vector, during one period, is an ellipse. To present the given state of polarization in a convenient mathematical manner, one uses the super-position of two linearly polarized light waves within an arbitrarily chosen orthogonal coordinate system [Born85],

$$\vec{E}(\vec{r},t) = \begin{pmatrix} |E_p| \cos(2\pi vt - \vec{k}.\vec{r} + \delta_p) \\ |E_s| \cos(2\pi vt - \vec{k}.\vec{r} + \delta_s) \end{pmatrix} \tag{5.1}$$

where $|E_p|$ and $|E_s|$ are the amplitudes, δ_p and δ_s the phases (along parallel (p) and perpendicular (s) vectors to the withdrawing vector-$\vec{r}$), $|\vec{k}| = 2\pi / \lambda$ is the magnitude of the wave vector and v is the frequency. The phases and the amplitudes are required to represent the states of polarization, assuming that the time dependence can be neglected. Hence, so called Jones vector states [Jon49]:

$$\vec{E} = \begin{pmatrix} |E_p| e^{i\delta p} \\ |E_s| e^{i\delta s} \end{pmatrix} = \begin{pmatrix} E_p \\ E_s \end{pmatrix} \tag{5.2.}$$

In next figure one represents examples of polarization state, given versus the phases δ_p and δ_s.

a   **b**   **c**
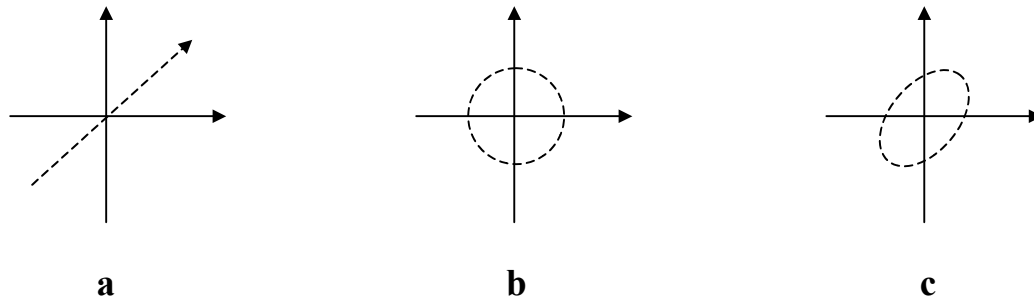
Figure 5.1. Jones representation of polarized light. The states of polarization are presented as a linear combination of two orthogonal linearly polarized light waves. a) linearly; $\delta_p - \delta_s = 0$, b) circularly; $\delta_p - \delta_s = \pi/2$ and $|E_p| = |E_s|$, c) elliptically polarized light; $\delta_p \neq \delta_s$ and $|E_p| \neq |E_s|$.

The interaction between the light and a matter can be described by a complex refraction index:

$$\overline{N} = n - i.k \tag{5.3.}$$

where n is the refraction number, that can be expressed by the ratio of the speed of light c_v in vacuum and the speed of the light in a medium c_m.

$$n = \frac{c_v}{c_m} \tag{5.4.}$$

The extinction coefficient k is given by:

$$k = \frac{\lambda.\beta}{4\pi} \tag{5.5.}$$

where β is the adsorption coefficient [Tomp93]

The reflection and transmission of the beam at a thin polymer layer (one or more) on a solid are shown in the next Figure.
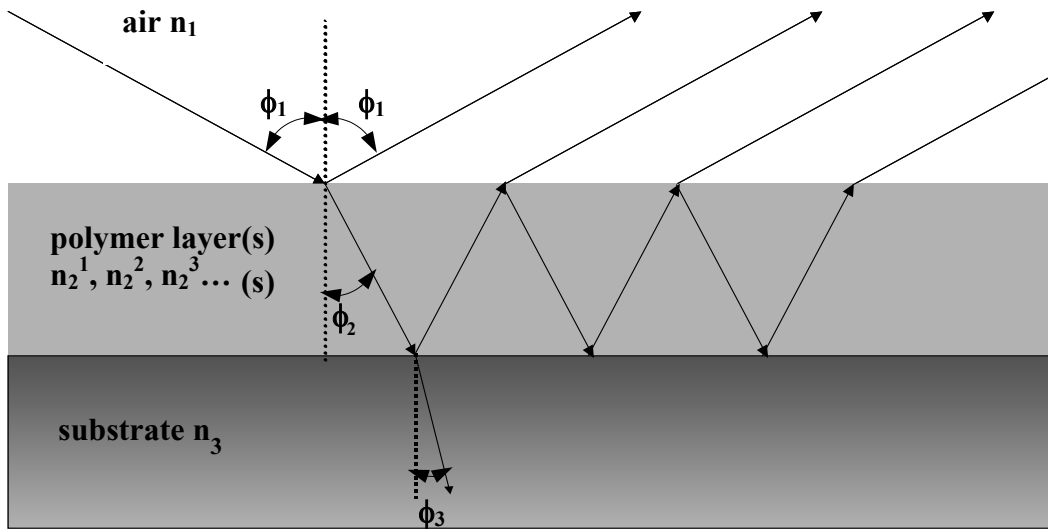
Figure 5.2. Reflection and transmition at a multiplane interface.

The refracted at the interface beam forms with a normal an angle ϕ_1, which can be connected to the incident angle ϕ_0 by equation 5.6. [Gert93]

$$\overline{N}_1.\sin\phi_1 = \overline{N}_2.\sin.\phi_2 \tag{5.6}$$

The reflected beam consists of two parts. One is reflected at the top of the polymer thin film and second one appeared by a reflection at thin film-substrate interface. The ratio of the amplitudes of the reflected and the incident waves can be expressed through the Frensel reflection coefficients for the two interfaces and the thickness of the thin layer [Born85, Röm94]:

$$r^p{}_{12} = \frac{E_p{}^r}{E_p{}^e} = \frac{\overline{N}_2.\cos\phi_1 - \overline{N}_1.\cos\phi_2}{\overline{N}_2.\cos\phi_1 + \overline{N}_1.\cos\phi_2} \tag{5.7}$$

$$r^s{}_{12} = \frac{E_s{}^r}{E_s{}^e} = \frac{\overline{N}_2.\cos\phi_1 - \overline{N}_1.\cos\phi_2}{\overline{N}_2.\cos\phi_1 + \overline{N}_1.\cos\phi_2} \tag{5.8}$$

The ratio between the amplitudes of the reflected wave and the incident one can be expressed by complex components of the reflection coefficients of electrical field vectors [Azz79]:

$$R_p = \frac{r_{12}{}^p + r_{23}{}^p.\exp(-i.2\beta)}{1 + r_{12}{}^p.r_{23}{}^p.\exp(-i.2\beta)} = \frac{\left|E_p{}^r\right|}{\left|E_p{}^e\right|}.\exp(i(\delta_p{}^r - \delta_p{}^e)) \tag{5.9}$$

$$R_s = \frac{r_{12}{}^s + r_{23}{}^s.\exp(-i.2\beta)}{1 + r_{12}{}^s.r_{23}{}^s.\exp(-i.2\beta)} = \frac{\left|E_s{}^r\right|}{\left|E_s{}^e\right|}.\exp(i(\delta_s{}^r - \delta_s{}^e)) \qquad (5.10)$$

The Frensel coefficients r_{12} and r_{23} at two interfaces are stated above. The phase thickness of a thin film, β, correlates with the real thickness, d, via next equation.

$$\beta = 2\pi.\frac{d}{\lambda}.\overline{N}_2.\cos\phi_2 \qquad (5.11)$$

A multiplayer system is treated similarly, but on the basis of the matrix formalism [Azz79, Mots91, Tomp93].

5.2.2. Basic equation of ellipsometry.

An incident (with a defined polarization state) light is reflected at the sample surface and as a result, the state of polarization changes. These variations can be measured and quantified by ellipsometry.
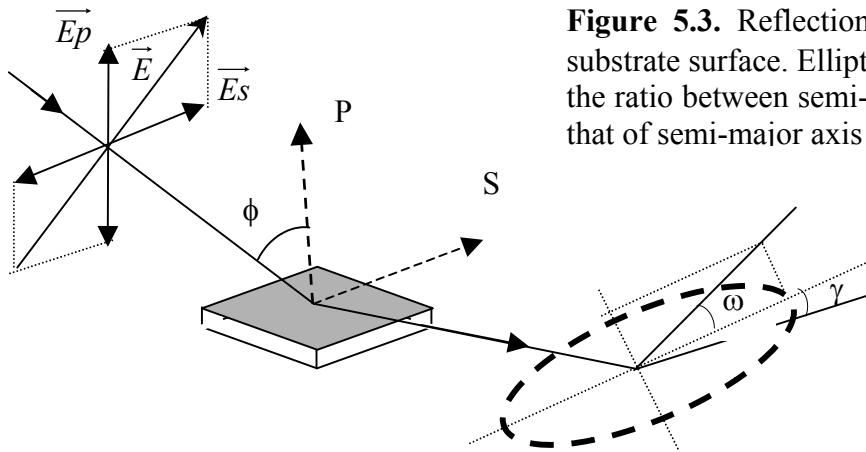
Figure 5.3. Reflection coordinates at the substrate surface. Ellipticity ω is defined by the ratio between semi-minor axis length to that of semi-major axis (dashed ellipse).

To describe mathematically the reflectivity experiment, a coordinate system, which consists of unit vectors, perpendicular and parallel to the plane of incidence, and an exit vector z is chosen (Figure 5.3). This coordinate system allows a description of every state of polarization as superimposition of two linear polarized waves. The plane of incidence is defined by the propagation direction of the beam together with the normal of the reflecting surface. Light

with an electric field vector, oscillating within the plane of incidence ($\hat{p}$ light), remains linearly polarized upon reflection and the same holds for $\hat{s}$-light with $\vec{E}$, perpendicular to the plane of incidence. Considering this fact, $\hat{p}$ and $\hat{s}$ light are also called Eigen-polarizations of isotropic media or uni-axial perpendicular media. The incident and reflected beam can be described by their corresponding Jones vector:

$$\vec{E}_{inc} = \begin{pmatrix} \left|\vec{E}_p^i\right| e^{i\delta_p^i} \\ \left|\vec{E}_p^i\right| e^{i\delta_s^i} \end{pmatrix} \qquad \vec{E}_{refl} = \begin{pmatrix} \left|\vec{E}_p^r\right| e^{i\delta_p^r} \\ \left|\vec{E}_s^r\right| e^{i\delta_s^r} \end{pmatrix} \qquad (5.12)$$

In order to evaluate dissimilarities in the polarization states, one introduces two quantities- ψ and Δ.

$$\Delta = (\delta_p^r - \delta_s^r) - (\delta_p^i - \delta_s^i) \qquad (5.13)$$

$$\tan\psi = \frac{\left|E_p^r\right| / \left|E_p^i\right|}{\left|E_s^r\right| / \left|E_s^i\right|} \qquad (5.14)$$

Changes in the amplitudes ratio are presented as the tangent of the angle ψ that can be measured directly.

So called reflection coefficients r_p and r_s give the reflectivity properties of the sample. The reflection coefficient is considered as a complex quantity, counting the changes in phase and amplitude of the reflected electric field E^r with respect to the incident one E^i.

$$r_p = \frac{\left|E_p^r\right|}{\left|E_p^i\right|} e^{i(\delta_p^r - \delta_p^i)} ; \; r_s = \frac{\left|E_s^r\right|}{\left|E_s^i\right|} e^{i(\delta_s^r - \delta_s^i)} \qquad (5.15)$$

As it is known, there is no interference between orthogonal beams, hence, $\hat{p}$ - and $\hat{s}$ -light are not in an influence and can be treated in a separate way. Regarding these definitions, one can derive the basic equation of ellipsometry [Azz79].

$$\tan\psi . e^{i\Delta} = \frac{R_p}{R_s} \qquad (5.16)$$

5.2.3. Ellipsometer design.

The set-up of an typical ellipsometer is given in Figure 5.4. The basic components are a polarizer, which turns the light to the polarized state, a compensator, introducing a defined phase retardation of one field component with respect to the orthogonal one, a sample, an analyzer and a detector [Erb93, Erb97, Mots91] .
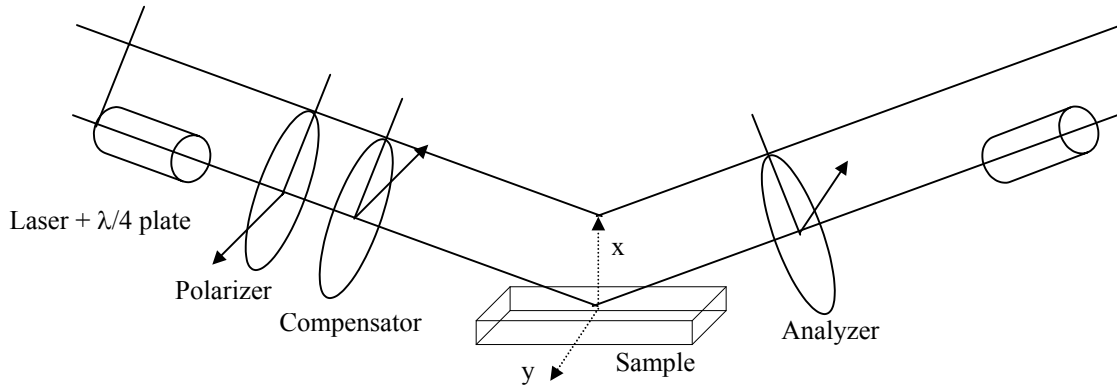
Figure 5.4. Schematic depiction of an ellipsometic set-up.

The ellipsometer determines the ellipsometric angles, and by additional parameter set can operate in various modes.

The null-ellipsometry is a successive implement, which eliminates many system errors, that can occur by a small-scale sample misalignment. As a light source, a red He-Ne laser with a wavelength 632.8 nm was used. The motorized polarizer and the compensator generate elliptically polarized light, which, afterwards, reflects from the substrate surface. For dry state measurements, the incident angle normally is set to 70^{0}, appropriate for silica wafers with native SiO_2 layer. After the sample surface is reached, the reflected light passes through the analizer and drops onto a photo multiplier, which operates as a detector. The control of the ellipsometer and the data evaluation, requires a special software. The ellipsometric quantities ψ and Δ were derived from positions of the polarizer (P) and analyzer (A) which led to zero intensity of the beam at the detector:

$$\psi = E , \ \Delta = 2P + 90° \tag{5.17}$$

There are different methods for determination of ψ and Δ parameters [Azz77]. He-Ne laser, producing monochromatic red light ($\lambda = 632.8$ nm) was utilized as a light source. The beam passes through the polarizer and compensator, adopting elliptical polarization, and was

incident at 70° to the sample (optimal for Si substrates with native SiO_2 layer). The reflected beam passed through the analyzer and its intensity was measured with the 4-section photodiode. In such cases the refractive index is measured in an independent experiment on a thick film or is taken from literature.

5.2.4. Liquid state measurements.

Instead studying the film growth after processing in air conditions, the null-ellipsometry is a sensitive technique for evaluation of thin films swelling and adsorption kinetics under appropriate conditions. Since most of the adsorption and surface processes, studied here, take a place at solid/liquid interfaces of water solvent, the ellipsometric measurements were adapted and optimized for experiments at aqueous/solid interfaces.

Dealing with such matter, one can face difficulties related to independent estimation of thickness, d, and n. When the thickness of a layer is less than 10 nm (in dry state), a correlation between the thickness, d, and the refractive index of the layer, n, is in presence. That means, that both parameters cannot be independently determined accurately. "In situ" ellipsometric measurements were performed to examine the swelling behaviour of the binary polyelectrolyte brush in variable media quality. Figure 5.5 gives a simplified view of the experiment.
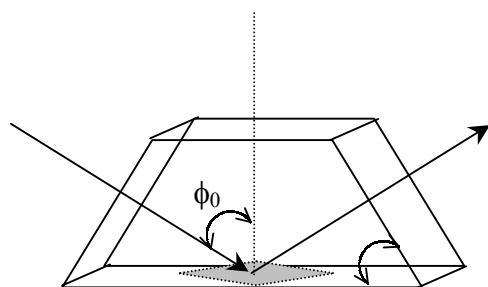
Figure 5.5. Ellipsometric set-up for "in situ" experiments.

For "in situ" studies of polymers at solid/liquid interface, one can use a cell with thin, stress-free glass windows at a fixed angle. For a single, sharp, interface between two transparent media (water-polymer) Δ passes through an abrupt step between 0 and 180 ^{0} at certain angle, called the Brewster angle ϕ_{Br}. Varying the wall-angles allowing one to stay closer to the Brewster angle of the system under investigation.

5.3. Fourier Transforming Infrared Attenuated Total Reflection

5.3.1. Introduction.

The ATR-IR spectroscopy (attenuated totally reflected infrared light spectroscopy) is a method, which permits the infrared-spectroscopic investigation on thin polymer layers of some nanometers scale. The infrared spectroscopy is based on the phenomenon that by infrared light irradiation, oscillations and rotations of atoms and atomic's groups become lively. Suggestion condition is that during the oscillation the dipole moment of the molecule changes. Different atomic's groups within the examined polymer layers absorb infrared light of different frequency, which is characteristic of the groups. So the groups can be identified within the polymer layer [Hess91, Göp94].

The difference between ATR and conventional IR spectroscopy in reflection mode is that by the ATR the infrared light is irradiated and reflected by an optically closer to the polymer layer side [Fahr61, Müll93, Urb93].

5.3.2. Totally internal reflection of light.

When light passes from a first into a second, less dense medium, it bends away from the normal. At a particular incident angle, the angle of refraction will be 90^0, and the refracted ray would travel along the boundary between the two media.

The incident angle at which this occurs is called the critical angle. This angle can be calculated, using Snell's Law:

$$\sin(\phi_{cr}) = (n_2 / n_1)(\sin(90^\circ)) = (n_2 / n_1) \qquad (5.18)$$

where n_2=index of refraction in denser medium, n_1=index of refraction in 2nd medium.

If the angle of incidence is increased beyond the critical angle, the light rays will be totally reflected back into the incident medium. This effect is called total internal reflection (Scheme 5.1). It is important to note, that total internal reflection cannot occur if light is propagating from a less dense medium to a denser one.
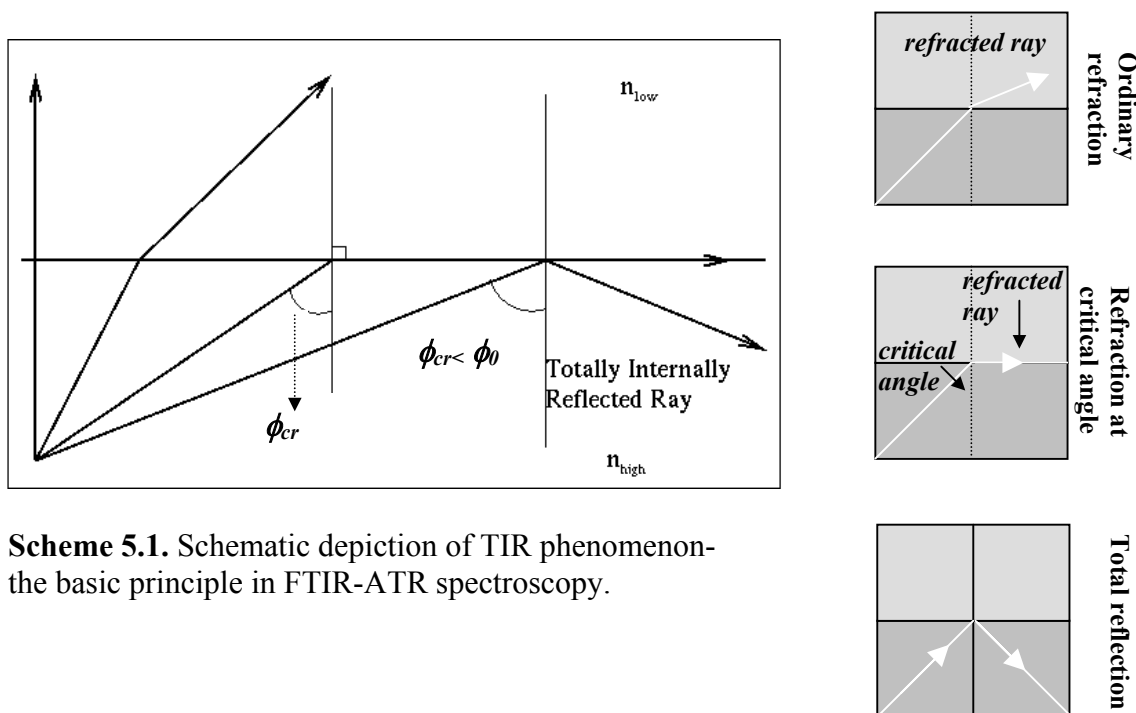
Scheme 5.1. Schematic depiction of TIR phenomenon- the basic principle in FTIR-ATR spectroscopy.

5.3.3. Basic principles of FTIR-ATR.

FTIR-ATR differs from commonly used FTIR techniques. In common circumstances, the IR beams pass through the sample (liquid or solid), otherwise in ATR, sample is contacted with the ATR crystal which is made of IR transparent material with high refractive index, typically including zinc selenide, KRS-5 (thallium iodide/thallium bromide), germanium and silicon. Scheme 5.2 shows the schematic diagram of ATR principle. Considering a trapezoidal ATR crystal (also called an internal reflection element or IRE), one can focus the infrared light onto one of the ATR crystal sides, using an appropriate optical setup.
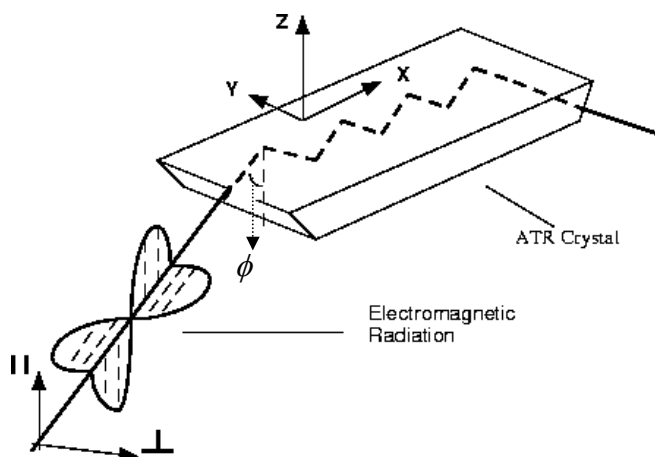
Scheme 5. 2. ATR crystal and principle of light propagation.

If the angle ϕ, at which the infrared light impinges upon the interface between the ATR crystal (the dense medium) and the

air (or water, buffer, etc.- the rare medium), is greater than the critical angle, then the light will totally internally reflect within the IRE.

By appropriately choosing the thickness (W) and the length (L) of the crystal, one can control the total), that the light will undergo as it propagates down the crystal, before emerging at the other end:

$$N_r = \frac{L}{W} \cot angent(\phi) \tag{5.19}$$

At each reflection, an evanescent electric field (E) is generated in the rare medium, whose intensity decays exponentially with distance (z) into the same medium, i.e.,

$$E = E_0 e^{-z/d_p} \tag{5.20}$$

where E_o is the intensity of the incident radiation and d_p the depth of penetration, representing the distance at which the evanescent wave drops to $1/e$ times the intensity at the surface. The magnitude of d_p gives us an idea of how deep we can see into the rare medium. This is true for both the electric and the magnetic components of the light. Using a device called a polarizer, we can selectively absorb one of these components. Perpendicularly polarized light (or the transverse electric wave perpendicular to the plane of incidence on the IRE, the xz plane) when travelling through the ATR crystal will result in an electric field on the surface of the ATR crystal with a component only on the surface of the crystal. When the light is polarized parallel to the incident plane, then:

$$E_0 = E_y \tag{5.21}$$

and

$$E_0^2 = E_x^2 + E_z^2 \tag{5.22}$$

Consideration of the two components of the travelling light beam will be important for understanding and interpreting calculations of molecular orientations on the ATR surface. The intensity of the reflected light at each reflection point will be reduced by the presence of infrared absorbing material in the rare medium. The surface sensitivity of ATR results from the addition of a number of small absorbances from each reflection. The depth of penetration can be calculated using the following formula:

$$d_p = \frac{\lambda}{2\pi n_1 \sqrt{(\sin^2 \phi - n_{21}{}^2)}} \qquad (5.23)$$

where λ is the wavelength of the light (note that the depth of penetration is a function of wavelength), n_1 is the refractive index of the ATR crystal, n_2 is the refractive index of the rare medium (this value is a function of wavelength), ϕ is the angle of incidence and n_{21} is n_2/n_1. Considering equation (5.23) one can easily calculate, that thin films with up to 100 nm thickness can be successfully investigated [Müll96, Müll97].

5.4. Zeta Potential.

5.4.1. Streaming potential.

The electrostatic potential near a surface is called zeta potential. Electrokinetic techniques, determining the zeta potential can be summarized in four groups: 1) Streaming Potential, 2) Electro-Osmosis, 3) Electrophoresis and 4) Sedimentation Potential.

For measuring zeta potential of thin films, the streaming potential method is applicable. The measured quantity by this method is given by the correlation between the zeta (ζ) and the streaming (U_s) potentials derived by Smoluchowski [Jac84, Jac96]:

$$U_S = \frac{\zeta \cdot \varepsilon \cdot \varepsilon_0 \cdot Q \cdot \Delta p}{\eta \cdot L \cdot R} \qquad (5.24)$$

where η is the viscosity, ε is the relative dielectric constant, ε_0 the absolute dielectric constant, Δp-the pressure difference, R the externally applied voltage, L the capillary channel length and Q is the cross-section channel area. The set up of the experimental cell is presented below.
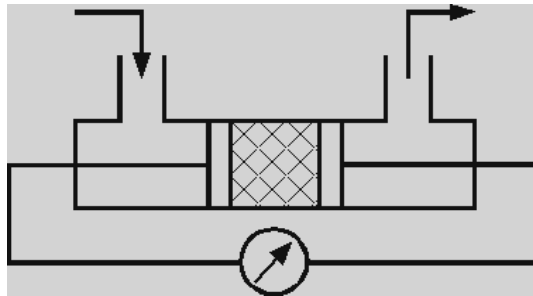
Scheme 5.3. Simplified scheme of a streaming potential cuvette.

In order to determine ζ as function of pH, the pH value of the liquid phase was adjusted with 1 mol/L HCl and 1 mol/L KOH, and measured at a constant ionic strength of 10^{-3} M KCl.

The charge on a colloidal surface can arise from a number of different mechanisms, including dissociation of acidic or basic groups at the substances, or adsorption of charged species from solution. The substrate charge is balanced by an equal and opposite charge carried by ions in the surrounding liquid. These counter ions tend to cluster around the surface in diffusive

clouds. This arrangement of the surface charge, surrounded by a diffusive cloud of counter charge, is called electrical double layer (see Figure 5.6).
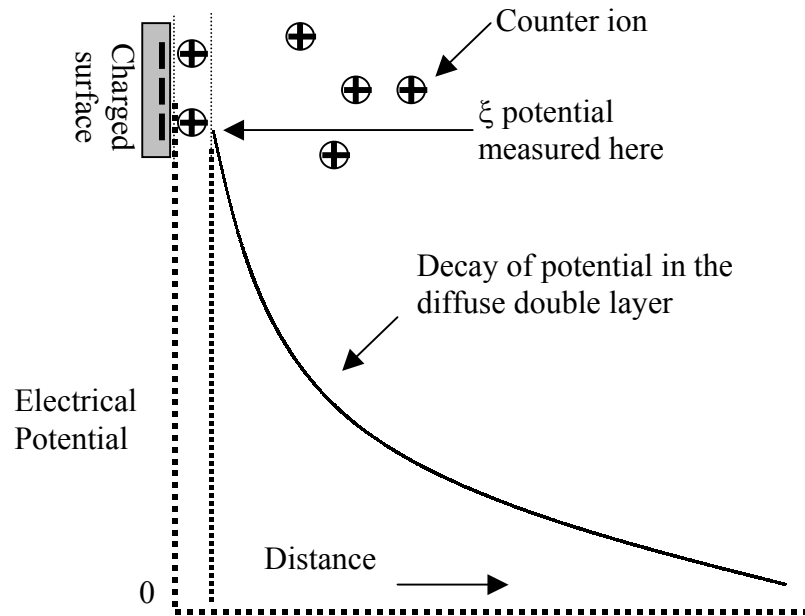
Figure 5.6. The electrical double layer and the zeta potential.

The electrical potential drops off exponentially with distance from the surface.

5.4.2. Isoelectric point.

The isoelectric points (IEP) of the brush modified silicon wafers were determined by means of streaming potential measurements. The experiment runs, using an Electrokinetic Analyser (company Anton Paar KG, Austria), whereby the electrical potential is determined here as function of the pressure loss in a flow channel between two wafer plates (2 cm x 1 cm). The correlation between the Zeta potential, ζ, and the Streaming potential, U, is given by the Smoluchowski equation enabling calculation of the zeta potentials from streaming potential measurements.

The zeta potential depends on the surface charge density and the double layer thickness. The surface charge density, in turn, depends on the concentration of "potential-determining ions" in the solvent-ions that have a particular affinity for the surface. In many systems, the H^+ ion is potential-determining, and so the zeta potential depends on pH. The zeta potential is

positive for low pH values and negative for high pH values. The pH at which the zeta potential is zero is the IEP of the sample.

5.5. Contact Angle Method.

5.5.1. Introduction.

Drop shape analysis is a convenient way to measure contact angles, and thereby to determine the surface energy. The principal assumptions are: a) the drop is symmetric about a central vertical axis and it is irrelevant from which direction the is viewed. b) the drop is not in motion in the sense that viscosity or inertia are playing a role in determining its shape, i.e., the interfacial tension and gravity are the only forces shaping the drop.

5.5.2. Wetting phenomenon.

The phenomenon of wetting or non-wetting of a solid by a liquid is better understood by studying what is known as contact angle. The drop of liquid forming an angle may be considered as resting in equilibrium by balancing the three forces involved. Namely, the interfacial tensions between solid and liquid (γ_{sl}), that between solid and vapour (γ_{sv}) and that between liquid and vapour (γ_{lv}). The angle within the liquid phase is known as the contact angle or wetting angle. It is the angle included between the tangent plane to the surface of the liquid and the tangent plane to the surface of the solid, at any point along their line of contact. Three types of equilibrium wetting regimes, in respect to drop-surface interaction mode, can be distinguished. The wetting is partial in case of a finite contact angle, occurring at the interface, i.e. $\Theta > 0$ (Figure 5.7a and b) The energetic state corresponding to such a contact angle is a hydrophobic one. The liquid does not spread down to a mesoscopic or a microscopic thickness. Thus, it can be described in terms of macroscopic quantities discussed above. When the contact angle overcomes 90 ^{0} (a), the state is called „non-wetting"and the liquid tends to ball-up and to run off the surface easily.

Figure 5.7. Variety in wetting phenomenon of a water droplet in contact with a solid surface. a) non-wetting, b) partial wetting, c) completely wetted surface.

The wetting is complete when the contact angle between a liquid and a solid surface is zero ($\Theta = 0$, Figure 5.7c). In this case, the liquid forms a thin film on the solid surface, which allows the long range molecular interactions to operate within the system. A substrate having such characteristics is called a hydrophilic one [Grah48, Leg92, Caz89].

5.5.3. Interfacial tension, Young and Laplace equation

The surface tension of the solid will favor spreading of the liquid, but this is opposed by the solid-liquid interfacial tension and the vector of the surface tension of the liquid in the plane of the solid surface (Figure 5.8).
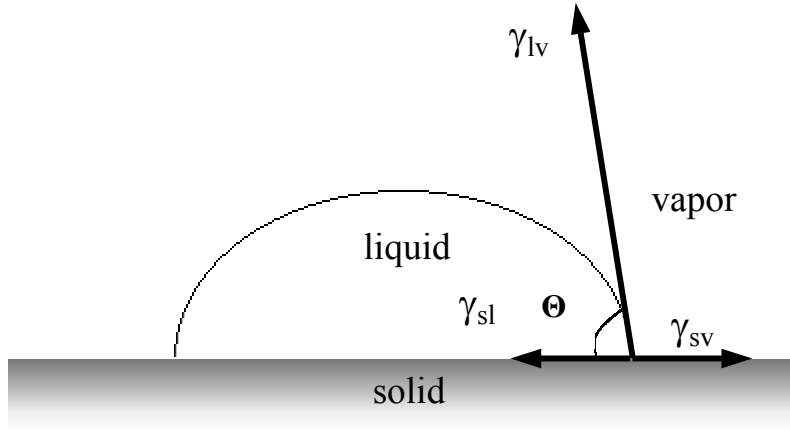
Figure 5.8. Interfacial tension balance between solid, liquid and vapor.

Surface tension is used to describe the equilibrium within a boundary region, formed between two bulk phases. Mathematically, the surface tension is often presented by its equivalent-the surface free energy.

The terms „interfacial tension" or „interfacial free energy" are used in a more general sense to describe the free energy of solid-liquid, solid-vapor, liquid-vapor and liquid-liquid interfaces. The surface tension can be defined as a force per unit length [Gru01] and then the work done for extending a movable side to distance dR:

$$W = \gamma \, dR \qquad (5.25)$$

where γ (dyne/cm or mN/m, but also in erg/cm^2 or mJ/m^2) represents the work required by any reversible process to form a unit area of new surface. According to the thermodynamics of interfaces, γ_{ij} can be written in terms of the surface excess free energy. That is, γ_{ij} is the change in surface excess free energy produced by a unit increase in area, either of a solid-vapor, solid-liquid, liquid-liquid or liquid-vapor interface, respectively. In general,

$$\gamma_{ij} = (\frac{\partial G}{\partial A_{ij}})_{T,p,n} \qquad (5.26)$$

or

$$\gamma_{ij} = (\frac{\partial F}{\partial A_{ij}})_{T,V,n} \qquad (5.27)$$

where G is the Gibbs free energy of the system, F-the Helmholtz free energy, and A_{ij} the area of the interface between phases i and j. The subscript "n" denotes the assumption of adsorption equilibrium, in the case of multicomponent systems. In the thermodynamics of interface systems, both quantities, the Gibbs and the Helmholtz free energy are defined as excess quantities, drawing an imaginary and arbitrary dividing mathematical surface (Gibbs surface) between the two phases separated by the interface.

In Figure 5.8 one can observe three interfaces formed if a liquid drop is deposited on a solid surface, and hence, three interfacial tensions are involved: γ_{sv}, γ_{sl}, γ_{lv}, respectively the solid-vapor, solid-liquid, and liquid-vapor interfacial tensions. The balance between the forces at these three boundaries is given by Young's equation:

$$(\gamma_{lv}\cos\Theta + \gamma_{ls}) = \gamma_{sv} \qquad (5.28)$$

In the case of partial wetting, the shape of a liquid drop is determined by a combination of surface tension and gravity effects. Surface forces tend to make drops spherical, whereas gravity tends to flatten a sessile drop or to elongate a pendant drop. The shape of the drop is governed by the Laplace equation of capillarity, as follows:

$$\Delta P = \gamma \; (\frac{1}{r_1} + \frac{1}{r_2}) \qquad (5.29)$$

According to this well known equation, the pressure difference ΔP across a liquid-fluid interface is related to its interfacial tension γ and curvature, where r_1 and r_2 are the principal radii of curvature. Derivations of this equation, which describes the mechanical equilibrium condition for the liquid-fluid interface, can be found [Gru01, Row82]. The Laplace equation is the basis for drop shape analysis techniques including a very powerful contact angle method based on axisymmetric drop shape analysis.

5.6. Atomic Force Microscopy (AFM).

5.6.1. Introduction.

Scanning probe microcopy (SPM) designates a range of novel techniques for imaging and analysis of surfaces on a microscopic scale. The invention of the scanning tunneling microscope (STM) by G. Binnig and H. Rohrer at IBM in 1982 initiated a scientific research in the general field of scanning probe microscopy. In 1986 Binnig, C. Quate, and C. Gerber [Binn86] invented the atomic force microscopy (AFM), enabling one to image surfaces on the nanometer scale [From92, Göp94, Tsuk97]. Since SPM deals with detection of specific forces, it can be adapted to be sensitive to always existing van der Waals forces, and hence, practically all materials can be examined by this method [From92, Hart92, Stam92].

5.6.2. AFM device design.

The key components for a SPM include a tip, a scanner, an approach mechanism, a pre-positioning mechanism, a motion detector for the SPM, an electronic feedback control, and a computer controlled acquisition and imaging system. Rather than using a beam of light or electrons, SPM uses a fine probe that scans over a surface. By using such a probe, there are no restrictions, concerning the wavelength of light or electrons. The resolution obtainable with this technique can resolve atoms, and true 3-D maps of surfaces. Scanning Probe Microscopy is a general term, used to describe a growing number of techniques that use a sharp probe to scan over a surface and measure some property of that surface. Some examples are STM (scanning tunneling microscopy), AFM (atomic force microscopy), and NSOM (Near-Field Scanning Optical Microscopy).

The set up of an Atomic Force Microscope is presented in the Figure 5.9.

Figure.5.9. Schematic view on an AFM set up.
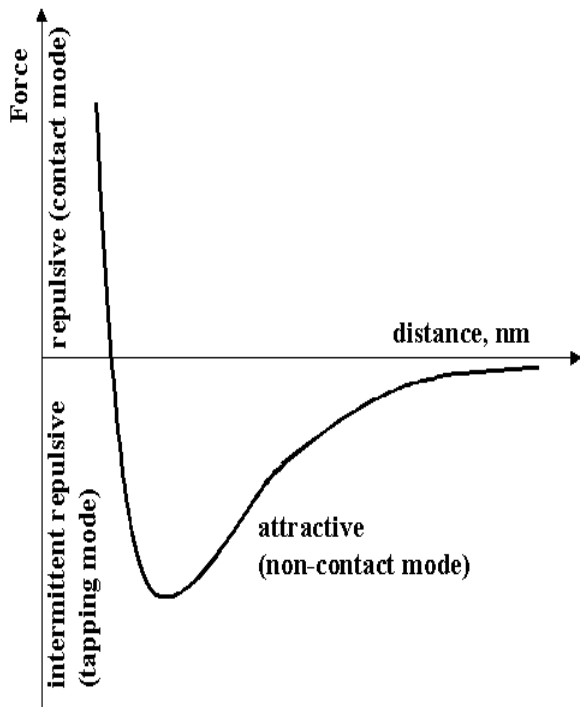
Figure 5.10. Force interactions between the sample surface and the probing tip.
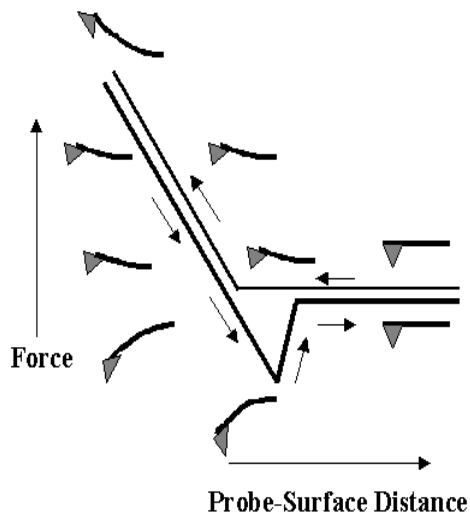
Figure 5.11. Force-curve representing the distance separating the tip and the sample surface and the nature and magnitude of the interacting forces. The thinner line shows the forces as the tip approach the surface and the thicker line shows how the force varies as the tip is retracted.

A common AFM device comprises a multi-sectional piezo element which allows the cantilever to move in x, y and z direction, depending on bias applied to it. It determines motion of a cantilever (a plate-like spring) with a probing tip or (in some microscopes) the piezo moves the sample.

5.6.2.1. Contact mode. As the name suggests, the tip and sample remain in close contact as the scanning proceeds.

In the contact mode, the probe is sensitive to the forces operating perpendicular (normal forces) and parallel (lateral forces) to the surface.

By "contact" one means the repulsive regime of the inter-molecular force curve as it is shown in Figures 5.10. and 5.11. The repulsive region of the curve lies above the x-axis. One of the drawbacks of remaining in contact with the sample is that there exist large lateral forces on the sample as the drip is "dragged" over the specimen. In the contact mode, when the tip interacts with the sample, the cantilever bends, according to the Hooke's law:

$$F = kz, \qquad (5.30)$$

where F, k, and z are the applied force, the cantilever spring constant, and cantilever deflection, respectively. To minimize the amount of applied force, used for sample scanning, one normally uses low spring constant probes (k<1 N/m) [Di99].

The laser beam reflects from the upper side of the cantilever at different angles depending on the cantilever bending (Figure 5.11.) to a four-section photodiode (Figure 5.9.). The difference in photo current between the upper and lower sections of the photodiode relates to the cantilever deflection in the vertical plane, while the photo current difference between the left and right sections corresponds to cantilever twisting due to friction between the probing tip and the sample. The sample is scanned in lateral (x, y) directions at constant deflection set point maintained by the feedback loop of the microscope by means of extending and retracting the piezo. The constant tip-sample interaction force (cantilever deflection) means the constant tip-sample distance (Figure 5.10.), which allows recording the vertical (z) piezo extension versus (x, y) location on a sample as the topography signal.

In a typical force microscope, cantilever deflections ranging from 0.1 Angstrom to a few micrometers and the typical forces range from 10^{-13} to 10^{-5} Newtons. There are varieties of forces in Force Microscopy that one should pay attention to. For example: a) Pauli repulsion and ionic repulsion which are very short range and negligible beyond about 1 nm, b) van der Waals force that are forces between electric dipoles and quite long ranged being significant up to 10 nm, c) capillary forces, and d) magnetic and electrostatic forces. Based on the signal detected, and the 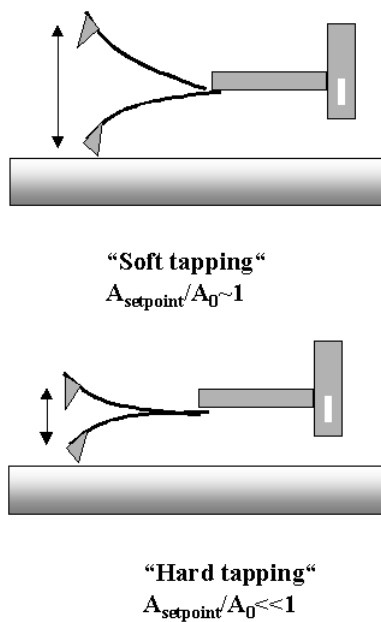spring constant of the cantilever, a force-curve can be constructed to determine the distance separating the tip from the sample surface and the magnitude and nature (attractive or repulsive) of the forces interacting between them. One of the main advantages of contact AFM is the high spatial resolution. Variations in height as small as 0.01 nm can be easily detected in the constant height mode.

5.6.2.2. Dynamic Force / Intermittant-contact / "tapping mode" AFM is the most common mode used in AFM of obtaining image contrast and was solely used in this work. When operating in air or other gases, the cantilever is oscillating at its resonant frequency (ω_0- about hundreds of kilohertz-normally between 50 and 500) and positioned above the surface so that it only taps the surface for a very small fraction of its oscillation period. That means the amplitude is required to be sufficiently high to overcome adhesion forces. Typically, amplitude changes are of magnitude of 100 nm.

This is still contact with the sample, but the very short time over which this contact occurs means that lateral forces are dramatically reduced as well as the amplitude of oscillation linearly decreases and is maintained constant (by the feed-back loop of the microscope) at a known value (amplitude set-point). In constant force mode the feedback loop adjusts, so that the amplitude of the cantilever oscillation remains (nearly) constant. An image can be formed from this amplitude signal, as there will be small variations in this oscillation amplitude

The oscillation amplitude is selected ($A_{setpoint}$) and kept constant while scanning (via a

"Soft tapping"
$A_{setpoint}/A_0 \sim 1$

"Hard tapping"
$A_{setpoint}/A_0 << 1$

Figure 5.12. Tapping modes in AFM

feedback loop), relative to the amplitude of free oscillation (A_0).

The lower is the set-point (or the amplitude set-point ratio $A_{setpoint}/A_0$, where $A_{setpoint}$ is the amplitude in contact), the closer the tip can come to the sample. Changes in the vertical coordinate (z) of the sample (or the cantilever) upon scanning the surface needed to keep constant amplitude of oscillation, are monitored, and displayed as a topography signal. The typical amplitude while imaging in air allows the tip to contact the sample surface through an adsorbed liquid layer without being stuck. The time of contact of the tip with the surface and the friction energy are from one to two orders smaller in the tapping mode than in the contact mode [Tam96]. The contact time increases upon decreasing the amplitude set-point ratio.

It should be noted that imaging at constant amplitude leads to higher indentation depth on softer materials than on harder ones. Choice of the amplitude set-point affects the relative topography signal on a heterogeneous sample. At certain conditions, an inversion of topography contrast can occur as the set point is changed [Bar00, Kopp00, Mag97]. Deduction of the true sample surface is discussed in [Kno01].

When imaging poorly immobilized or soft samples, tapping mode may be a far better choice than contact mode for imaging.

More recently, there has been much interest in **phase** imaging, by measuring the phase difference between the oscillations of the cantilever driving piezo and the detected oscillations. It is thought that image contrast is derived from image properties such as stiffness and viscoelasticiy. In the phase mode imaging, the phase shift of the oscillating cantilever relative to the driving signal is measured. This phase shift can be correlated with specific material properties that effect the tip/sample interaction. The phase shift can be used to differentiate areas on a sample with such differing properties. Figure 5.13 illustrates how phase data are obtained.
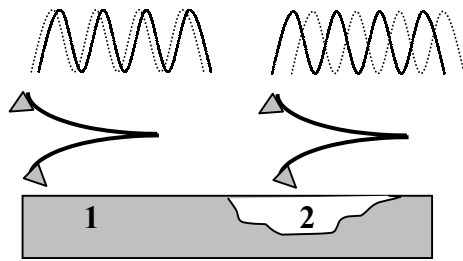
Figure 5.13. Phase offset of two different sample areas. Solid line represents the driving force, whilst the dashed one the tip response. Various samples characteristics cause a shift in the amount that they offset.

Phase is useful because different materials will cause different offsets in phase, because it depends on differences in adhesion, friction, and viscoelasticity. In Figure 6.13, region 1 has much smaller phase offset than region 2, so they will be very distinguishable in phase imaging. Phase images will also display great sensitivity to fine ridges in materials, often helping the user to locate areas of interest.

Nanoscope 3100/Digital Instruments at air carried out all investigations performed in this study in tapping mode. All of the topographies were taken in the tapping mode. The measurement frequencies were set to around 80 kHz. The cantilevers were made from microfabricated silicon (Nanosensors). Spring constant was 1.3-3.6 N/m.

5.6.2.3. Non-contact mode operation is another method, which may be employed when imaging by AFM. It differs from tapping mode by smaller amplitude of cantilever oscillation, which is < 10 nm. The cantilever must be oscillated above the surface of the sample at such a distance that we are no longer in the repulsive regime of the inter-molecular force curve. This is a very difficult mode to operate in ambient conditions with the AFM. The thin layer of water contamination, which exists on the surface of the sample, will invariably form a small capillary bridge between the tip and the sample and cause the tip to "jump-to-contact".

Even under liquids and in vacuum, jump-to-contact is extremely likely, and imaging is most probably occurring using tapping mode.

A different geometry is possible using the shear-force microscope (SHFM), and here true non-contact operation is possible.

5.6.3. Roughness analysis.

The smoothness of the polymer layer on a solid substrate one can measure, using root mean square (RMS) roughness parameter, using the tools at the AFM program.

RMS roughness parameter of a measured topology is calculated like:

$$RMS = \sqrt{\frac{\sum_{i=1}^{N}(Z_i - Z_{ave})^2}{N}} \ ,$$ (5.31)

where $Z_{ave} = \dfrac{\sum_{i=1}^{N} Z_i}{N}$, Z_i is height at certain point of measured area, Z_{ave} is average Z value

within the area, N is number of measured points within the area. The parameter shows how the measured surface area is not smooth. This parameter is always positive. Then a measured surface is rougher when the RMS is larger. On completely smooth surfaces, the parameter is zero.

Chapter 6

Synthesis of Polymer Brushes.

6.1. Synthetic routes.

The strategy for synthesis of binary amphiphilic and polyelectrolyte brushes is based on the combination of concepts that are typically used for synthesis of homopolymer brushes. Two main approaches were developed by a limited number of research groups [Sid99, Min01, Min02, Bie99, Bie00], comprising step-like "grafting to" a planar surface of two incompatible polymers (see chapters 7 and 8), or "grafting from" the surface of a defined number of monomer units, polymerizing under appropriate conditions.

6.1.1. "Grafting to" method. Step by step grafting of two end functionalized polymers.

The "grafting to"approach implies immobilization of pre-synthesized end-functional polymers onto a solid substrate. Multi-component polymer brushes can be synthesized via step-by-step binding of end-functional homopolymers to one type of surface functional groups. Maximal thickness of the brushes prepared by this technique is limited by disability of polymer molecules to diffuse through the already anchored polymer layer and does not exceed 8-9 nm.

6.1.2. "Grafting from" method. This method can be successfully used to prepare high grafting density and thickness binary brushes [Sid99, Min01]. The surface of silica wafer is functionalized with (3-glycidoxypropyl)-trimethoxysilane (GPS) and treated with diaminopropane. Chloranhydride of 4, 4′-azobis (4-cyanopentanoic acid) (Cl-ABCPA) was chemically grafted to hydroxyl and amino groups on the Si-wafer surface. Step by step two different monomers, styrene and 2-vinylpyridine, were polymerized on the surface. The ratio between two grafted polymers is regulated by temperature and time. In the second step polymerization is initiated by the residual fraction of the chemisorbed azo-initiator left after the first step. Molecular weight of the grafted polymers was regulated by monomer concentration, temperature and concentration of initiator in the bulk.

## 6.2. Mixed polymer brushes synthesized via "grafting to" approach.

We synthesized two different types of polymer brushes, used as substrates for adsorption of particles, polyampholytes and proteins. The synthetic route, covered by the procedures,

developed for "grafting to" method, and a consecutive analogous chemical reaction for converting the non-polar constituents to polar, was applied.

6.2.1. Materials. Carboxyl terminated poly(*tert*-butyl acrylate) (PBA-COOH, Mn =42 000, Mw= 47 000 g/mol), polystyrene (PS-COOH, Mn = 45 900, Mw = 48 400 g/mol) and poly(2-vinylpyridine) (P2VP-COOH, Mn =39 200, Mw =41 500 g/mol) were obtained from Polymer Source, Inc, Canada. GPS (Aldrich) was used as received. Silicon (Si) wafers (100) with ca. 1.5 nm native SiO_2 layer thickness were obtained from Wacker-Chemitronics.

The Si wafers were rinsed several times in dichloromethane in an ultrasonic bath and afterwards placed in a cleaning solution of NH_4OH and H_2O_2 for 2 h at 60 °C. The cleaned wafers were exposed to 1% GPS solution in toluene for 16 h. The thickness of the rinsed and dried layer of the chemisorbed GPS was 1.3 ± 0.2 nm.

6.2.2. Grafting procedure. The first type polymer brush we synthesized, PS-P2VP, consists of the non-polar PS and the polyelectrolyte P2VP. The polymers were spin-casted onto Si-substrate, enriched with epoxy groups after GPS chemisorption (Scheme 6.1). PS-COOH was grafted from melt at 150 ^{0}C in vacuum for 15 min, then rinsed in soxhlet for 2 h and dried in flow of dry nitrogen. Afterwards P2VP-COOH was deposited on the same substrate from 1% THF solution. The grafting time consumed 15 h at the same conditions, followed by Soxhlet extraction in tetrahydrofuran (THF) for 3 h and dried in N_2 flow.
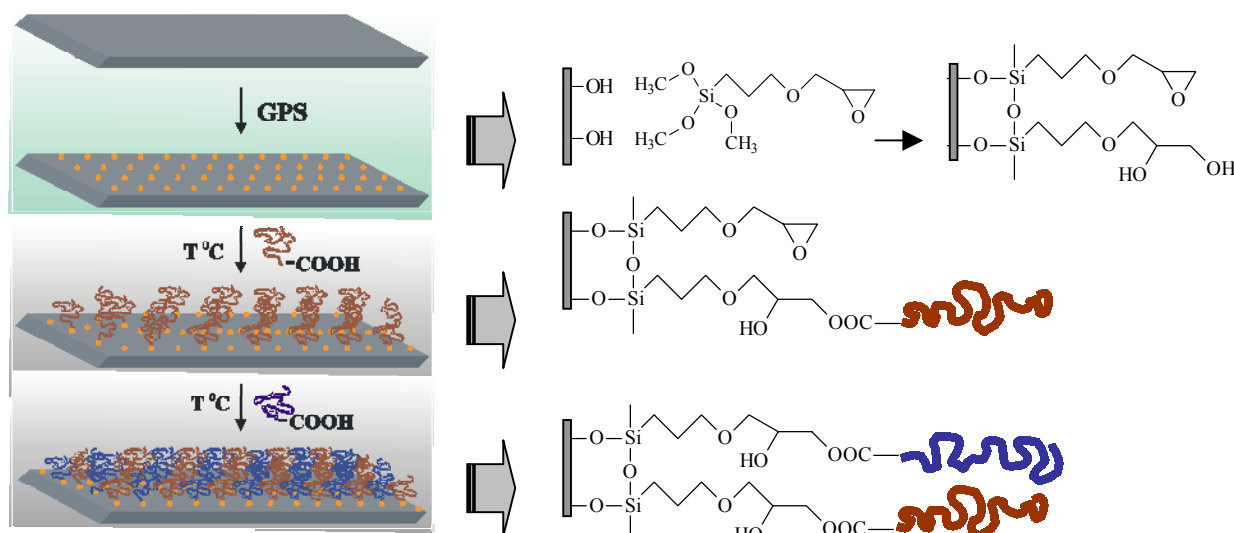
Scheme 6.1. "Grafting to" approach; I-attachment of epoxysilane, II- grafting of the first (nonpolar) polymer, III-grafting of the second polymer.

The second substrate, Polyacrylic acid-Poly(vinyl pyridine) (PAA-P2VP) binary polyelectrolyte brush, has the particularity to be composed of two polymers that are both

polyelectrolytes- a weak base (P2VP) and a weak acid (PAA), and was synthesized from PBA and P2VP by converting the first one to a polyelectrolyte-PAA (see 6.2.3).

PBA-COOH was selected to be the first grafted polymer, whilst P2VP-COOH was grafted in the second step. The opposite order of grafting gave no reproducible results, because of the high affinity of P2VP-COOH chains to the substrate, which suppressed essentially penetration of the second polymer through P2VP brush. The first grafted layer of PBA-COOH was prepared via deposition of the polymer film on the GPS modified Si wafer by spin-coating from 1% methanol solution and following annealing in a vacuum oven at 150 °C for 15 min. After the grafting procedure, the ungrafted polymer was removed by a Soxhlet extraction in methanol for 3 h. The second polymer P2VP-COOH was then grafted using the same procedure, when a thin film of P2VP-COOH was spin-coated on top of the PBA-COOH brush. The grafting time was 15 h. Afterwards, the ungrafted polymers were removed by Soxhlet extraction in THF. Polymer brushes, synthesized by this method, do not exceed a grafted amount of 10 mg/m^2, because of the "volume excluded effect", operating in the system. The effect is based on the kinetic inability of chains, reaching the top surface, to penetrate already grafted layer and to react with the active groups of GPS. Figures 6.1 and 6.2 represent the grafting kinetics, measured for PS-P2VP and PBA-P2VP brushes.
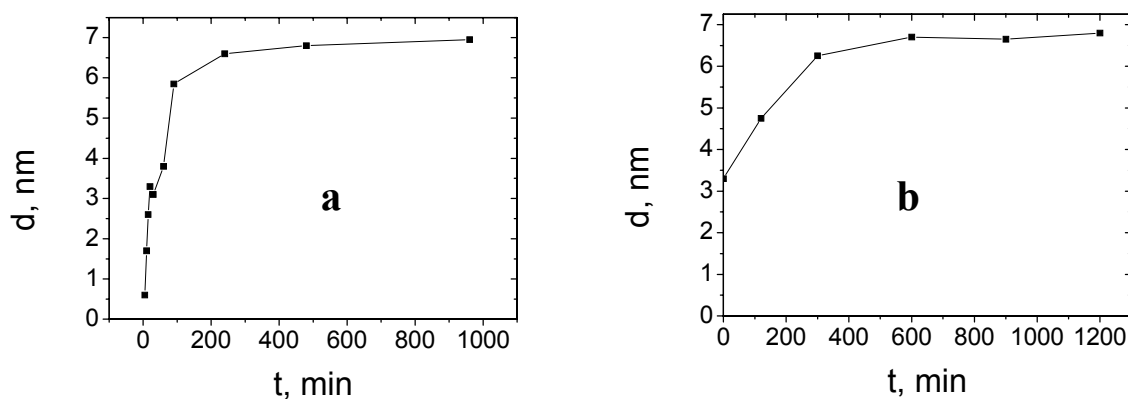
Figure 6.1. Grafting kinetics on the modified with epoxy groups Si wafer, 150 °C, melt: a) PS-COOH, b) P2VP-COOH after grafting of 3.4 nm of PS-COOH. Total grafted layer thickness-6.7 nm.

In Chapters 7 (Table 7.1) and 8 (Table 8.1), the characteristics, obtained for various binary brushes, synthesized by both approaches are presented.
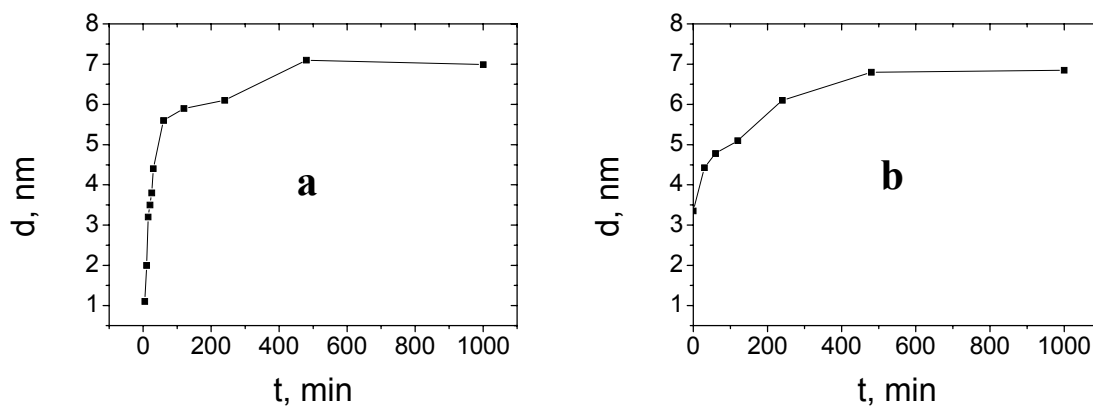
Figure 6.2. Grafting kinetics on the modified with epoxy groups Si wafer, 150 °C, melt: a) PBA-COOH, b) P2VP-COOH after grafting of 3.5 nm of PBA-COOH. Total grafted layer thickness-6.8 nm.

6.2.3 Polyelectrolyte brush composed of oppositely charged polymers.

PBA–P2VP mixed amphiphilic brush was prepared as it was described above. After the synthesis, PBA component was hydrolyzed by treatment in benzene saturated with *p*-toluenesulfonic acid monohydrate at 55 °C for 1 h, to yield PAA. Scheme 6.2 represents the mechanism of the conversion reaction.
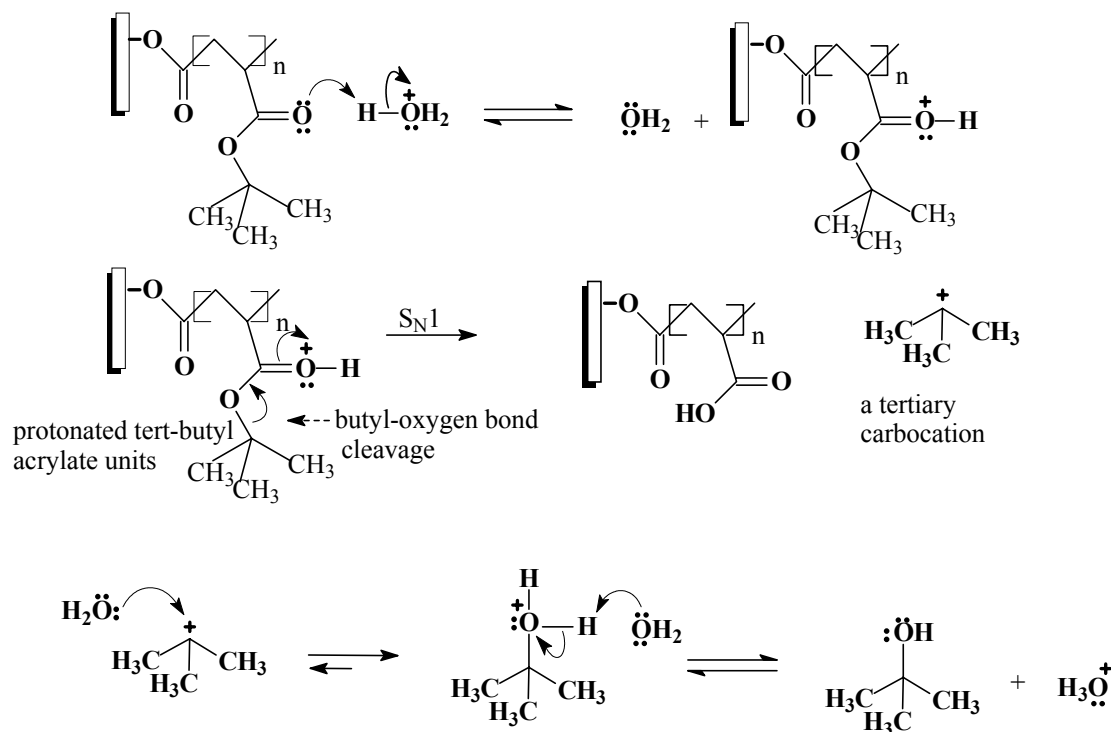
Scheme 6.2. Conversion of the neutral PBA to the polyelectrolyte PAA.

The first step in the hydrolysis is the protonation of the carbonyl oxygen. The protonated ester dissociates by an S_N1 mechanism into a tertiary carbocation and carboxylic acid. After the hydrolysis, a no significant decrease (about 5%) of the brush thickness was observed [Hou03, Brue97]. To prove stability of the formed PAA film, the brush was treated in ethanol by Soxhlet extraction over 5 h.

The layers structure was investigated using FTIR-ATR analysis, performed on silicon ATR prism surface. The spectrum of the chemisorbed GPS was used as reference. Spectra b-d in Figure 6.3 are plotted after subtraction of the GPS spectrum (Figure 6.3.a). The characteristic bands detected at 1730 cm^{-1} (-C=O) and 1370 cm^{-1} (-C(CH$_3$)$_3$) refer to butyl ester groups of the firstly grafted PBA (Figure 6.3b).

The grafting of the second polymer P2VP was proved by the characteristic bands at 1568 and 1590 cm^{-1} (Figure 6.3c).
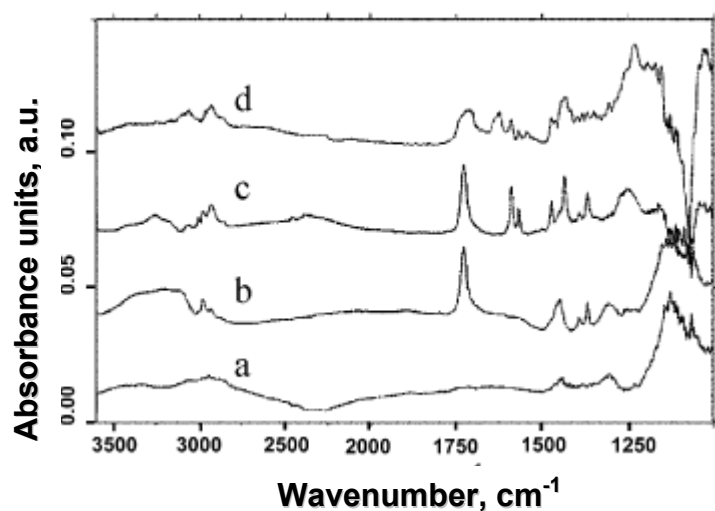
Figure 6.3 FTIR-ATR spectra of grafted layers on Si prism:
(a) GPS, (b) PBA brush, (c) PBA-P2VP mixed brush, (d) PAA-P2VP polyelectrolyte brush. Spectra (b)-(d) are plotted after subtraction of spectrum (a).

After conversion of PBA to PAA via hydrolysis of the *tert*-butyl ester groups, new bands at 1710-1730 cm^{-1} (acid carbonyl), 1230 and 3200 cm^{-1} (-OH), together with the peak at 1610 cm^{-1} (presence of -COO- grops) identify the existence of PAA within the film (Figure 6.3d). Dramatically decreased intensity of the band at 1370 cm^{-1} proves a complete hydrolysis of PBA as well.

Chapter 7

Mixed Amphiphilic Polymer Brush for Switching of Energetic state and Surface Charge in Aqueous Media

7.1. Abstract. "Grafting to" and "grafting from" surface approaches, for synthesis of binary polymer brushes from two incompatible polymers of different polarity were applied. The synthetic route is based on a subsequent step-by-step grafting of carboxyl-terminated polystyrene and poly(2-vinylpyridine) to the surface of a Si wafer, functionalized with 3-glycidoxypropyltrimethoxysilane (GPS). This method provides a smooth and homogeneous polymer film on the macroscopic scale, as it can be evaluated by root mean square roughness analysis (RMS), at the AFM program. Polymer brushes, synthesized by grafting to approach do not exceed 1nm roughness (RMS (root-mean-square) roughness parameter- 5.6.3. in Chapter 5), while for thicker ones, fabricated via "grafting from" method, one can measure a RMS roughness value between 1 and 4 nm. On the nanoscopic scale the system undergoes phase segregation affecting the switching/adaptive properties of the film. Such a material was an object of intensive research during last few years. Here, a different aspect of its switching properties is on focus, namely, the response to an aqueous media upon exposure to various pH. The film morphology reversibly switches from "ripple" to "dimple" structures as well as the surface energetic state switches from hydrophobic to hydrophilic.

7.2. Introduction.

Thin films with polymer chains grafted to the solid substrate by only one end are a very suitable subject for theoretical analysis and experimental study, because its behavior can be easily modeled and interpreted. If the distance between grafted chains is smaller than an average end-to-end distance of the polymer chain, the layer of the grafted chains is in the regime of a polymer brush. In this case, grafted chains are forced to stretch in the direction normal to the plane of grafting and the conformation is determined by the energy balance between the elastic free energy of the stretched chain and the energy of the interaction between statistical segments [Ale77, Mil91]. Such an arrangement offers many interesting applications of the brushlike layers [Hal92] that have stimulated great interest in synthesis and investigation of polymer brushes [Tha00]. The questions of the regulation of thin polymer film stability [Zer94], wettability [Man97], adhesion [Raph92, Ruth00], reactivity and cell

protein interaction [Aks96, McPher98], micro/nano-patterning [Niu98, Huss00], swelling [Hab98], friction [Kle94], stabilization of colloids [Ber98], core-shell structures [Guo99], and so forth, were addressed with respect to the employment of such an advanced material.

The theoretical analysis of phase segregation within binary brushes results in a complicated phase diagram [Mar91, Lai92, Lai94, Bro94, Sog96] and plenty of the thin film morphologies. Depending on solvent quality, layered and rippled phases, or their mixture, were observed experimentally. The transition between different morphologies upon external stimuli (solvent, temperature, etc.) results in switching of surface properties of the film, for example, from hydrophilic to hydrophobic. Such surfaces partially mimic a cell membrane. Regarding these properties, the mixed amphiphilic PS-P2VP brush was used successively in tuning adsorption of polyampholytes and proteins further in our studies.

7.3. Experimental.

7.3.1. Synthesis and characteristics.

Mixed polymer brushes were fabricated via "grafting to" [Mir95, Zaj95, Kop96, Tra99a, Tra99b] and "grafting from" [Kno96, Rüh00, Bie99, Boe00, Bie02] approaches, with some additional particularities developed by a limited number of researchers [Sid99, Min01, Min02a, Min02b]. The particular procedure is extensively described in 6.2.2 of Chapter 6 and includes the next methods and steps:

1. Thin polymer brushes produced by "grafting to" approach.

a) wafers cleaning (dichloromethane) and surface OH groups yielding ($NH_4OH+H_2O_2$).

b) chemisorption of GPS-epoxy groups for esterification reaction with carboxyl groups ends of the polymer chains.

c) grafting of PS (spin casted from 1 % w/w toluene solution and grafted from melt for15 min, at 150 ^{0}C in vacuum oven), followed by soxhlet extraction in toluene

b) grafting of P2VP (spin casted from 1 % w/w THF solution and grafted from melt-15 h, 150 ^{0}C, vacuum), followed by soxhlet extraction in THF.

2. Thick polymer brushes produced by "grafting from" approach.

The surface of Si-wafer already functionalized with GPS (see case 1.) is treated with diaminopropane. Chloranhydride of 4,4'-azobis(4-cyanopentanoic acid) (Cl-ABCPA) was chemically grafted to hydroxyl and amino groups on the Si-wafer surface. Step by step two different monomers, styrene and 2-vinylpyridine, were polymerized on the surface. The ratio between two grafted polymers is regulated by condition of polymerization in each step of grafting (temperature and time). In the second step polymerization is initiated by the residual

fraction of the chemisorbed azo-initiator left after the first step. Molecular weight of the grafted polymers was regulated by monomer concentration, temperature and concentration of initiator in the bulk.

By these two approaches, one synthesizes mixed amphiphilic PS-P2VP brushes, differing in their molecular size and physical-chemical characteristics (Table 7.1)

Grafted amount of a polymer, A, is calculated by:

$$A = \rho.d \tag{7.1}$$

where ρ is the polymer density (for PS $\rho = 1.045$ g/cm^3 and P2VP $\rho = 1.18$ g/cm^3) and d is the dry state thickness.

From the molecular weight Mn and the dry thickness, d, the distance between two grafting sites d_g is derived as:

$$d_g = M_n^{1/2}\left(N_A.d\rho\right)^{-1/2} \tag{7.2}$$

where N_A is Avogadro's number. The polymer layer is thicker than the distance between two grafting sites even in the dry state. The system therefore certainly is well in the brush regime and significant chain stretching is expected.

The grafting density of a polymer brush layer one can obtain from d_g by:

$$\sigma = \frac{1}{d_g^{\,2}} \tag{7.3}$$

Table 7.1. Characteristics of the mixed amphiphilic PS-P2VP brush.

Method and composition	Grafting to PS-P2VP			Grafting from PS-P2VP		
	PS-P2VP	PS	P2VP	PS-P2VP	PS	P2VP
Grafted layer thickness, d, nm	6.1	3.4	2.7	24.7	13.5	11.2
Grafted amount A, mg.m^{-2}	6.8	3.6	3.2	27.3	14.1	13.2
Grafting distance, d$_g$, nm	3.2	4.6	4.5	3.3	4.9	4.5
Grafting density, σ, nm^{-2}	0.10	0.05	0.05	0.09	0.04	0.05
Mn, kg.mol^{-1}		45.9	39.2		197.7	162.5
Mw, kg.mol^{-1}		48.4	41.5		361.5	284.8

7.3.2. Responsive properties.

Mixed amphiphilic PS-P2VP brush can be considered as a limiting case of the homopolymers PS and P2VP at symmetrical layers ratio. Responsive properties are determined from a combination of the behavior of uncharged PS brush and an additional performance originating from the electrostatic inter- and intra-chain repulsion at the charged P2VP in acidic media. The chains of PS display collapsed conformation and are located near the substrate surface, at the entire pH scale of our experiment, since for non-polar polymers the aqueous medium is a poor solvent in general. The contact angles variety (for the binary brush) is originating from the stretched P2VP chains, as the ratio between PS (hydrophobic) and P2VP (hydrophilic) within the surface mixed layer is regulated via pH signal. The main result of such a combination lies on an extension of the range of switching: charges make the surface more hydrophilic and introduce specific electrostatic interactions. Below we present several examples of responsive switching.
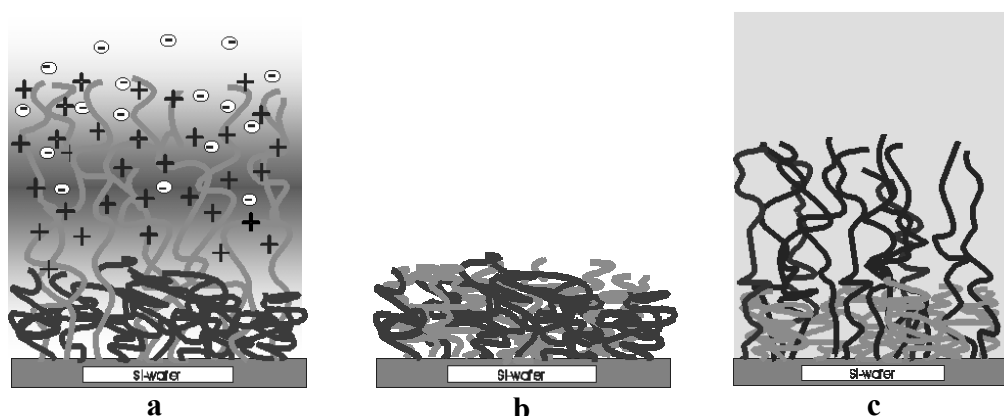
Figure 7.1. Illustration of a PS-P2VP brush behavior at different conditions: a) acidic water- a selective solvent for P2VP component, b) neutral and basic water-poor solvent for both components and c) selective organic solvent for the non-polar PS component.

The switching behavior was measured by electrokinetic test, contact angle method and AFM. Isoelectric point (IEP) of the mixed PS-P2VP brush, grafted onto GPS modified Si-wafer, was determined to be at pH 5.9. That is between IEPs of the homopolymer brushes of PS (at pH 4.3) and P2VP (at pH 6.7) (Figure 7.2).

Figure 7.2. Zeta-potential plotted as a function of pH for thin mixed and homopolymer brushes: P2VP brush (circles), PAA brush (squares), mixed PS-P2VP brush (triangles).

Mixed brush undergoes switching of the surface energetic state (wettability) upon exposure to different pH of the aqueous medium (Table 7.2), and similarly morphology transitions from dimple to ripple regime (Figure 7.3). Exposed to neutral and basic water the brush becomes hydrophobic. Its wettability increases with decrease of pH. At low pH values, protonated hydrophilic P2VP chains preferentially occupy the top of the film. As reference, we introduced wettability test of homopolymer PS (non-polar) and P2VP (weak polyelectrolyte) brushes. It is clearly seen that the 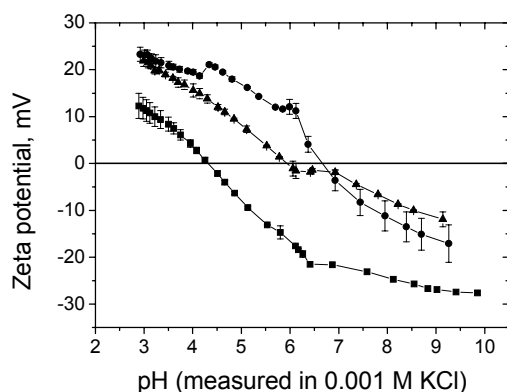electrostatic interactions extend switching of wettability of the brushes to broader range from highly hydrophilic (contact angle 22^0) to hydrophobic (90^0), and it is in agreement with literature [Min99, Min01]

Table 7.2. Water contact angles $(\Theta \pm 3)^0$ of binary (1:1) thin and thick PS-P2VP brushes.

Sample	PS-P2VP	PS-P2VP	PS	P2VP
A, mg.m^{-2}	27.3	6.8	6.8	7.2
Water pH				
1.5	22	28	-	19
3.0	41	50	87	29
5.0	-	-	-	-
7.0	74	76	86	66
9.0	79	81	88	78
Methanol	54	52	88	50
Toluene	90	88	90	79

The switching of morphologies upon exposure to different aqueous media quality was measured for thick and thin mixed PS-P2VP polymer brushes. Its origin is affected by the phase segregation at nanoscopic scale, which results in a reproducible surface features and patterns, successively detected using AFM technique and confirmed literature data [Min01]. Morphological transition from clustered large structures (dimples) at low pH to lamellas (ripples) with lateral characteristic size in the range of 50-100 nm and 20-50 nm respectively, was measured (Figure 7.3). In the case of thin mixed brushes PS-P2VP brush (Figure 7.5), one can observe the same transition, but the roughness (RMS) decreases in order of several magnitudes, because of the lower brush thickness. Since the chain length asymmetry is very small (see Table 7.1), the solvent selectivity is dominating factor for the switching. In the case (A) at Figure 7.3, the top layer is seen as grains of segregated P2VP, preferentially occupied the surface at pH 2. At pH 10, a smoother layer (RMS 2.4 nm), caused by the poor solvent conditions for both polymers was measured.

Figure 7.3. 1x1μm AFM topography images (Z range 32 nm) with corresponding cross-sections of PS-P2VP brush (24.7 nm thick) after exposure to: A) pH 2 (RMS 4.05 nm), B) pH 10 (RMS 2.4 nm).

The draws between the images represent an idealization of dimple/ripple morphology. The switching mechanism is sketched between the cross-section plots.

A medial, between a good to bad quality solvent, morphology is presented in the Figure 7.4, where surface topography was measured in a slightly acidic, through neutral pH region.

Figure 7.4. 1x1μm AFM topography images (Z range 32 nm) with corresponding cross-sections of PS-P2VP brush (24.7 nm thick) after exposure to: A) pH 3 (RMS 4.22 nm), B) pH 5 (RMS 4.71 nm), C) pH 7 (RMS 2.11 nm).

Exploring thin PS-P2VP brushes, one can observe similar tendencies in switching of the surface morphology. Comparing to the results, obtained for brushes with higher grafted amount, on can observe differences only concerning the magnitude of lateral size and height of the features (provided by cross section analysis). It is obvious, that brushes, synthesized via polymerization from the surface (thick PS-P2VP brushes) segregate better, as the effect is amplified by the chain size, exceeding sufficiently that of thin brushes. It is also of importance, to mark the prolonged time, required for equilibrium state morphology to be reached to, and it is devoted to the grafting density and thickness effect.
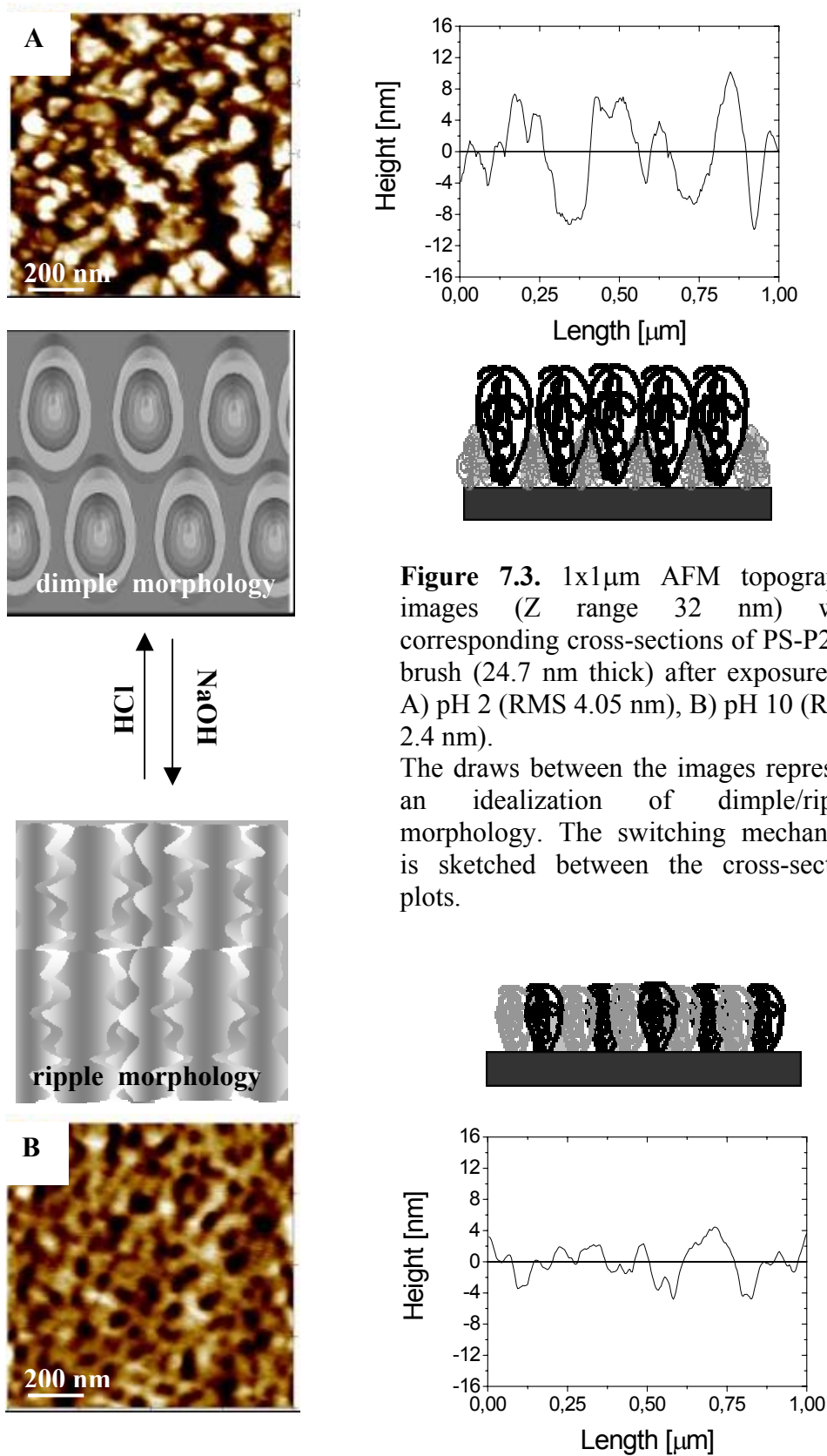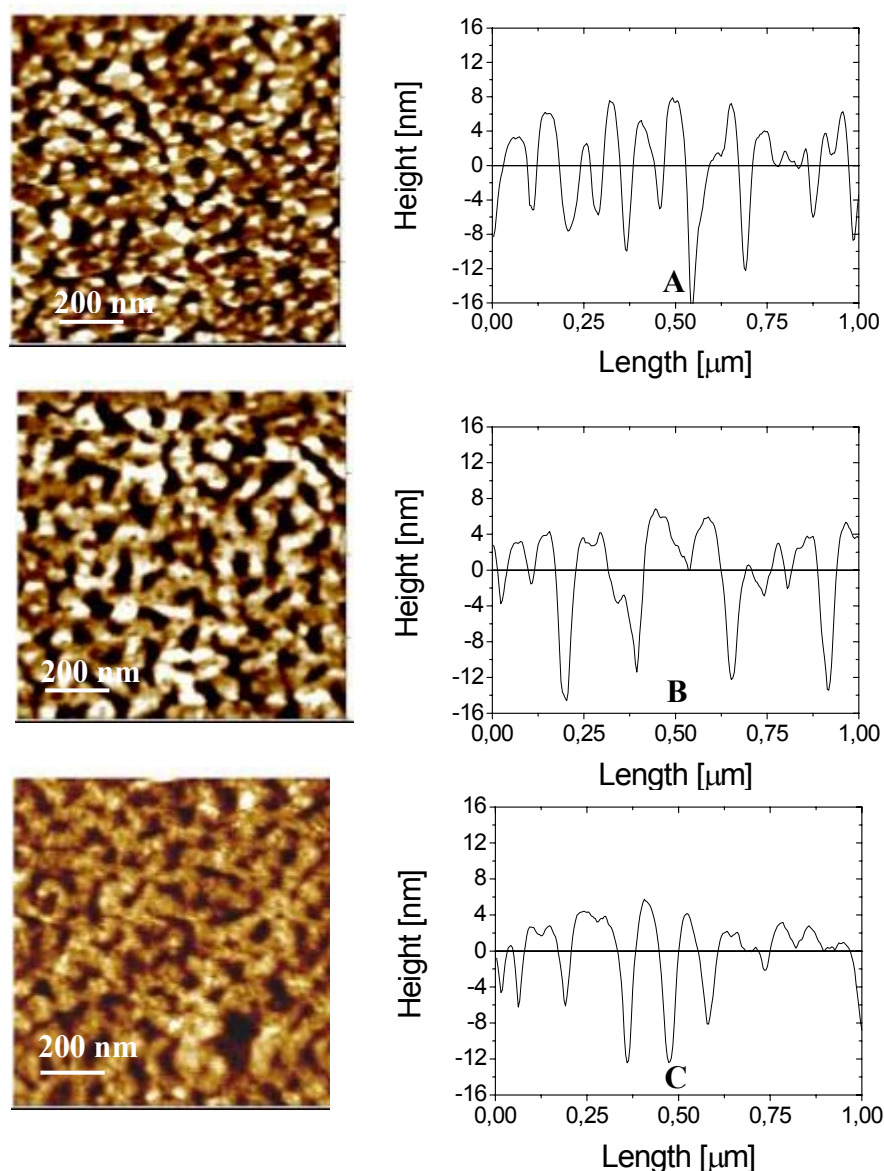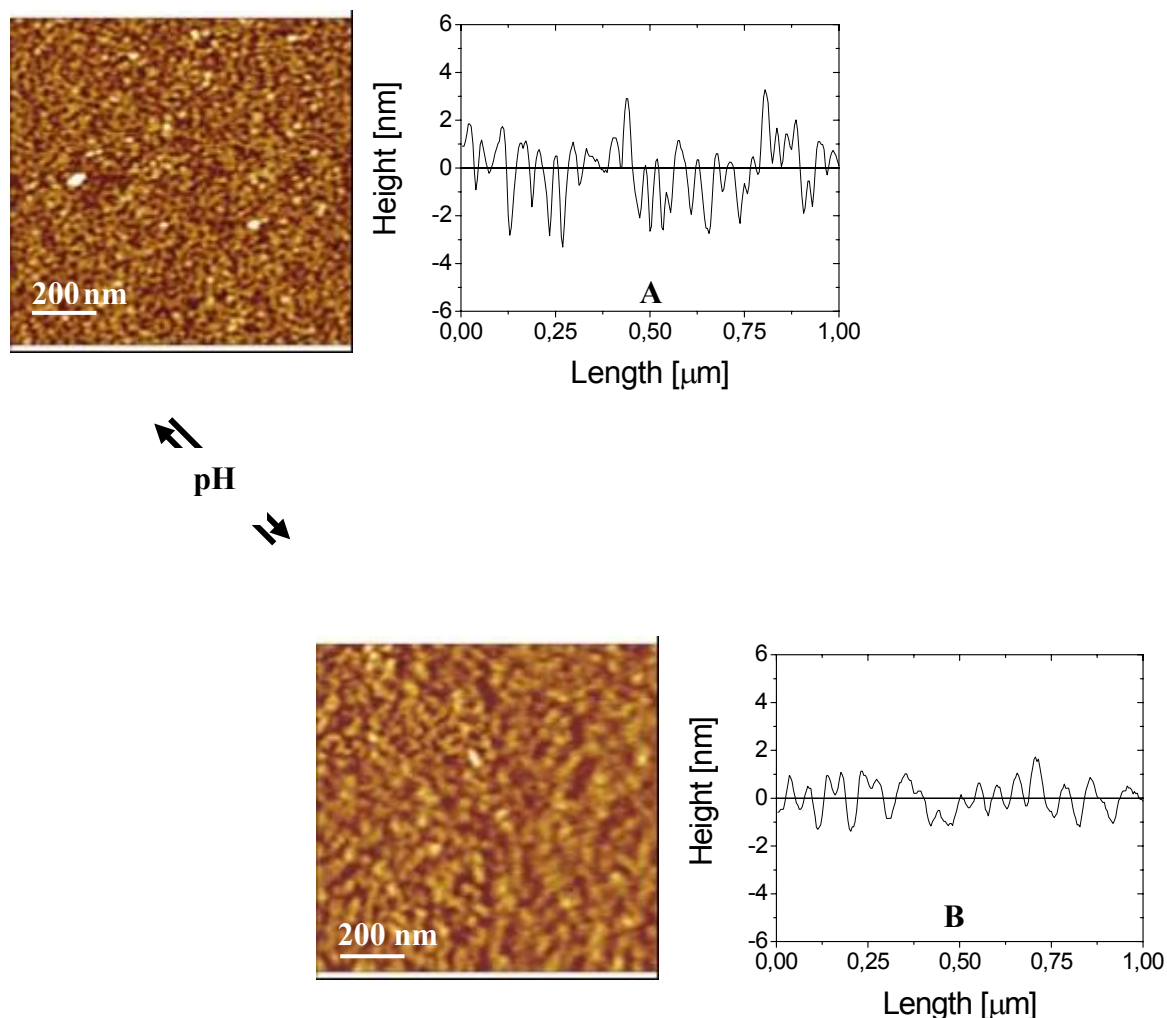
Figure 7.5. 1x1μm AFM topography images (Z range 12 nm) with corresponding cross-sections of PS-P2VP brush (6.1 nm thick) after exposure to: A) pH 2 (RMS 0.98 nm), B) pH 10 (RMS 0.71 nm).

7.4. Conclusions.

By use of two-step grafting procedure, we fabricated mixed polymer brushes with prominent amphiphilic properties. The mixed brushes showed reversible switching properties, when they were exposed to different selective/non-selective solvents. In acidic aqueous medium, a selective solvent for the hydrophilic P2VP, its chains are highly swollen, while the hydrophobic PS adopts collapsed state conformation. The top brush layer consists in this case mainly of P2VP chains, and the surface of the layer becomes hydrophilic. To adopt a hydrophobic energetic state, the amphiphilic brushes were exposed to neutral or alkali aqueous conditions, enriching the top layer with PS in expense of collapsed in this environment non-charged P2VP chains. The surface morphology in this case showed transition from well-segregated clusters to ripple-like structures, originating from the incompatibility between PS and P2VP, both exposed to poor solvent conditions.

The experiments demonstrated that with these materials one can reversibly and precisely to regulate the wettability and surface morphology, just by simple treatment of the samples with solvents of different quality. Our findings are in agreement with the literature and expand the application possibilities for such materials in fields, where a fine tuning of interfaces is required.

Chapter 8

Properties of Binary Polyelectrolyte Brush Composed of Oppositely Charged Polymers.

8.1. Abstract. In this chapter the environmental response of the binary polyelectrolyte brush polyacrylic acid-poly(2-vinylpyridine) (PAA-P2VP) is extensively discussed.

The brush was synthesized according to the "grafting to" procedure of poly(tert-butyl acrylate)-poly(2-vinylpyridine) (PBA-P2VP) and consequentially performed acid catalyzed ester hydrolysis, converting the precursor PBA to PAA. The switching/adaptive properties were examined, concerning the mechanism of surface charge replacement, swelling behavior and wettability.

Further, the influence of a monovalent salt on the brush behavior in aqueous solution was studied by null-ellipsometry, building a special set-up for "in situ" tests. Both, low and high, salt concentration regimes were distinguished in respect of swelling-deswelling performance of the polyelectrolyte brushes in good and poor aqueous solvent media.

Different morphologies were measured by Atomic Force Microscopy (AFM), adjusting the pH of the salt free medium below, at, and above the isoelectric point (IEP) of the material. Coil-globule/toroidal transitions were observed from good to poor (for both polyelectrolytes) solvent media, as the toroidal geometries have been detected to originate mainly from the collapse of P2VP component.

8.2. Introduction.

Polyelectrolyte systems exhibit a variety of phenomena, which find a wide application in many fields of science and industry. Modifying substrates with polyelectrolytes plays a significant role in adsorption processes of synthetic and natural molecules in industry and biomaterials sciences [Ber00, Schle01, Grau99, Dub99, Sukhor96, Kot98, Fish99]. Recently polymer layers, covalently attached by one end to the substrate and called polymer brushes attract a sufficient interest, due to their well defined surface properties and environmental

response [Min01, Min02a, Min02b, Sid99, Hou03]. This allows one to consider them as a good candidate for surface manipulation, adjustment, and nano-objects adsorption.

On mono-component brushes, a number of studies, experimental and theoretical, are reported [Zhu96a, Zhu96b, Bie99a, Bie99b, Bie99c, Bie02]. On binary mixed polymer brushes, recently, one can find several studies, concerning the synthetic procedures and environmental responsive switching [Min00a, Min00b, Min02, Min03, Us02]. In respect of binary brush, composed of oppositely charged polyelectrolytes, only some theoretical approaches are available [Shu01a, Shu01b].

Theory predicts that in contrast to equally charged homopolymer brush, when the intra- and inter- chain Coulomb repulsions lead to reversible stretching of the chains, the oppositely charged mixed brush has other possibilities to reduce the electrostatic repulsion. It depends on charge ratio (degree of compensation of the total charge of the homopolymer A, consisting of N_A segments, by the total opposite charge of the homopolymer B, consisting of N_B segments). At $N_A > N_B$ polymer A chains are coiled due to the electrostatic attraction between A and B, while at $N_A = N_B$ both chains form a compact brush. Addition of salt leads to screening of this attraction, and the brush expands. At a low charge ratio, further increase of the salt concentration causes a decrease of brush thickness due to screening of the repulsion between equally charged segments, thus exhibiting a maximum. Consequently, the larger variety of combinations of electrostatic and short-range interactions leads to much more complex response, compared to mono-poylelectrolyte brushes.

In this chapter, the first attempt to synthesize and experimentally investigate such brushes is presented.

8.3. Experimental.

8.3.1. Synthesis.

The synthesis of the binary polyelectrolyte brush onto Si-wafer planar surface is reported elsewhere (Chapter 6-6.2.2 and 6.2.3, [Hou03]), and covers the "grafting to" procedures, developed for fabrication of amphiphilic polymer brushes, with some additional modifications. Briefly reviewed, the synthesis includes: alkali cleaning procedure via rinsing the Si-wafer in NH_4OH/H_2O_2 for 2h at 60^0C; enriching the surface with epoxy groups by attachment of GPS (1% solution of dried toluene for 16 h); consecutive two step grafting procedure of carboxyl terminated PBA and P2VP for 15 min and 15 h, respectively, from melt at 150 ^0C. Characteristics of the binary amphiphilic brushes, as well as of the

homopolymer constituents, were calculated by 7.1, 7.2, and 7.3 (see Chapter 7) and are reported below. The density of PBA is ρ=1.04 g/cm^3.

Table 8.1. Characteristic of binary and mono polyelectrolyte brushes.

Composition	Binary brush PBA-P2VP			Mono-component brushes	
	PBA-P2VP	PBA	P2VP	PBA	P2VP
Grafted layer thickness, d, nm	5.74	3.13	2.61	6.79	6.84
Grafted amount A, mg.m^{-2}	6.33	3.25	3.08	7.06	8.06
Grafting distance, dg, nm	3.33	4.62	4.59	3.14	2.84
Grafting density, σ, nm^{-2}	0.1	0.05	0.05	0.10	0.12
Mn, kg.mol^{-1}		42.0	39.2	42.0	39.2
Mw, kg.mol^{-1}		47.0	41.5	47.0	41.5

Acid catalyzed hydrolysis of the tert-butyl ester groups at PBA was the second key step performed to convert the neutral PBA to weak poly(acrylic acid) (PAA). The chemical reaction runs on S_N1 mechanism in presence of p-toluenesulfonic acid monohydrate in benzene at 55 ^{0}C It is noteworthy that hydrolysis of tertiary esters by this mechanism involves breaking the alkyl-oxygen bond in contrast to primary and secondary esters. FTIR-ATR investigations, of the transition from a system including two incompatible homopolymers to a system with a high affinity between the components, were performed (Figure 6.3-Chapter 6)

8.3.2. Ellipsometry.

8.3.2.1. Dry state measurements. Null ellipsometry was applied to determine the thickness of chemisorbed GPS and grafted amount of the polymers after the grafting procedure. All the measurements were carried out using null-ellipsometer in a polarizer-compensator-sample-analyzer (Multiscope, Optrel Berlin) mode. As light source a He-Ne laser with λ= 632.8 nm was applied and the angle of incident was set to 70^0. A multilayer model for homogeneous films covering the silicon substrate has been used for calculation the thickness of chemisorbed GPS and grafted polymer layers in air from the ellipsometric angles ψ and Δ. The refractive indexes used in the calculations were n= 3.8850 for the silicon substrate, n=1.4598 for GPS, n=1.466 for PBA and n=1.595 for P2VP. After the hydrolysis of PBA, refractive index of 1.527 for PAA was used in the thickness evaluations.

For the mixed brush a three layer model was used, as SiO$_2$ and GPS layers were considered as one layer with effective n = 1.445. We found that this approach results in an error not larger than 5%.

8.3.2.2. "In situ" experiments. Null-ellipsometry is a sensitive technique for evaluation of thin films swelling under appropriate conditions. "In situ" ellipsometric measurements were performed to examine the swelling behaviour of the binary polyelectrolyte brush in variable

media quality, varying the ionic strength, the pH and the brush composition. The scheme in the Figure 8.1 gives a simplified view on the experiment. An ellipsometric cell with thin glass walls, fixed at a known angle (68^0) from the sample plane, was used. The angle of incidence of the light was settled such that its path was normal to the window.

It is noteworthy to mention the difficulties, concerning an independent estimation of swollen layer thickness, d_S, and n. Such a matter takes place when the thickness of a layer is below ca. 20 nm [Styr00]. The correlation between d_S and n at the solid/liquid interface means that both parameters cannot be independently determined with a high accuracy. Despite of that, we were able to measure their magnitude together, obtaining an inverse dependence between them, as it is shown in Figure 8.3.
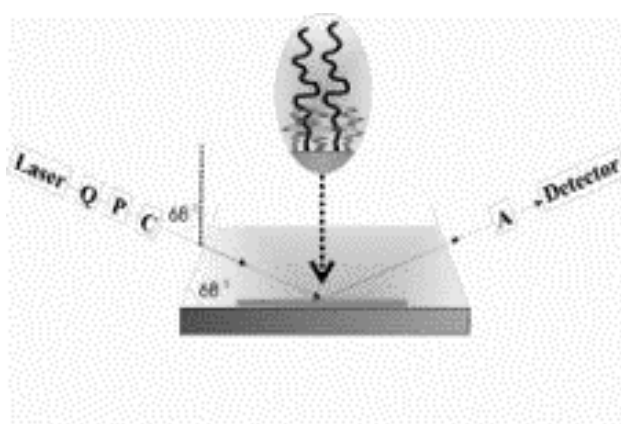

Figure 8.1. Schematic illustration of the "in situ" ellipsometric set-up for swelling phenomenon investigations. Q- $\lambda/4$ plates, P- polarizer, C- compensator, A- analyzer, Detector

8.4. Responsive/Switching Behavior.

8.4.1. Switching of the surface charge.

The binary polyelectrolyte brush is capable for a sharp switching of the surface charge upon change of the pH. The switching mechanism can be followed in Figure 8.2, where the binary, polyelectrolyte and amphiphilic brushes are studied by the electrokinetic method.
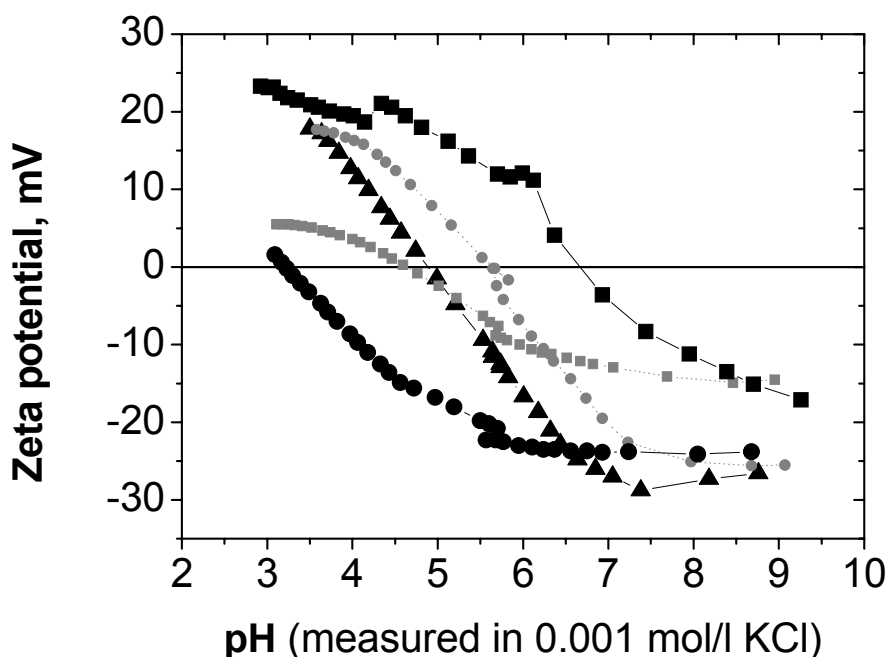
Figure 8.2. Zeta-potential plotted as a function of pH for: homopolymer P2VP brush (black squares), homopolymer PAA brush (black circles), mixed PAA-P2VP brush (black triangles).
As a comparative case, the electrokinetic behavior of the precursor system was studied as well: PBA (grey squares) and PBA-P2VP (grey circles).

Homopolymer P2VP and PAA brushes were measured as a reference. Isoelectric points at pH 6.7, 3.2, and 4.9 were determined for P2VP, PAA, and the binary polyelectrolyte P2VP-PAA brushes, respectively. The data demonstrate the switching ability of the binary brushes when the isoelectric point is located in between the values corresponding to each of homopolymer constituents. Small shift of pH away from the isoelectric point results in a sharp linear change of surface charge within an extended range of pH.

The surface charge changes are accompanied by a U-shaped change of the swollen film thickness, revealing an adaptive brush response (Figure 8.3). In this experiment, the thickness and the refractive index of the layer were obtained as dependent parameters from the fitting procedure.

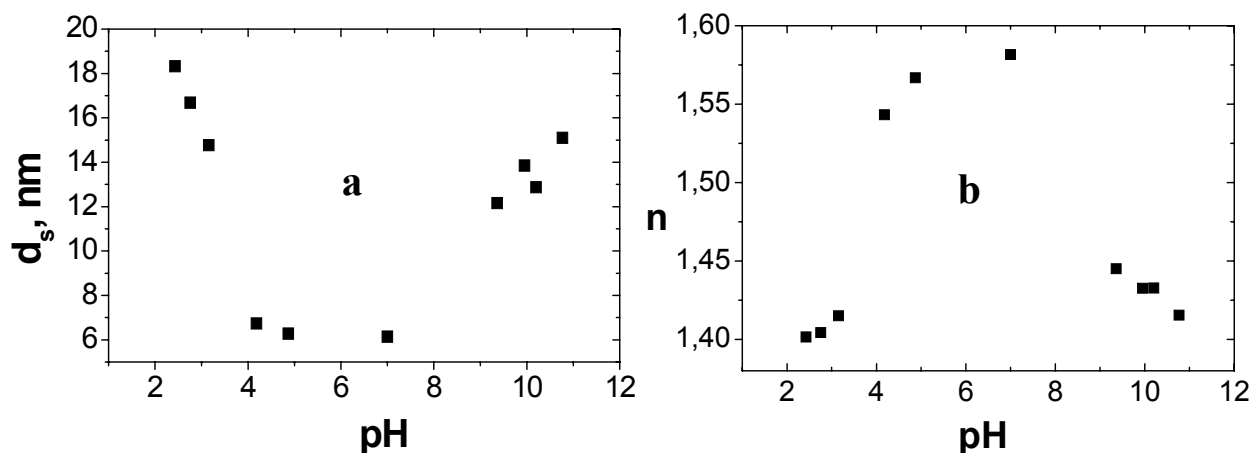**Figure 8.3.** Influence of the pH on the (a) swollen thickness, d_S, and (b) the refractive index, n, of the swollen PAA-P2VP brush. The thickness in dry state was measured to be 5.7 nm (Table 8.1).

The switching route for the binary polyelectrolyte brush is schematically shown in Figure 8.4. Each homopolymer in the mixed brush is a weak polyelectrolyte. The charge density of the weak polyelectrolytes depends on pH. At pH <6.7, P2VP is protonated, and a further decrease of pH results in an increase of density of positive charges at P2VP chains.
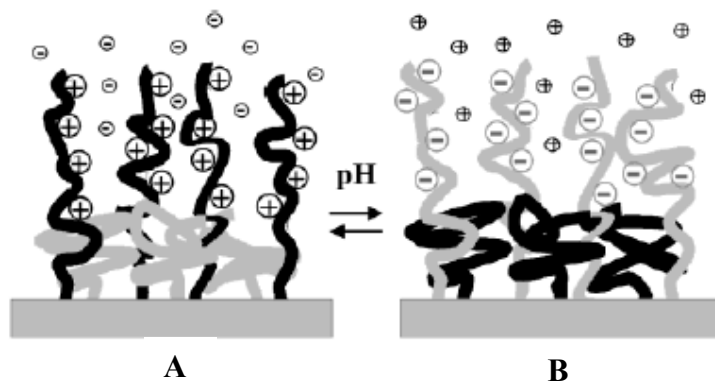
Figure 8.4. Schematic representation of switching behavior of a binary polyelectrolyte brush upon adjusting the pH below (A) and above its isoelectric point (B)

The inverse scenario may be assigned to PAA chains, which are negatively charged at pH > 3.2. In the range of 3.2 < pH < 6.7 the charged P2VP and PAA interact so that at pH 4.9 the charges are completely compensated, that results in a neutral surface. "In situ" thickness of the brush at the isoelectric point was ca.7 nm-close to the thickness of the dry film (Figure 8.3). Out of this region, at low pH, PAA chains adopt a compact conformation on the bottom of the film, while P2VP is highly protonated and stretched away from the surface. The thickness of the swollen brush measured at pH 2 was 18 nm; P2VP preferentially occupies the top of the film. At high pH value, the inverse transformation takes place. P2VP is collapsed to the surface, while negatively charged PAA chains are on the top, electrostatically expanded

by repulsion between dissociated carboxylic groups at the monomer units. The thickness of the swollen brush was 15 nm at pH 10. The binary polyelectrolyte brush allows approaching a much larger range of switching between values of surface charge (from negative to positive surface) as compared to the homopolymer brushes (Figure 8.2). The absolute values of zeta potential in acidic and basic pH regions for PAA-P2VP are close to the corresponding values for the P2VP homopolymer brush for acidic pH values and for the PAA homopolymer brush for basic pH values, respectively. That indicates the possibility to switch the surface composition of the brush via small change of pH, as the top layer is enriched with the charged polymer, while the uncharged one occupies the bottom layer. This possibility demonstrates the substantial difference of the binary polylelectrolyte brush from the mixed uncharged amphiphilic brush, investigated in the previous Chapter 7. In the latter case, the switching of the surface composition can be approached by a general change of the solvent [Min00a, Min00b], while the layered segregation of two different polymers in the binary polyelectrolyte brush can be easily approached by a small adjustment of the pH.

Such a behavior of the polyelectrolyte brush is promising for the precise regulation of adsorption/desorption processes of charged particles, cells, and protein molecules and controlled release or tuneable catalysis in aqueous environment.

8.4.2. Switching of the energetic state.

Further, we demonstrate how the pH signal may be used to switch the wetting behavior of polyelectrolyte brushes. At low and high pH values, protonated hydrophilic P2VP molecules or dissociated acrylic acid segments along the PAA chains, occupy the top of the sample, respectively. Therefore, the brush remains hydrophilic in the entire range of pH, except within the neutral part, where a compensation of the charges takes place. If the brush is rapidly removed from the solvent bath and dried, the lateral surface morphology of the film is assumed to be "frozen". Thus, we assume that the ratio between concentrations of different polymers in the top layer of the mixed brush is not much changed during fast collapse, when water is rapidly evaporated. The brush can be easily probed, using the contact angle method. Results of such experiments are presented in Figure 8.5c, as the same test was performed with single polyelectrolyte brushes for a reference (Figure 8.5a, b).
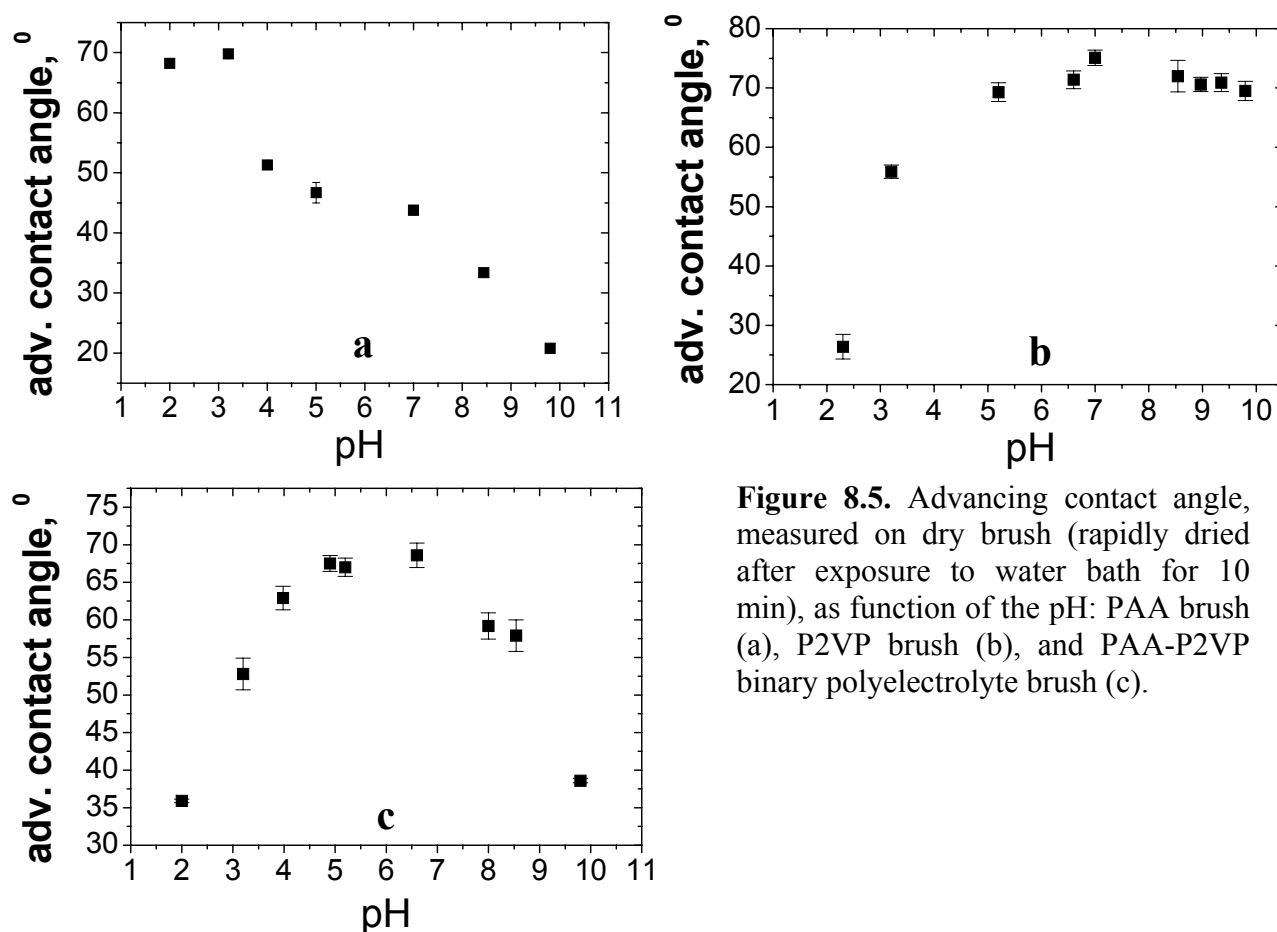
Figure 8.5. Advancing contact angle, measured on dry brush (rapidly dried after exposure to water bath for 10 min), as function of the pH: PAA brush (a), P2VP brush (b), and PAA-P2VP binary polyelectrolyte brush (c).

The wetting experiments confirmed that in acidic media, P2VP preferentially occupies the top of the substrate, while in basic media PAA replaces P2VP in the top layer. Despite different compositions and charge signs of the surface, the binary polyelectrolyte brush demonstrates very similar wetting behavior after acidic or basic treatment. Measured contact angles were 36° for pH 2 and of 39° for pH 10. In contrast, mono-PAA brush is hydrophilic at pH 10 and more hydrophobic at pH 2 (Figure 8.5a), while mono-P2VP brush demonstrates the inverse behavior (Figure 8.5b). The values measured for the binary polyelectrolyte brush in between the limiting points of the range 2<pH<10 represent the stepwise transition, showing more hydrophobic behavior near the IEP of the brush ($\Theta = 70°$). The reason for this performance was already explained in the terms of complexation between the oppositely charged polyelectrolyte chains. The step-like change in contact angle values deals with the weak polyelectrolyte behavior, originating from the dependence of degree of dissociation on the pH.

8.4.3. Ionic strength influence on the swelling of polyelectrolyte brushes.

The influence of the solution ionic strength onto the degree of swelling at different pHs was examined for binary and mono-component weak polyelectrolyte brushes. The monomer units at the polyelectrolytes bear weak acidic or basic groups, as only a fraction of their charge is compensated by condensed counterions. In this case, the degree of dissociation or association of ions at the polymer chain is controlled by the environmental pH. Furthermore, an addition of salt induces a collapse of the chains by screening intra- and inter- electrostatic interactions in the system, as the behavior of weak and strong polyelectrolyte brushes is qualitatively different [Zhu95, Lya95]. At high salt concentration, their response to the media is comparable, as both type of brushes shrink in a very similar way, while in low salted solutions one can observe considerable dissi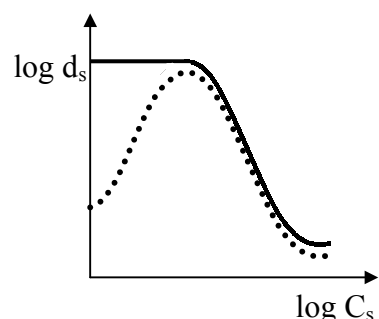milarities, originating from the unfixed degree of charge at the weak ones. Our experiments confirmed qualitatively the non-monotonic dependence between the weak brush swollen height and the external salt concentration, C_s, shown in Figure 8.6.

Fig. 8.6. Influence of the external salt concentration, Cs, on the swollen brush height, d_s: Weak (dashed line) and strong (solid line) polyelectrolyte brushes behavior.

The binary PAA-P2VP brush was examined at acidic, neutral and basic conditions as well as at its isoelectric point (Figure 8.7a). The reference cases of mono-component brushes are shown in plot 8.7b. The amount of added salt was increased step-wisely till a range of that it totally collapses the chains to the substrate. At both pHs- 2 and 10 (Figure 8.7a), the high ionization degree in salt free solution, i.e. high charge density of the P2VP or PAA, induces swelling of the brush due to inter- and intra-repulsive electrostatic forces, arising from the equal charged segments, and the osmotic pressure of the counter-ions. At low salt concentration and pHs 2 (protonated P2VP chains) and 10 (dissociated PAA monomer units) the swollen brush thickness reaches a maximum, which can be explained in terms of equalized concentrations of external salt and the free mobile counterions inside the brush. At these conditions, the brush is in so-called "osmotic regime", in which all counterions are trapped within the brush volume and stretch the chains via an osmotic effect. This process was predicted by Zhulina [Zhu95], Ross [Ross92] and Fleer [Fle93] to follow a $d_s \propto C_s^{1/3}$ power law. Beyond this salt concentration, a crossover occurs, and the osmotic pressure of the counterions decreases as the brush height decreases accordingly. For planar geometries, after the crossover, mean-field theories, as well as experimental studies [Bie02d], predict that, the brush height, d_s, follows a $d_s \propto C_s^{-1/3}$ law.

The scaling of the brush height with ionic strength in this study is in qualitative agreement with the theoretical predictions.

At C_s=0.001 M (the lowest salt concentration) and pHs 2 and 10, the brush remains in swollen state. If the concentration of added salt is increased, the brush height increases further. At salt concentrations of between 0.005 and 0.01 mol/L, one can observe maximums at both pHs. Over C_{NaCl}=0.01 mol/L the brush collapses ("salted regime") and reaches approximately its dry state height at C_{NaCl} between 0.1 and 0.5 mol/L.

At pH 4.9 (IEP) and pH 7, we found that PAA-P2VP brush effectively behaves as neutral.
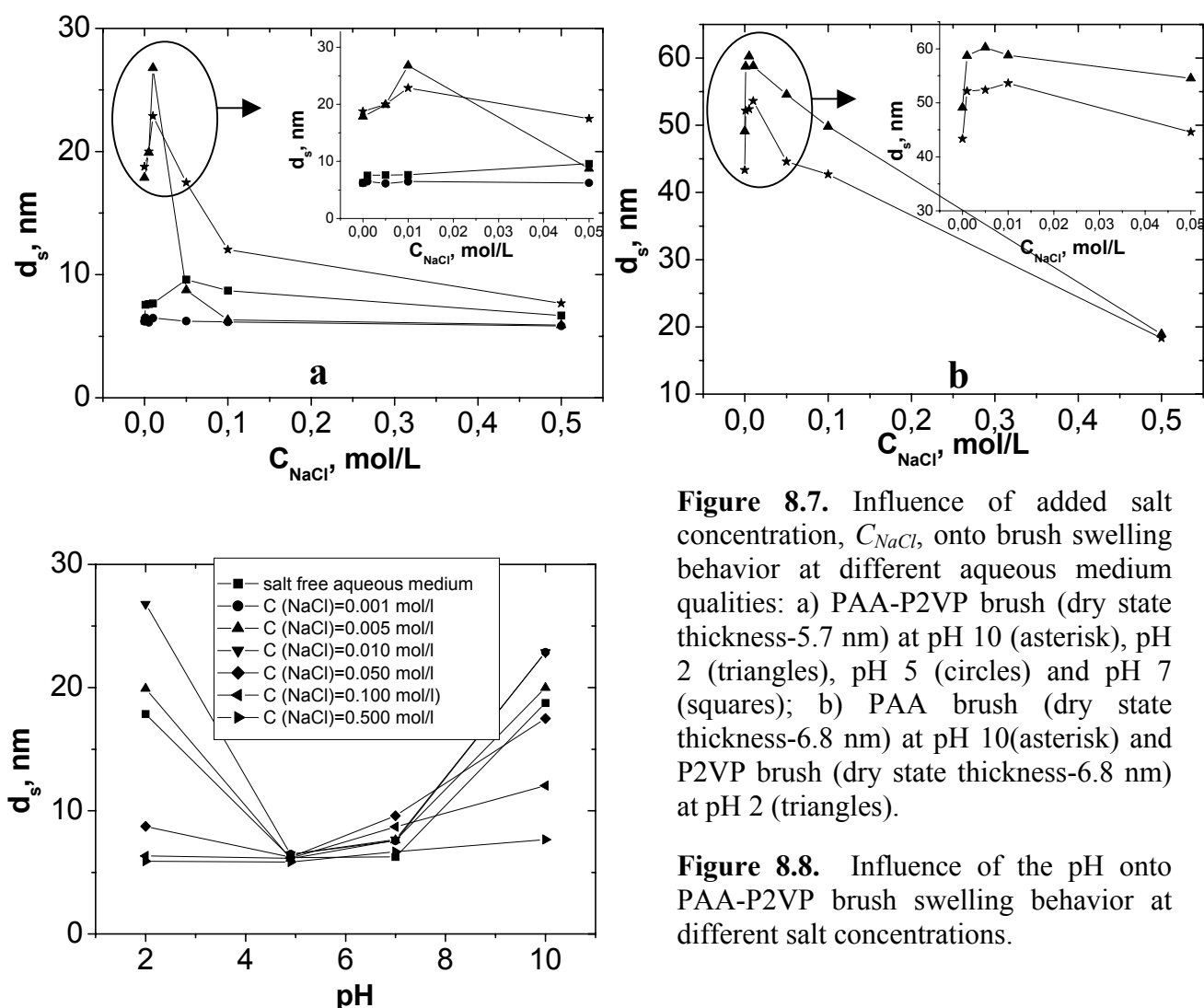
Figure 8.7. Influence of added salt concentration, C_{NaCl}, onto brush swelling behavior at different aqueous medium qualities: a) PAA-P2VP brush (dry state thickness-5.7 nm) at pH 10 (asterisk), pH 2 (triangles), pH 5 (circles) and pH 7 (squares); b) PAA brush (dry state thickness-6.8 nm) at pH 10(asterisk) and P2VP brush (dry state thickness-6.8 nm) at pH 2 (triangles).

Figure 8.8. Influence of the pH onto PAA-P2VP brush swelling behavior at different salt concentrations.

The complexation between PAA and P2VP via –COO⁻ and -NH⁺ reactive groups at the monomer units in sligthly acidic and neutral media, keeps the binary polyelectrolyte brush in colapsed state at any salt concentration, since the absence of binding ionic sites, and hence, reduced osmotic presure in the brush volume. In Figure 8.8 one can follow the thickness variations, affected by pH, at seven different ionic strengths.

The behavior of a homopolyacid (PAA) and homopolybase (P2VP) brushes in salt solution was examined separately. The tendency of continuous swelling at low salt content did not reverse, as it is shown in Figure 8.7b. In the initial swollen state, at pH 10, PAA reaches a height of ca. 43 nm-approximately six times of its dry state thickness. The swelling continues at C_{NaCl}=0.001, 0.005 and 0.01 mol/L, as the curve forms a plateau with a maximum value of 54 nm. The homo-polyelectrolyte base P2VP at pH 2 expresses a similar behavior. The primary swelling in salt-free media turns the brush height to ca. 49 nm. At C_{NaCl}=0.001-0.01 mol/L the swollen thickness reaches ca. 60 nm. Over this point (C_{NaCl}=0.01 mol/L) the chains adopted a collapsed conformation and the average thickness for both P2VP and PAA was measured to be 20 nm at C_{NaCl}=0.5 mol/L. These experiments provide a good agreement to the theoretical predictions discussed above.

8.4.4. Switching of surface morphology upon pH variance.

Morphologies of the mixed amphiphilic (precursor system) and polyelectrolyte brushes were investigated in variable points of interest and accomplished by AFM in air. The top layer structures differ significantly after exposure of the brushes to pH variable aqueous media.

As a reference, the morphologies of the precursor system (PBA-P2VP brush), treated at the same conditions as the polyelectrolyte binary PAA-P2VP brush, were measured (Figure 8.9). Before the conversion one can observe dominating toroidal structures with diameter of about 55 nm (pH 7) and 67 nm (pH 10) (discussed latter) and lamellar features (pH 4.9), originating from the incompatibility of both polymers and the quality of the media, which do not favors a swelling of neither components. At pH 2, the swollen P2VP chains cover the surface, while PBA remain collapsed to the substrate. After drying one can measure a smooth interconnected network.

Figure 8.9. 1X1 µm AFM images (left, topography-Z range 12 nm; right, phase) and corresponding cross-sections, representing morphology of mixed PBA-P2VP brush at: A) pH 2.0 (RMS 0.99 nm), B) pH 4.9 (RMS 2.17 nm) C) pH 7.0 (RMS 1.37 nm), D) pH 10 (RMS 1.70 nm).

Conversion of PBA to PAA within the binary brush composition reflects in prominent changes in respect to the size and shape of the features, detected on the surface, and showed in Figures 8.10 - 8.13.
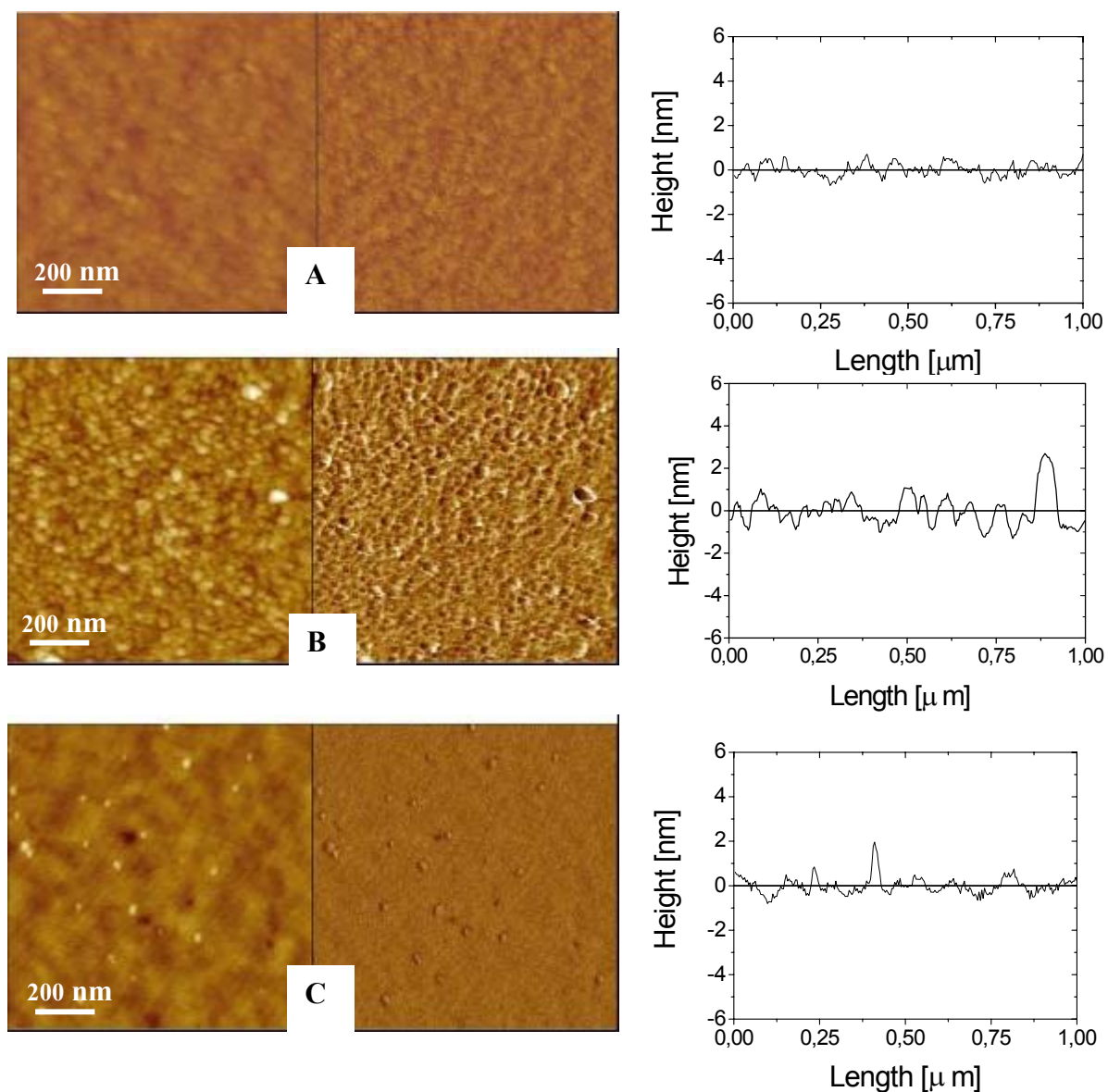
Figure 8.10. 1X1 μm AFM images (left, topography-Z range 12 nm; right, phase) and corresponding cross-sections, representing morphology of: A) PAA (RMS 0.21 nm), B) PAA-P2VP (RMS 0.58 nm) C) P2VP (RMS 0.33 nm) at **pH 2**.
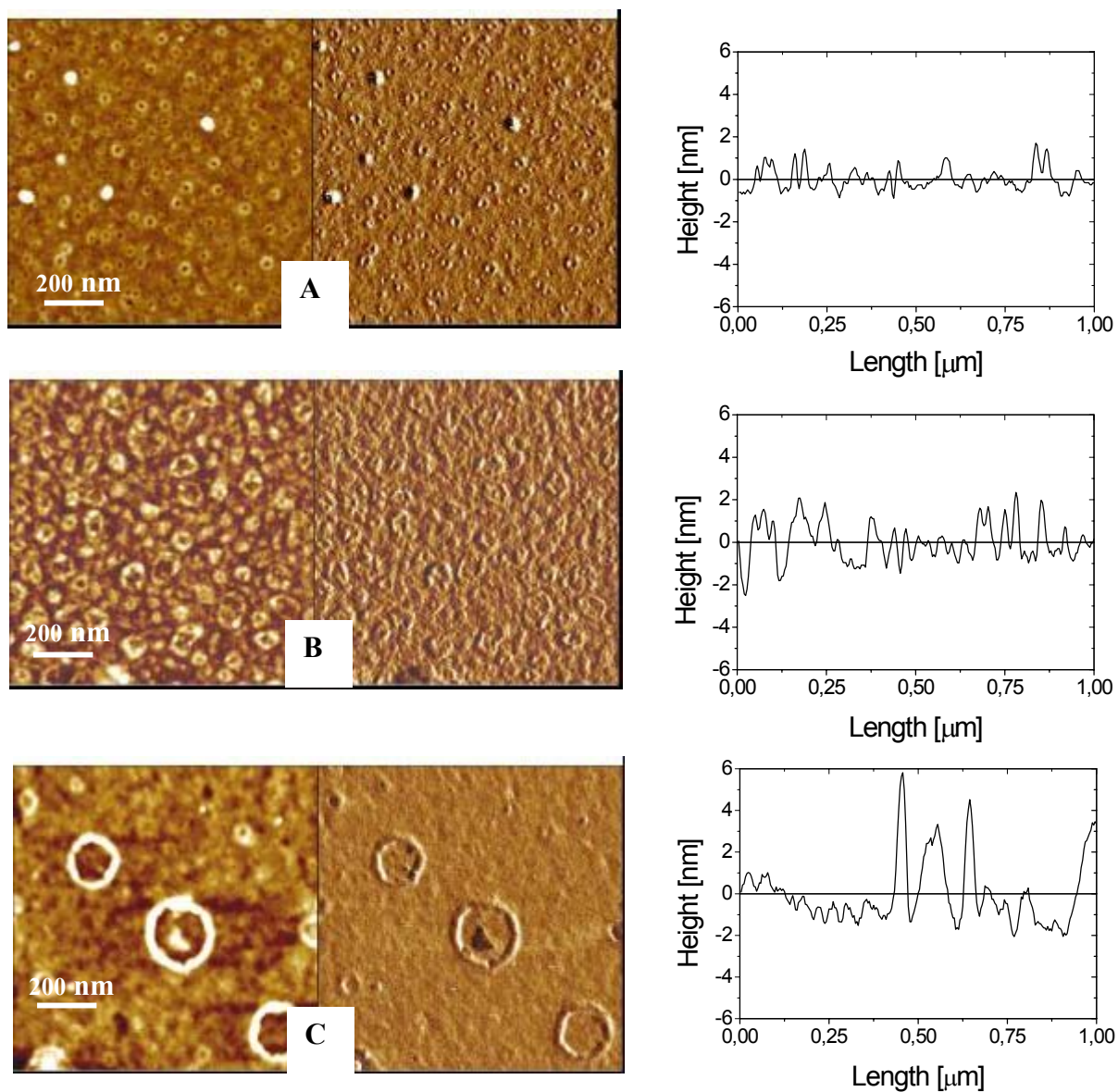
Figure 8.11. 1X1 µm AFM images (left, topography-Z range 12 nm; right, phase) and corresponding cross-sections, representing morphology of: A) PAA (RMS 0.61 nm), B) PAA-P2VP (RMS 0.92 nm) C) P2VP (RMS 1.18 nm) at **pH 4.9**.
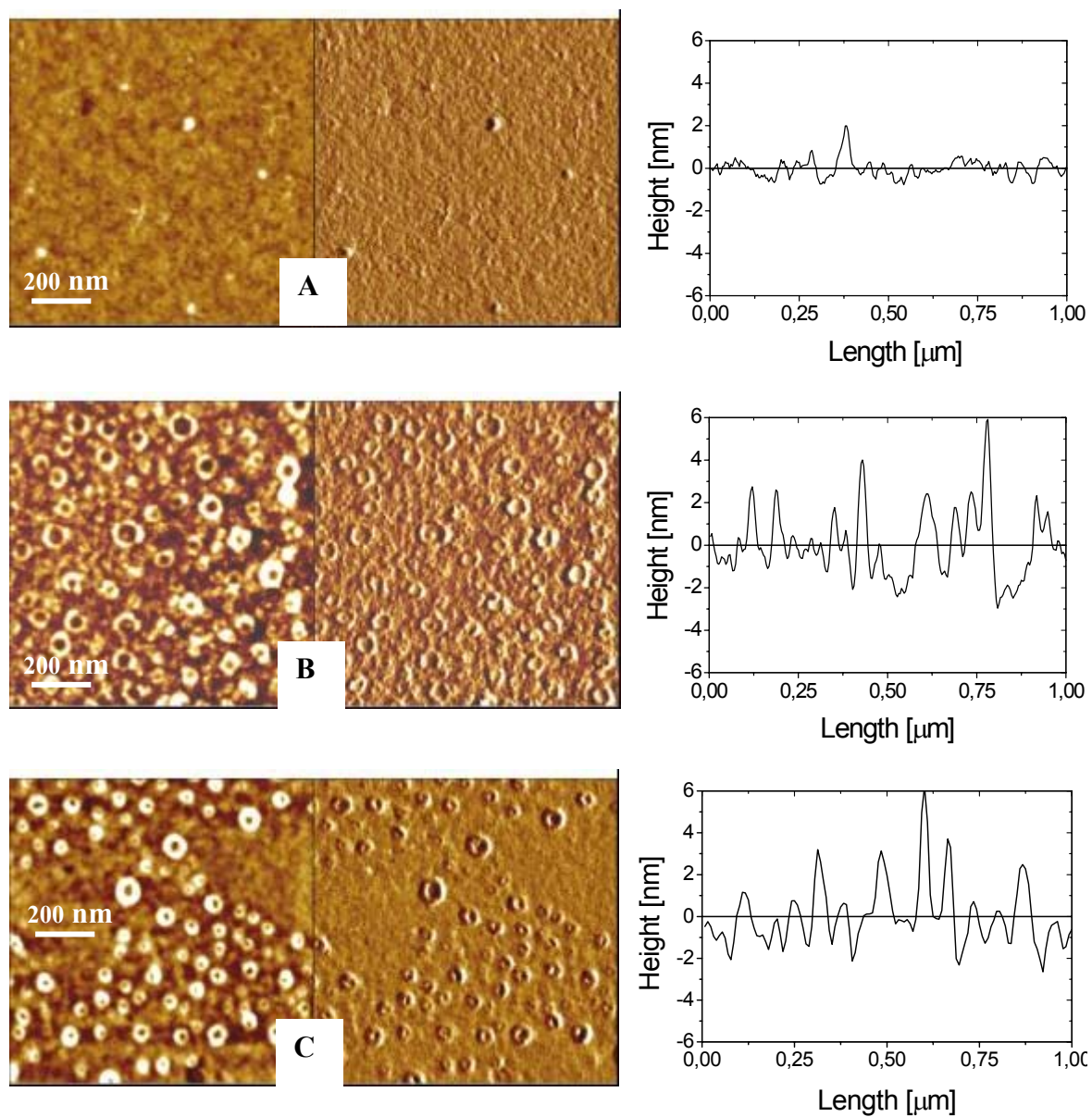
Figure 8.12. 1X1 μm AFM images (left, topography-Z range 12 nm; right, phase) and corresponding cross-sections, representing morphology of: A) PAA (RMS 0.43 nm), B) PAA-P2VP (RMS 1.30 nm) C) P2VP (RMS 1.54 nm) at **pH 7.0**.
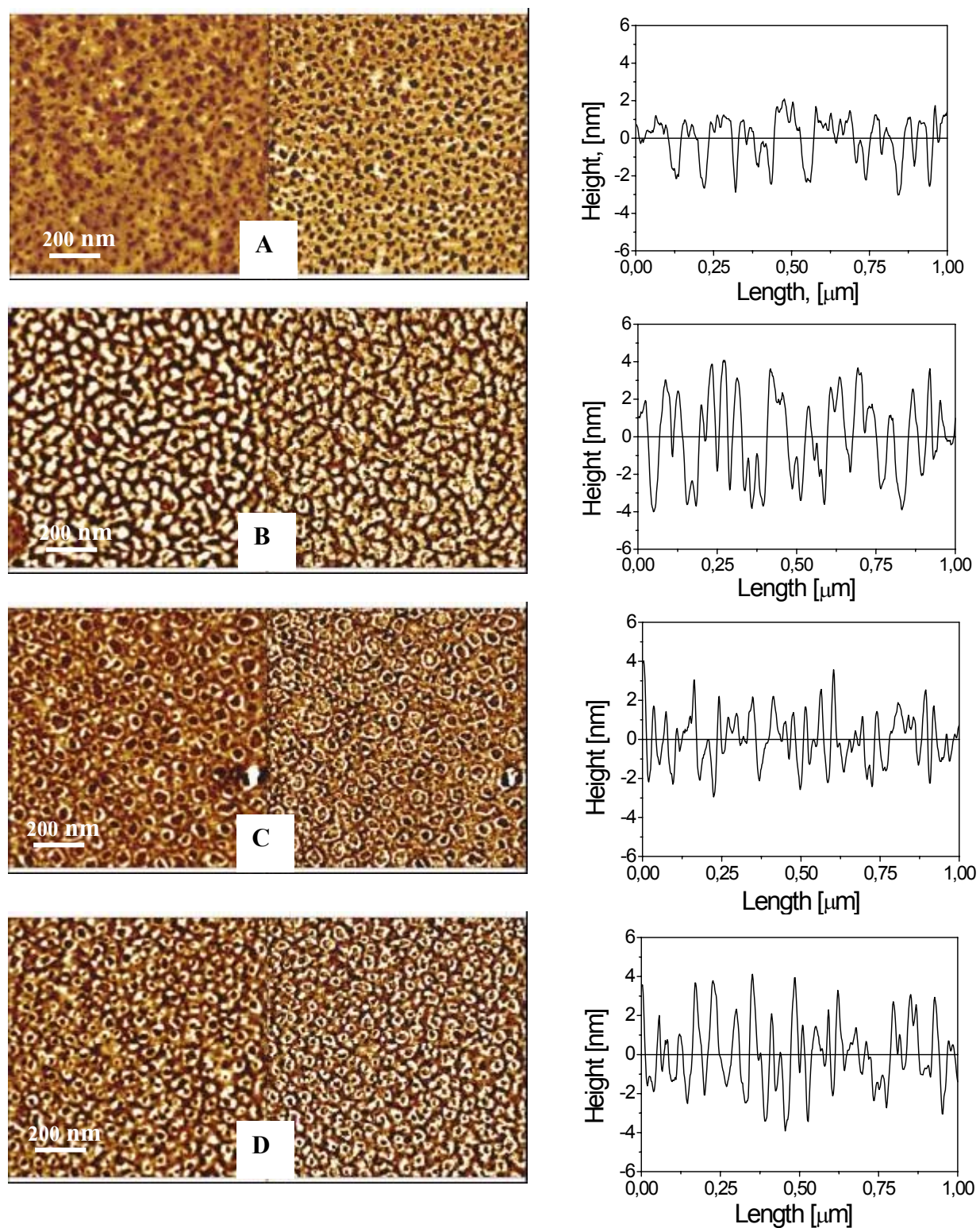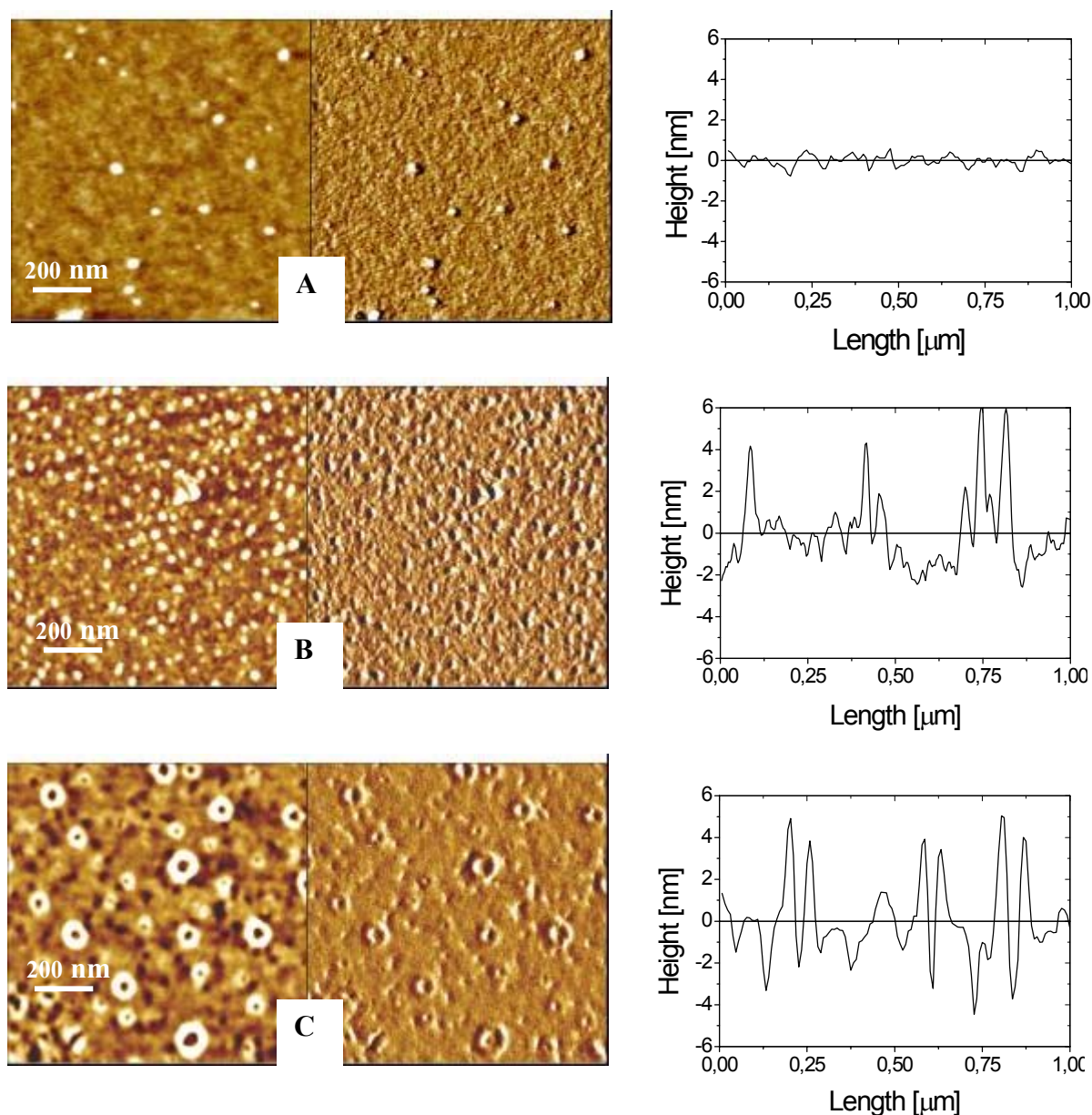
Figure 8.13. 1X1 μm AFM images (left, topography-Z range 12 nm; right, phase) and corresponding cross-sections, representing morphology of: A) PAA (RMS 0.21 nm), B) PAA-P2VP (RMS 0.58 nm) C) P2VP (RMS 0.33 nm) at **pH 10.0**.

The toroidal geometries, observed on the binary PAA-P2VP polyelectrolyte brush surface at pH 4.9 and 7 (diameters (evaluated between the tops of two peaks in the cross-sections) L ~ 45 and 59 nm respectively), required one to measure the referent morphologies of the constituents PAA and P2VP separately, in terms to identify their origin. It was clearly figured out, that the toroidal shaped surfaces originate mainly from the condensation of P2VP component (pH 4.9 - L ~ 190 nm; pH 7 - L varies between 23.5 and 55 nm), which collapses

to such structures even at pH 10 (L between 39 and 75 nm). For PAA only at pH 4.9 smaller, compared to P2VP brush, toroidal shapes of L ~ 25 nm were detected.

The origin of such surface geometry is not recently described enough accurately in the literature. A number of studies have attempted to cover the reasons of such features occurring in poor solvents for flexible and semi-flexible polymers [deGen85a, b, Daw97, Halp00, Schnu02]. However, attempts to explain the collapse from coil through globule to toroid were theoretically made [Schnu00, Sak02]. It is known, that when a flexible polymer is exposed to a poor solvent it passes by a collapse transition to a globular state, as it minimizes the contact with the solvent by decrease of surface area. It occurred, that for the investigated system, at specific conditions, the transition ends to submicron toroidal structures. The components in the polyelectrolyte brush, P2VP and PAA, are both relative flexible polymers (glass transition temperatures (Tg) are at 104 ^{0}C and 87 ^{0}C respectively), but far from fully flexible ones and require a higher energy to form a bend. The globular state is energetically unfavorable for them because it includes highly bent states. The collapsed ground state is then a toroid, benefiting a reduction of the monomer-solvent contact, excluding an additional bending penalty. Hence, the toroidal "state" acts for balance between a trend of the surface area to be minimized and the energetic penalty of bending the chains. An important limiting factor, contributing to such surface arrangement, one can find the volume-excluded regime, operating within the brush volume. The brush-like architecture of the polyelectrolyte layers provides a dense package of the polymer chains (dg~3 nm, grafting density~0.1 nm^{-2}) as well as an immobilization of one of the chain ends. Therein, one can apply this information, together with the assumptions above, to the specific behavior of weak polyelectrolytes in aqueous solutions. During drying of the samples, the slightly swollen P2VP chains (homopolymer brush), segregated from the fully collapsed ones at neutral and basic media, shrink rapidly (in the range of few seconds) back to the surface, excluding water molecules, already penetrated brush volume in the aqueous media. The surface capillary forces then imply a collapse of a number of assemblies of polymer chains, attached to a number of grafting sites, forming a concave structure in its virtual centre, which finally results in the surface toroidal shapes. Such structures were not observed for PAA in neutral and basic media, because the polyacid chains are substantially swollen in neutral and alkali water (IEP of PAA is at pH 3.2), and during the drying, form easily a homogeneous layer, shown in Figures 8.11a, 8.12a and 8.13a. In case of the binary PAA-P2VP polyelectrolyte brush, such geometry was detected only at pH 4.9 and 7. Referring to the homopolymer brushes morphology, observed at the same

conditions (see Figures 8.11 and 8.12), one could assume the same model, already applied for the P2VP brush, to explain the origin of the toroids on the samples surfaces.

Focusing on this approach, we explained the collapsed toroidal features, observed on the binary and mono-component polyelectrolyte brushes. We assume that this additional bending limitations as well as excluded volume effect at the brush contribute to the toroidal arrangement. Reduced electrostatic repulsion between the polyelectrolyte segments in neutral-basic aqueous media for the P2VP, and neutral for PAA-P2VP brushes, limits the supposition for toroidal formation to energetic factors such as bending, entropy loss and capillary interactions.

The AFM images measured after immersing the samples in a good solvent for one of the components show segregated clusters with PAA on the top at pH 10 and P2VP top layer phase at pH 2. In a good solvent for either component (relatively strong acidic or basic medium), the surface is enriched with protonated P2VP or dissociated PAA. The electrostatic repulsion between the likely charged segments and the osmotic pressure of the counterions expand the brush up to 7 times of its dry state thickness (in respect only to the component which undergoes elongation, not to the total brush thickness, as it is shown in Figure 8.7). In those cases a mono phase dominates on the surfaces and the contact angles values indicates highly hydrophilic properties (35.9^0 for pH 2 and 38.6^0 for pH 10). As result, the surface follows a typical clustered morphology, shown in Figures 8.10b and 8.13b.

8.5. Conclusions.

In conclusion, we synthesized binary polyelectrolyte brush from two oppositely charged weak polyelectrolytes via the "grafting to" approach. The novel material in such architecture was fabricated for first time. The adaptive behavior of the PAA-P2VP binary polyelectrolyte brush was investigated by tuning its acid-base properties. The polyelectrolyte brush demonstrates sharp switching behavior when the top of brush is occupied by negatively charged and stretched away from the substrate PAA or by positively charged stretched P2VP chains at pH values below and above of the isoelectric point, respectively. At the isoelectric point the brush forms a collapsed polyelectrolyte complex with zero charge.

The influence of a mono-valent salt was examined, covering 10^{-3}-5.10^{-1} M concentration range of NaCl in the solution and at pHs between 2 and 10. At acidic and basic medium the effect of added salt was more distinguishable, concerning higher initial swollen state of the brush. The decrease in thickness with the amount of added salt was found to be not

monotonic. A maximum occurs by the binary polyelectrolyte brush at low salt concentration at pH 2 and 10. An increase of the amount of NaCl induces almost fully collapsed conformation, caused by the balance of polyelectrolyte charge and increased ionic strength of the solution.

Different morphologies, generated by solvent quality variation were detected on the PAA-P2VP, PAA and P2VP brush surfaces. In a good solvent medium (acidic for P2VP and PAA-P2VP and basic for PAA and PAA-P2VP) cluster-like structures and layered mono-phase, originating from preferential occupation of the surface by PAA or P2VP (in case of the binary brush), were measured.

Decreasing the solvent quality for PAA-P2VP brush (neutral and IEP-pH 4.9), toroidal structures rising from the tendency of the polymer to exclude the solvent molecules and that way to minimize the surface area on one hand, and to decrease the energetic costs for bending on the other, were observed. Additionally, reference experiments were performed onto the mono PAA and P2VP brushes. They confirmed the trend toroids to be formed in poor solvents on polyelectrolyte surface.

The responsive/switching behavior of the polyelectrolyte brush can be explored to tune surface properties in aqueous environment by pH signal, which is of potential interest for microfluidic technologies, smart nanodevices, and drug delivery systems.

Chapter 9

Adsorption of Charged Nanoparticles onto Thin Polyelectrolyte Brushes Composed of Oppositely Charged Polymers.

9.1. Abstract. The unique properties of a binary polyelectrolyte brush [Bie99, Shu01a, Shu01b] were investigated by adsorption of charged nanoparticles from aqueous solutions.

Modifying the substrate with ultra-thin polyelectrolyte layers in brush-like configuration allows one to suppress or improve the adsorption of colloidal particles by changing the media quality and the composition of the brush.

Mixed amphiphilic polymer brush, consisted of an electrically neutral homopolymer such as poly(tert-butyl acrylate) (PBA) and a polyelectrolyte-poly(2-vinyl pyridine) (P2VP), was synthesized, using "grafting to" technique and converted to a binary polyelectrolyte brush with oppositely charged weak polyelectrolytes, polyacrylic acid- poly(2-vinyl pyridine) (PAA-P2VP).

Polystyrene latex particles, D =15 nm, with sufonic acid groups -SO_3H (negative Zeta potential) and quaternary amino groups -NR_3^+ (positive Zeta potential) functionalized surfaces, were adsorbed onto the PAA-P2VP polyelectrolyte brush at varied pH of the aqueous media. The functionalities of the adsorbate (the particles) have properties of strong electrolytes, i.e., their charge densities are independent on the pH. Therefore, one can adjust the surface charge of the binary brush, without affecting the adsorbate behavior, and in this way, easily to tune the adsorption only by switching the surface domination at the brush top layer.

Strong particles adsorption was detected at pH values, where the fraction of the charged units along the polymeric chain dominates over the number of their uncharged counterparts, and the colloidal particles bear an opposite charge to the polyelectrolyte brush surface.

9.2. Introduction. The behavior of polymers at interfaces and the interactions with the surrounding media is of importance for a large number of processes in industry and biomedical science [Fle93]. Particularly, the polymers grafted by one end to the substrate at high grafting density could play a significant role by modifying the adsorption properties of various substrates in contact with a heterogeneous environment [Cag01, Sof98]. Adsorption of nano-objects (proteins, synthetic polyelectrolytes, nanoparticles etc.) from aqueous media

attracts increasingly interest of many research groups [Hal99, McPher98, Jeo91a, Jeo92b]. Regarding well defined features of the polymer brushes [Min01, Min02a, Min02b, Sid99], one could vary the surface properties of the brush-like layer, and hence, to direct the adsorption processes to an aimed direction, altering the pH signal.

9.3. Experimental. Polystyrene latex particles, D =15 nm, with SO_3H (PS- SO_3H, negative Zeta potential, –50 mV) and NR_3^+ (PS-NR_3^+, positive Zeta potential, + 30mV) functionalized surfaces were purchased from Micromod Partikeltechnologie GmbH, Rostock-Warnemuende, Germany. The initial concentration of 10 mg/ml was reduced by factor of 50, to reach a final concentration of 0.2 mg/ml, used in our experiments.

We prepared the mixed polyelectrolyte brushes by "grafting to" approach using esterification reaction between carboxyl terminated polymers in thin melted film deposited on the substrate surface modified with epoxy groups and further performed acid catalyzed ester hydrolysis of the tert-butyl ester groups at PBA in benzene saturated p-toluensufonic acid monohydrate solution at 55 ^{0}C [Brue97, Hou03]. The entire procedure is described in Chapters 6 and 8 as well. Resumed, our route comprises four key steps: (1) chemisorption of (3-glycidoxypropyl) trimethoxy silane (GPS) on the surface of Si-wafer, (2) grafting of carboxyl terminated PBA-COOH, (3) grafting of carboxyl terminated P2VP-COOH and (4) hydrolysis of PBA, yielding polyacrylic acid (PAA).

The total grafted amount of the brush, obtained by this procedure and used in our adsorption experiments, was A_{total}= A_{PBA}+A_{P2VP}=3.7 mg/m^2+3.5 mg/m^2= 7.2 mg/m^2 (6.5 nm thickness).

9.4. Results and Discussion. The adsorption of PS latex particles was explored in the pH range between 2 an 10, adjusting the values by 0.1 N NaOH or HCl. No salt was used, i.e. the overall ionic strength was $\sim 10^{-pH}$. The preferable adsorption conditions were outlined, varying pH, particles type and brush surface composition.

9.4.1. Adsorption of negatively charged nano-particles. As first step, particles with negative charge were adsorbed onto PAA-P2VP. Referent adsorption cases for PAA and P2VP homopolymer brushes will be discussed later.

Figure 9.1 shows kinetic experiments performed "in situ", using a special designed ellipsometric set-up, described in Chapter 8 (Figure 8.1). The angle of incidence of the light was set to 68^0. The ellipsometric cell was properly cleaned and dried after every measurement session. The left plot represents the changes in ellipsometric angles ψ and Δ with time, while

the right one- calculated from the angles "in situ" thickness, ds, of the adsorbed particles layer. Region I shows the brush swelling before adding the particles, while the region II illustrates the progress in the adsorption of the particles from the 0.20 mg/ml stirred solution.
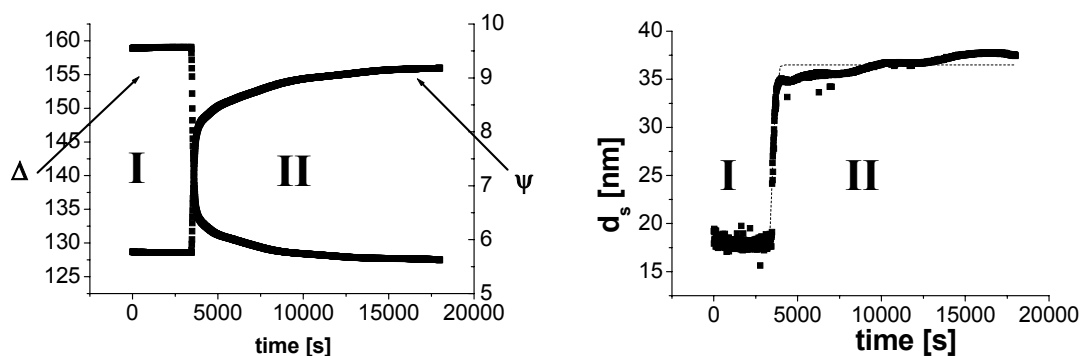
Figure 9.1. In situ measured adsorption kinetics of PS-SO$_3$H nanoparticles, adsorbing onto PAA-P2VP brush at pH 3; I-brush swelling: II-nanoparticles adsorption.

In Figure 9.2, we show the changes in the adsorbed layer thickness in dry state, upon varying the pH between 2 and 10. The reference case of the homopolymer components, composing the binary brush is shown as well.
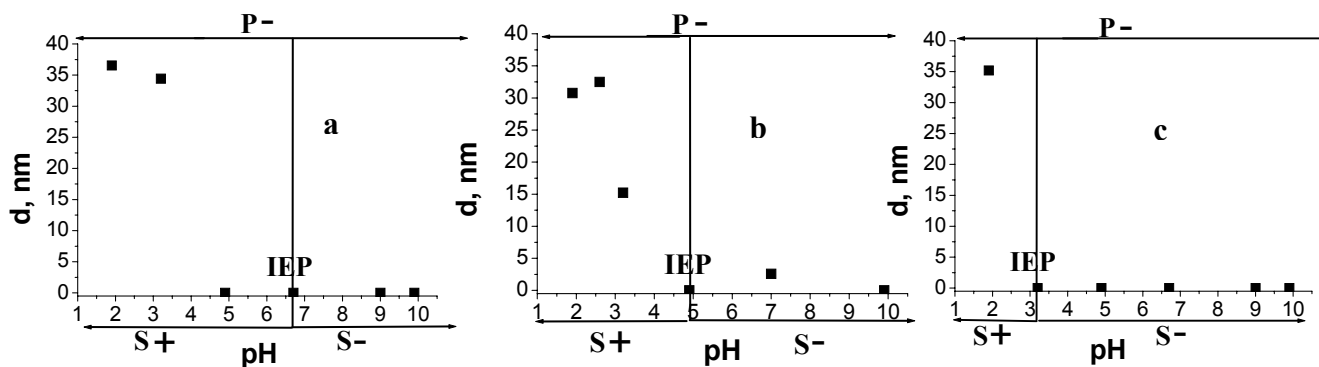
Figure 9.2. Dry state layer thickness, d, vs. pH plot of PS-SO$_3$H nanoparticles, adsorbed onto: a) P2VP, b) PAA-P2VP and c) PAA brushes. The arrows under and over the plots indicate the charge of the substrate-S and the particles- P, respectively.

As one can expect, the favorable conditions for adsorption occur below the IEP of PAA-P2VP brush (at pH 4.9). A nearly linear increase of the layer thickness was observed, which we devote to the increase of positive charges fraction along the extended P2VP chains, caused by the protonation of the N atoms at the pyridine rings. It results in appearance of positive charges on the surface, attracting the negatively charged PS-SO$_3$H particles. The value of Zeta

potential at pH 3 for the brush is ca. +20 mV (Chapter 8, Figure 8.2) and the particles potential is equal to –50 mV. By this pH the thickness of the adsorbed layer reaches 30 nm. This value is two times higher than the particles diameter. We commit this result to the grafting density (is $\sigma = 0.09$ nm^{-2}) of the brush and the differences in the electrical charges of the components. Among the different brush regimes, a value of 0.09 nm^{-2} correlates with an intermediate grafting density. The steric interactions within the brush plane at such conditions are minimized and the osmotic pressure decreases as well (comparing to a high grafting density, where the mentioned effect is in an opposite direction). The attractive force between the brush and the nanoparticles is balanced by the steric interactions, when the particles reach the inner part of the brush, i.e. the particles are not excluded from the intrinsic brush plane. This regime may allow to an increase of the effective adsorption sites, available for the particles, approached the surface. At higher grafting density, the particles may be positioned only on the upper part, because the attractive forces do not compensate the steric interactions within the inner brush volume.

By softening the media conditions to pHs 4.9-7, the adsorption tends to adopt zero value. This region complies with non-charged state of the polyelectrolyte brush, arising from the compensation of the opposite electrical charges at P2VP and PAA. Therefore, the overall surface charge becomes zero and the electrostatic interactions do not operate in. Studying the system in an alkali media, we did not detect a prominent adsorption process. Under basic conditions, the surface obtains negative charge, devoted to the carboxylic groups dissociation along the PAA chains. This results in electrostatic repulsion between the equally charged substrate and particles.

These findings, obtained by null ellipsometry in dry and liquid state, find their confirmation in the interpretation of AFM experiments in dried state.

Figure 9.3 shows several adsorption regimes from a favorable (acidic media) through an intermediate (neutral media) to a poor adsorption regime (basic media). The left parts of the images are denoted as height, while the right ones as phase. The cuts on the right side were obtained after cross-section analysis of the height images.

In image a) the particles can be easily recognized on the surface, by their circular shape and size. Measured by the ellipsometry overlapping of particles is well seen in the height image (Figure 9.3a). The increase in the layer thickness -about 30 nm, is believed to be due to localized aggregation mostly from overlapped particles, forming no uniform domains.

On images b) and c) the morphology is typical for a polymer brush at these conditions (lamellas and clusters) and shows an absence of nanoparticles on the top polymer layer.

The cross section analysis of height images b) and c) differ significantly from that one of image a), and prove the lack of adsorption under the conditions, applied to the system (see also Figure 9.2b).
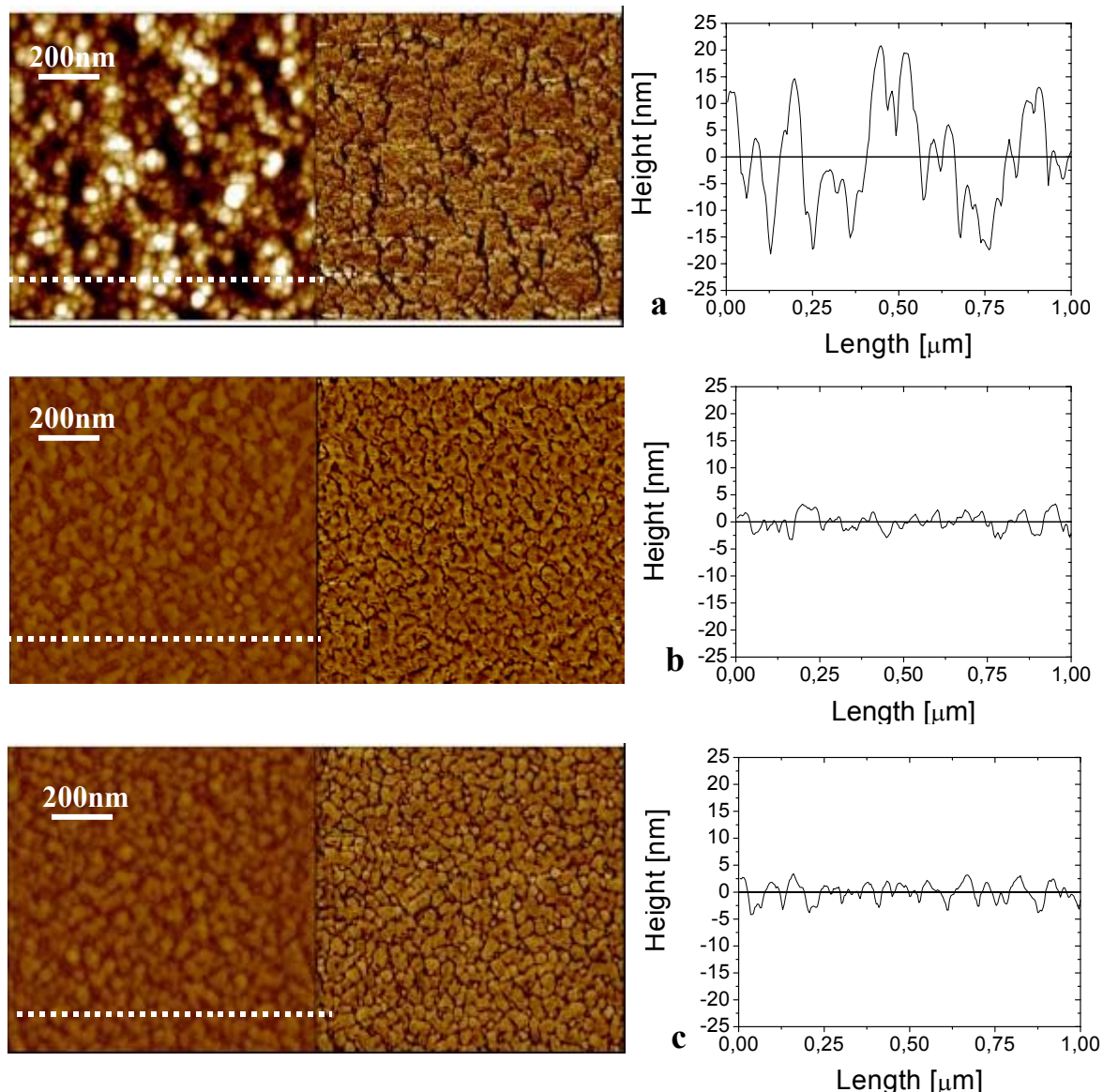
Figure 9.3. 1X1 μm AFM (left, topography, Z range=50nm; right, phase) images and corresponding cross-sections of PAA-P2VP brush after adsorption of PS-SO$_3$H particles at: a) pH 2.5 (favorable conditions); RMS 8.56 nm, b) pH 4.9 (unfavorable conditions); RMS 1.57 nm c) pH 9.8 (unfavorable conditions) RMS 1.72 nm.

9.4.2. Adsorption of positively charged nanoparticles. Continuing to study charged particles-binary polyelectrolyte brush interactions, we have exchange the sulfonic acid groups (−SO$_3$H) modified particles with quaternary amino groups (-NR$_3^+$) functionalized ones.

In this case, the surface and the particles may carry opposite charges only in the basic part of the pH scale and are supposed to interact via attractive electrostatic forces. In fact, there

occurred some deviations from the expected behavior of the system, but in general the trends were kept in the limits of our predictions. The ellipsometric results are shown in Figures 9.4 and 9.5.
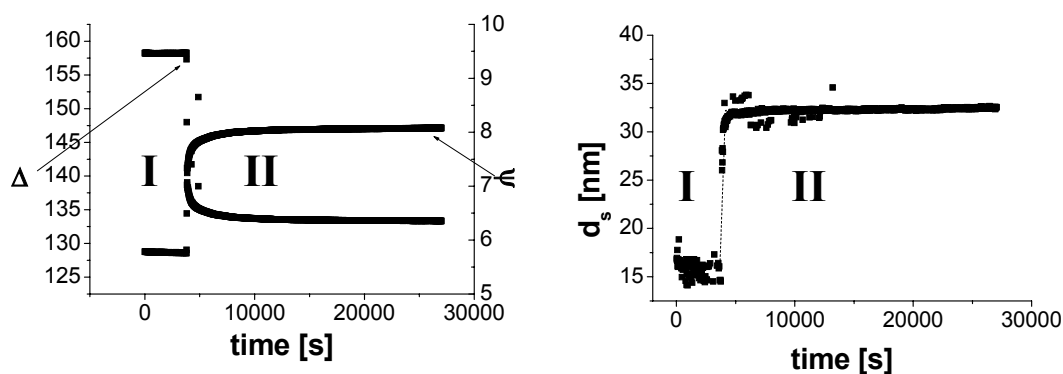
Figure 9.4. In situ measured adsorption kinetics of PS-NR$_3^+$ nanoparticles, adsorbing onto PAA-P2VP brush at pH 9.8; I-brush swelling: II-nanoparticles adsorption

The influence of pH on the adsorption strength is presented in Figure 9.5. In the acidic region, a weak adsorption was measured up to layer thickness 3 nm. The most interesting result in this system was the adsorption at the IEP point of the brush. About 7 nm thick layer of particles was measured at pH 4.9, where no electrostatic forces were expected to take part in the process. In this case, a contribution of hydrophobic interactions can be clarified.
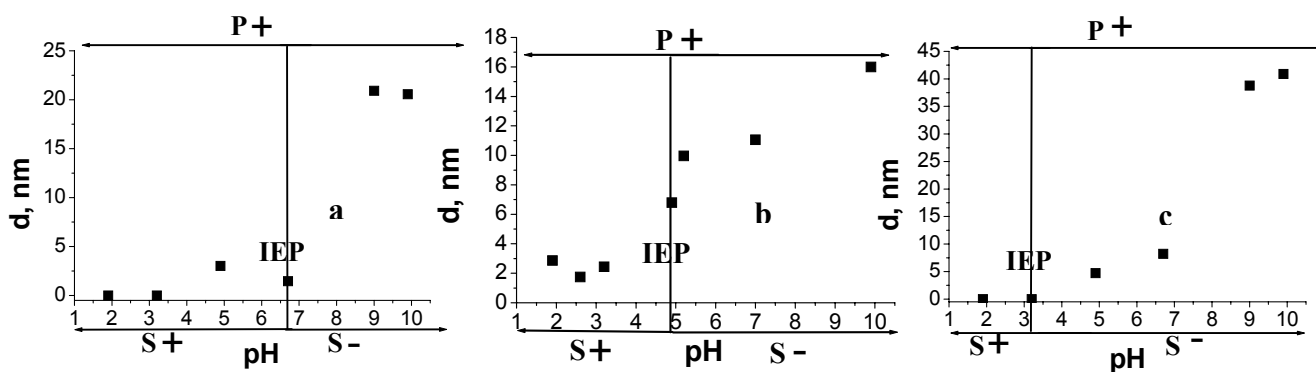
Figure 9.5. Dry state layer thickness, d, vs. pH plot of PS-NR$_3^+$ nanoparticles adsorbed onto a) P2VP, b) PAA-P2VP and c) PAA brushes. The arrows under and over the plot indicate the charge of the substrate-S and the particles- P, respectively.

The alkyl groups functionalities and the PS surface of the PS-NR$_3^+$ particles may interact with the hydrocarbon part of the PAA-P2VP brush chains, which results in such an anomalous,

from electrostatic point of view, adsorption. Another contribution may come from the charge inhomogenity along the brush chains, typical for weak polyelectrolytes. A pronounced charge accumulation appears at chain ends because there are fewer neighbors for the charges to interact with and the penalty in energy is therefore reduced. For end-grafted weak polyelectrolytes, a rather unusual regime can be obtained mainly due to the fact that the net charge of a chain as well as its distribution along the chain is not fixed but depends on its local environment.

Continuing to alkalize the media, the adsorption strength increases linearly up to pH 10 (the end point of our interest). In basic conditions, the carboxylic groups at PAA become dissociated, the brush adopts extended conformation and the surface turns to negatively charged. Hence, in the system a negatively charged component (the substrate surface) and a positively charged one (PS-NR$_3^+$ particles) are presented, which explains the linear increase of the adsorbed layer thickness. The maximum layer thickness is in the range of the particle diameter, i.e. ~15 nm. The difference with the adsorption of (-SO$_3$H) functionalized particles is obvious with respect to an absence of overlapping particles effect. We can assume that the equal absolute Zeta potential values of the brush surface (Chapter 8, Figure 8.2) and the particles, -30 and +30 mV respectively, may contribute to a compensation of the electrostatic charges at the adsorbing interface, which may prevent a double layer formation..

AFM investigations (Figure 9.6) give an additional illustration of these findings. On image a) one can observe circular shaped particles adsorbed on the surface. An overlapping regime cannot be detected on the image and on the cross-section graphic as well. At pH 4.9 (image b), the surface is uncharged, but some randomly distributed particles were detected on it. Image c) corresponds to pH 2.6 and a clear brush morphology was measured. As it was expected and found by ellipsometry, the acidic conditions do not favour adsorption in the system. The presence only of very low number of particles on the surface can be seen on the cross-section plot.
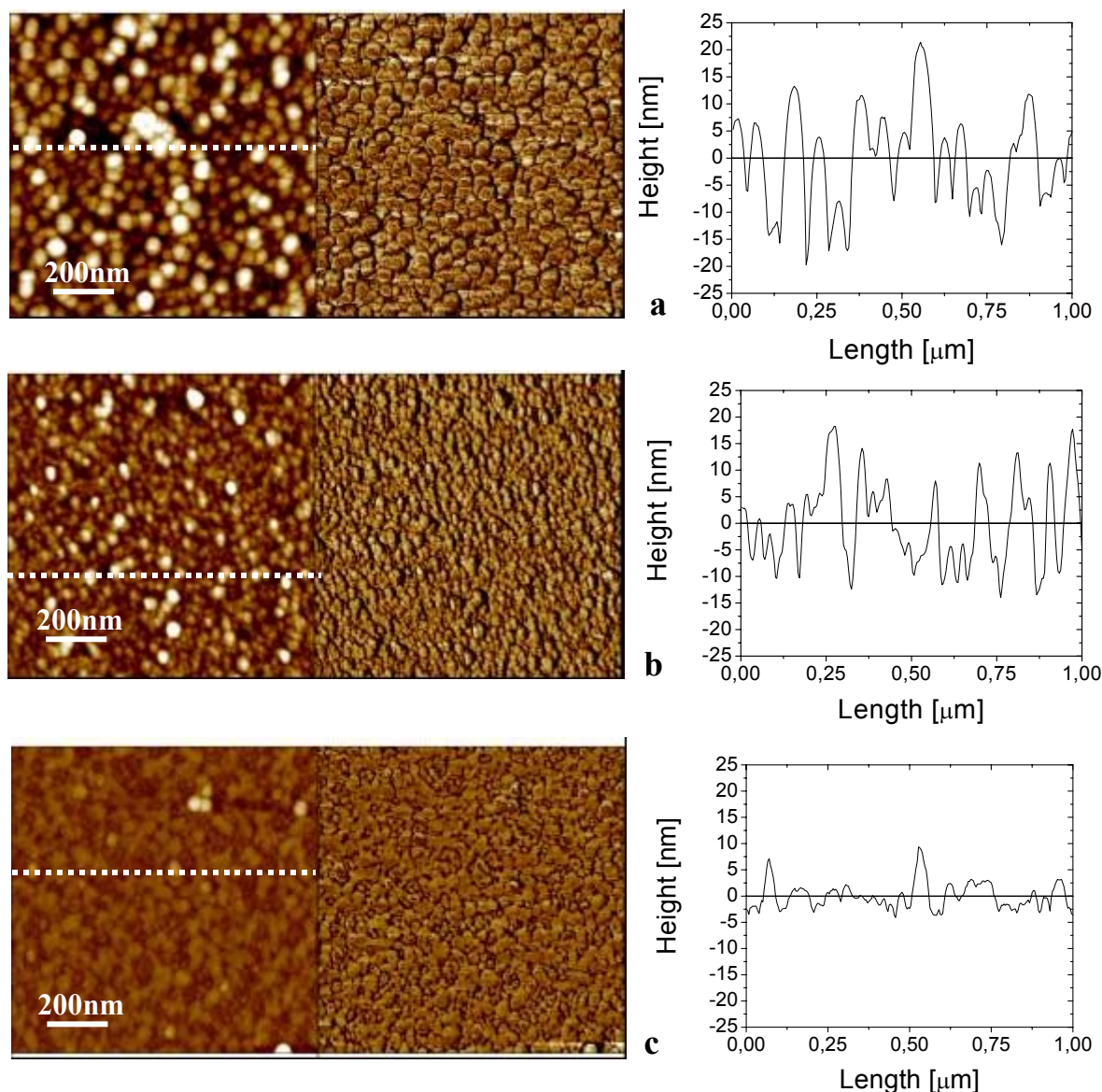
Figure 9.6. 1X1 μm AFM (left, topography, Z range = 50 nm; right, phase) images and corresponding cross-sections of PAA-P2VP brush after adsorption of PS-NR$_3^+$ particles at: a) pH 9.8 (favorable conditions); RMS 7.90 nm, b) pH 4.9 (unfavorable conditions); RMS 6.30 nm, c) pH 2.6 (unfavorable conditions); RMS 2.11 nm.

9.5. Conclusions. In the present study we have examined the adsorption of electrically charged nanoparticles onto binary polyelectrolyte brushes. The interactions within the system were controlled by pH adjusment, resulted in composition and surface charge replacement. The favourable conditions were outlined and the contribution of the different forces, driving the adsorption, were clarified. The pH responsible switching of the polyelectrolyte brush caused by preferential protonation of P2VP chains (acidic medium) and dissociation of PAA (basic medium), extends the brush in the adsorbing interface and facilitates the interaction

with the particles, i.e. the number of adsorption sites increases by swelling of the polyelectrolyte chains in the solution, and the particles can penetrate into the inner part of the swollen layer.

The adsorption strength increases significantly in that part of the pH scale, where the surface and the particles bear an opposite charge, i.e. the electrostatic interactions were classified as the main driving force for adsorption in the system. The contribution of hydrophobic contacts between the PS particles surface and the polyelectrolyte backbone, concerning an adsorption near IEP of the PAA-P2VP brush (PS-NR$_3^+$ particles) were taken into account as well.

Chapter 10

Regulation of Polyampholyte Adsorption by Responsive Binary Polymer Brushes

10.1. Abstract. In this chapter we are focusing on the effect, occurring by manipulation of "smart" responsive layers, tethered by one end to a planar solid surface, on the self assembly of polyampholyte molecules. Such system is more complex than that discussed in the previous Chapter 9, since the net charge of the polyampholyte molecules can be changed by varying the pH.

The adsorption of the ampholytic diblock copolymer poly(methacrylic acid)-block-poly((dimethylamino)ethylmethylacrylate) (PMAA-b-PDMAEMA) was investigated from salt-containing aqueous solutions onto heterogeneous surfaces with tuneable properties, as amphiphilic and binary polyelectrolyte brushes. The first type is composed of a neutral polymer- polystyrene (PS) and a polyelectrolyte-poly(2-vinylpyridine (P2VP), while the second type consists of two oppositely charged polyelectrolytes- polyacrylic acid (PAA) and P2VP. The amphiphilic polymer brush, PS-P2VP, provides hydrophilic-hydrophobic shift of the surface properties, while at the binary polyelectrolyte brush one can switch the surface charge via preferential swelling of one of the components.

To explore effectively the entire adsorbent-adsorbate interaction spectrum, we caused dissimilarity between the non-charged states of the adsorbing surface and the polyampholyte. The asymmetric block ratio (19:81) at the PMAA-b-PDMAEMA, results in different isoelectric points (IEPs) of the adsorbent and the adsorbate, placed far from each other on the pH scale. Subsequently, the adsorbed amount and surface morphology of the adsorbed polyampholyte were monitored as a function of pH, at constant ionic strength and concentration. Increasing pH, the adsorbed amount increases, and close to the non-charged polyampholyte state-its IEP, it diverges to very large values, tending to form micelles. Measured dependencies were explained by the adsorption of one or the other of the two blocks, strongly depending on the behaviour of the underlying tethered polymer layers, tuneable by the acid/base properties of the medium.

10.2. Introduction.

Polyampholytes are polymers which contain both, positively and negatively, charged monomers. A weak polyampholyte is one, where the overall charge can be adjusted by varying external conditions, usually the pH. The ability of polyampholytes to associate with various substances as well as their adsorption behaviour has been studied intensively during last years [Coh91, Ohl96, Kud99, Mahl99, Mahl00, Mahl01a, Mahl01b]. The application of such charged macromolecules in industry is of great importance in many fields, like paper production and waste water treatment [Dau94, Böh97]. An understanding of the route, in which polyampholytes behave at polymer brush heterogeneous surfaces and, particularly, how the brush switching properties regulate quantitatively and qualitatively the adsorption of polyampholytes, could play very important role for designing many systems performance, and therefore, opens large field of issues in science and industry. The behavior of polyampholytes is also of interest, because amongst their number are found the proteins. Investigating the performance of polyampholytes at solid/liquid interfaces enables one to simplify the view of biomolecules adsorption onto different targeted surfaces. It is important to notify the work, done by previous researchers in the direction of polympholyte adsorption onto non-modified silicon substrates [Mahl99, Mahl00, Mahl01a, Mahl01b].

10.3. Experimental.

10.3.1. Adsorbents.

Mixed amphiphilic PS-P2VP brushes were synthesized via grafting of carboxyl terminated PS and P2VP from melt. PAA–P2VP binary polyelectrolyte brushes were prepared using similar synthetic procedure by grafting of carboxyl terminated poly(tert-butyl acrylate) (PBA) and P2VP. The synthetic routes are described in 6.2.2. and 6.2.3 (see Chapter 6). Afterwards PBA was hydrolized in the presence of p-toluenesulfonic acid at 55 ^{0}C. For PS-P2VP (1:1) we obtained a layer thickness d=6.5 nm, which corresponds to grafted amount A= 7.2 mg/m^2 and grafting density σ =0.1 nm^{-2}, and similar values for PAA-P2VP: d=6.4 nm, A= 7.2 mg/m^2 and σ =0.1 nm^{-2}. For the homopolymer brushes, used in the adsorption experiments, the characteristics are: for PS d=6.6 nm, A= 6.9 mg/m^2 and σ =0.1 nm^{-2}; for PBA d=6.8 nm, A= 7.1 mg/m^2 and σ =0.1 nm^{-2} and for P2VP d=6.3 nm, A= 7.4 mg/m^2 and σ =0.1 nm^{-2}. A and σ were calculated by 7.1, 7.2 and 7.3 in Chapter 7.

10.3.2. Adsorbate.

Diblock ampholytic comolymer PMAA-PDMEAA (19:81, Mn=62 000 g/mol, ρ=1.3 kg/cm^3, isoelectric point (IEP) at pH 9.3) was synthesized by anionic polymerisation [Mahl00] and received from R. Jerome-Centre for Education and Research on Macromolecules, University of Liege. The synthesis and the determination of molecular weight are described elsewhere [Creu97a, Creu97b, Ant97]. The chemical structure is presented on the scheme below.

Scheme 10.1.
Polyampholyte structure:
Poly(methacrylic acid) *left* and
Poly((dimethylamino)ethyl methacrylate *right*
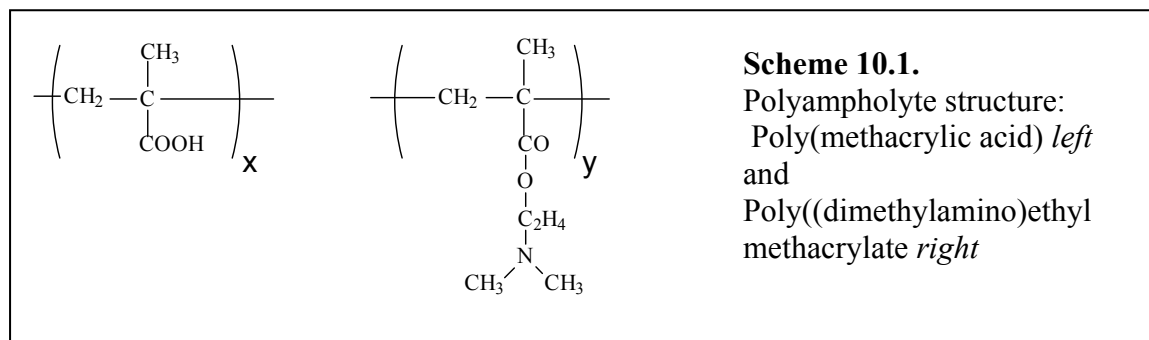
10.3.3. Adsorption Experiment.
The adsorption experiments were performed with ampholytic diblock copolymer onto both, amphiphilic and binary polyelectrolyte brushes from aqueous salt containing (C_{NaCl}=0.01 M), solutions at various pHs, for 10 h The polyampholyte concentration was set to 0.137 g/L.

10.4. Results and discussion

10.4.1. Polyampholyte adsorption onto amphiphilic PS-P2VP brush.

PS-P2VP amphiphilic polymer brush is a material that combines hydrophilic and hydrophobic properties, altering throughout the solution conditions. In aqueous medium, an adequate polyelectrolyte response can be obtained only by the P2VP component in acidic water. At low pH, the P2VP chains ability to swell (by intra/inter electrostatic repulsion and osmotic counter-ions pressure) and to cover preferentially the surface, results in a positive charged hydrophilic surface. Considering the polyampholyte, adsorbing to the surface, both components are responding to the medium, i.e. PMAA bears negative charges in alkali media, whilst PDMAEA become positively charged at acidic pH.

In Figure 10.1 one can follow the deposition efficiency, increasing the pH in steps from 2 to 11. Only weak adsorption occurred in the acidic region, up to, and not far after the IEP of the PS-P2VP substrate. This result was expected and finds its explanation in equally charged components of the brush and the polyampholyte. At low pH, the protonated nitrogen at pyridine rings (P2VP) and charged amino groups of PDMAEMA (both with positive sign),

turn the components to repel each other sufficiently, and contribute to a very poor adsorption, quantified with value of 1.2 mg/m^2 (A is calculated by 7.1., Chapter 7, as $\rho_{PMAA-b-PDMAEMA}$ =1.3 kg/cm^3) . Around the substrate IEP, at pH 5.9, relatively low polyampholyte coverage of 3 mg/m^2 was measured. The adsorbate molecules are immobilized on the surface by self hydrophobic parts, interacting with the likely parts at the polymer brush chains. Beyond the PS-P2VP IEP, a sharp jump in adsorbed amount was measured. Distinguishing the previous low pH conditions, a turn of the brush charge takes place, and therefore, an electrostatic attractive force leads to favorable adsorption in the system.
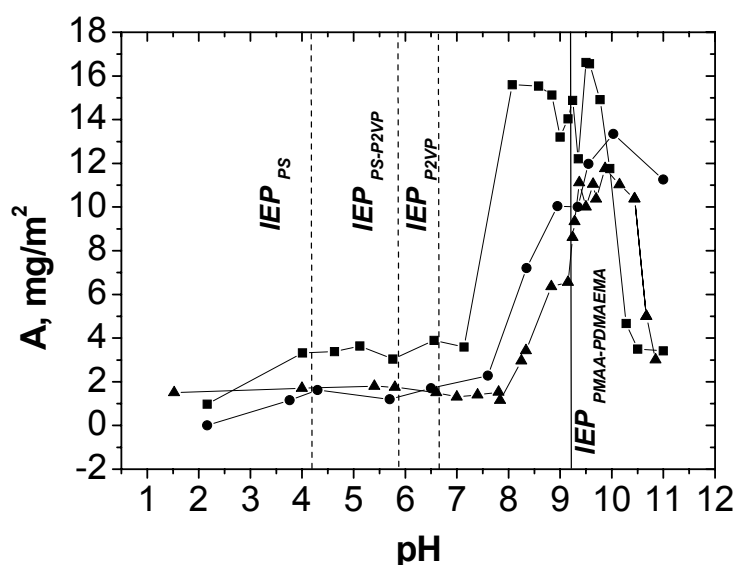

Figure 10.1. Amount of the poly-ampholyte PMAA-b-PDMAEMA, A, adsorbed onto: PS (circles), P2VP (triangles) and PS-P2VP (squares) brushes as a function of the pH. The mono-component brushes are taken as a reference of the binary brush. The dashed lines fix the non-charged states-*IEPs* of the brushes, while the solid one represents the neutral state of the polyampholyte.

This behaviour extends to the IEP of the polyampholyte, underlining the importance of the electrostatic interactions by weak polyelectrolytes. Over IEP of the PMAA-b-PDMAEMA, the adsorbed amount drops down again to values, measured before the PS-P2VP IEP to be reached. It does not occur as a sharp transition, as it is by the non-modified silicon substrates, described in the literature [Mahl99]. The adsorbed amount forms a plateau, extended from about pH 7 till pH 10, in difference with non-treated Si-substrates, where a maximum adsorbed amount can be extracted from a single peak. The non-zero adsorption values within the entire pH region (contrariwise to the PMAA-PDMAEMA adsorption onto pure silicon substrate), show the contribution of polymer brush adsorbent in the adsorption process.

In summary, concerning PS-P2VP brush, one can distinguish four types of adsorption response (positive-positive, neutral-positive, negative-positive and negative-negative charges interactions) and two energetic state transitions (hydrophilic/hydrophobic). Below pH 5.9 (brush IEP), the substrate is positively charged and hydrophilic. It repels the polyampholyte molecules, since the charges are equal. Not fully protonated P2VP does not cover the surface

completely and coexist with PS chains within the top layer near before the IEP. A hydrophobic adsorption, as well as hydrogen bonding between the functionalities in the system takes place, despite its relative insignificance. The uncharged surface state by PS-P2VP at pH 5.9 does not change the adsorption behaviour, i.e., there is a similarity between slightly charged surface and uncharged state in this system. At pH higher than IEP, the surface becomes negatively charged. Since P2VP adopts a non-charged state (PS is a non-polar polymer in general) there is no polyelectrolyte-like response to the environment. The negative charge is a result from a preferential adsorption of negative ions from the solutions, which form a diffuse layer near the surface. At this regime, the substrate and the polyampholyte molecules attract electrostatically each other, and maximum adsorbed amount of about 15mg/m^2 was measured. One can assume a synergic action of electrostatic attraction and short range hydrophobic contact between the constituents. Over pH 9.3 (IEP of PMAA-PDMAEMA), the smaller one, negatively charged PMAA block does not repels sufficiently the negative substrate, which results in continuous adsorption till about pH 10.

The adsorption response of the homo-polymer constituents were taken into account, as a reference case, as well. Considering their behaviour separately, one can find the advances of the switching phenomenon, expressed only by the binary PS-P2VP brush in direction of increased adsorbed amount and widened pH range of the adsorption jump. PS and P2VP homo-polymers form a synergic combination of properties well pronounced in the adaptive performance of the binary brush. AFM images (Figure 10.2) are shown as a confirmation of the ellipsometric findings. Regarding the degree of surface coverage and its correlation with the ellipsometric thickness, one can distinguish between both regimes-below and over the IEP of the polymer brush. At pH 5.67 (A) one can observe regular micellar polyampholyte coverage with lateral radius of about 220 nm (extracted from topography image in Figure 10.2 (5x5μm scan size) by PSD program tool- not shown here). Adjusting pH to 9 (B), the thickness values increase to about four times. One can observe a significant reduced 2D planar globule to globule distance, and average size of the structures of 120 nm. A previous study on this polyampholyte reports size of similar magnitude, which reveals already globules formed in the solution [Mahl99, Mahl00]. The role of the brush in the adsorption process is to control the adsorbed amount, by switching the surface composition, and hence to introduce into the system interactions of different type.

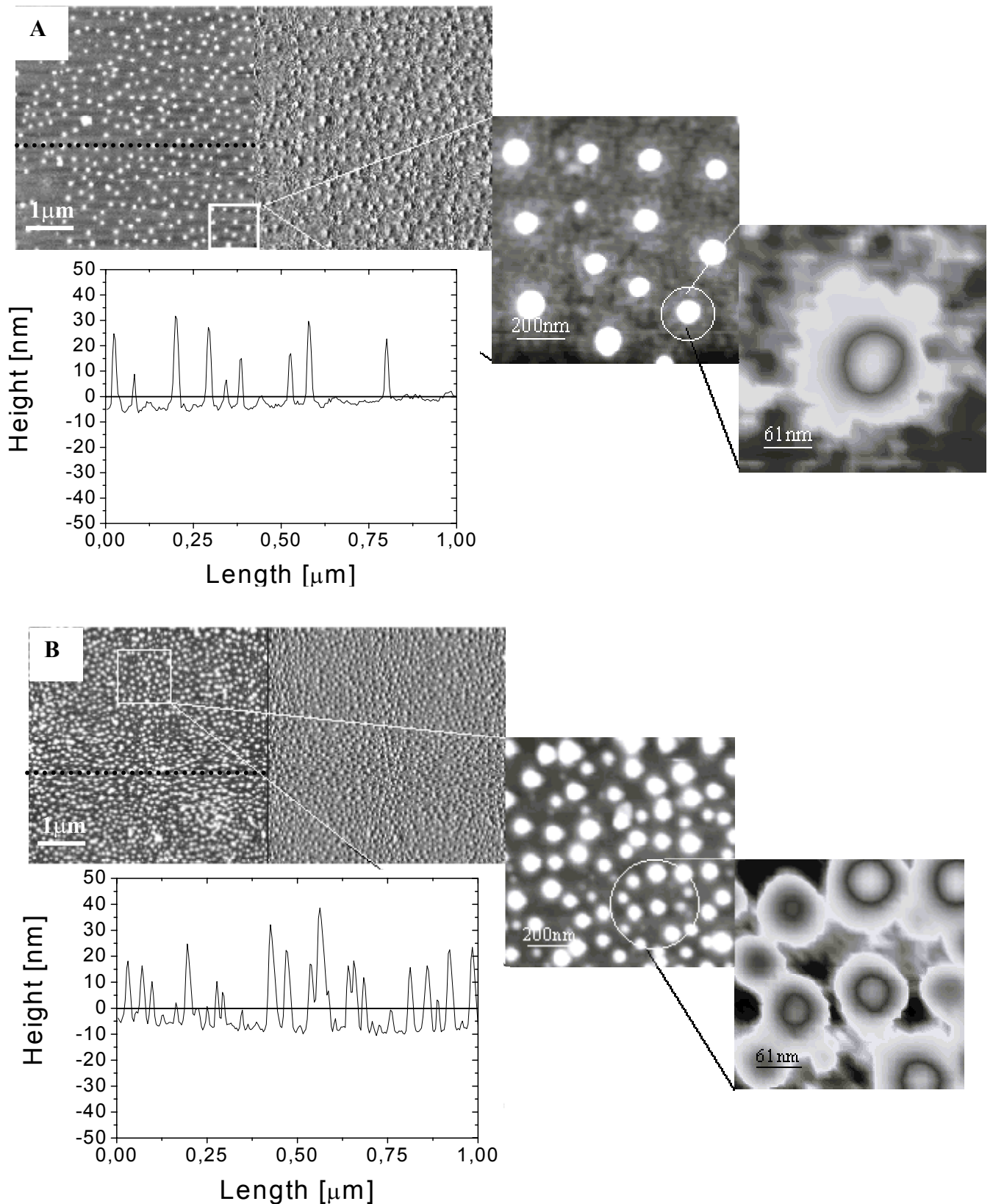**Figure 10.2.** 5X5 μm AFM images (left, topography, Z range 100nm; right, phase) of adsorbed onto PS-P2VP polymer brush polyampholyte PMAA-b-PDMAEMA at: A) pH=5.7 (RMS 5.17 nm) and B) pH 9 (RMS 9.12 nm). Sectional analysis from the topography images are plotted below. Right images represent zoomed spots from topography of the adsorbed polyampholyte dry layer, treated by contrast tools of the AFM program.

10.4.2. Polyampholyte adsorption onto PAA-P2VP brush.

Exploring PAA-P2VP brush adsorption response, one can expect even more interesting behaviour, regarding the adsorbent acid/base properties. Generally, we consider a system, in which both, the adsorbent and adsorbate, bare charged groups within the entire pH range. The polyelectrolyte brush is composed out of a weak base and a weak acid, similarly to the PMAA-b-PDMAEMA. By introducing such a substrate, composed of two oppositely charged polyelectrolytes, the importance of the electrostatic interactions is clearly shown. Below the brush IEP at pH 4.9, only insignificant PMAA-b-PDMAEMA deposition can be measured, devoted to repulsion between the equal charges within the system (Figure 10.3). Over pH 4.9, nearly linear growth of the adsorbed polyampholyte amount was detected, proving the electrostatic attraction, occurred at the interface. An interesting point is the continuing adsorption at pH over IEP of the polyampholyte at pH 9.3, where one can monitor even more adsorbed amount at pH 9.6 and 10 (proved by AFM as well). At pH ~10, the repulsion already becomes sufficient to overcome the hydrophobic forces, depositing the polyampholyte over pH 9.3.
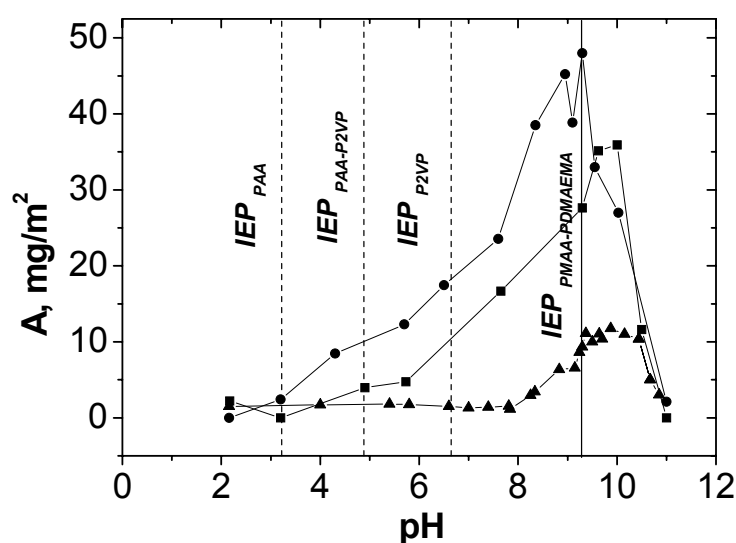
Figure 10.3. Amount of the poly-ampholyte PMAA-b-PDMAEMA, A, adsorbed onto: PAA (circles), P2VP (triangles) and PAA-P2VP (squares) brushes as a function of the pH. The mono-component brushes are taken as a reference of the binary brush. The dashed lines fix the non-charged states-*IEP* of the substrates, while the solid one represents the neutral state of the polyampolyte.

This finding was committed to the second weak polyelectrolyte, i.e. the PAA, which is getting dissociated in such alkali medium and occupies preferentially the top. Higher adsorbed amount on PAA and PAA-P2VP (as compared to the previous case of PS and PS-P2VP substrate) we allocate to the swollen PAA component on one hand, and to the bigger size of the positively charged PDMAEMA block, compared to the acidic PMAA one, on the other hand. Nevertheless, while formally both charges, operating within the system, are of equal (negative) sign, their magnitude is significantly different (since both uncharged states lie far

apart on the pH scale), due to a charge inhomogeneity, typical for weak polyelectrolytes. As another very important contribution one can assume the enlarged polymer surface area, available to contact for the depositing polyampholyte. The origin of that contribution is the swelling of PAA in basic water, providing "in situ" elongated chains. The hydrophobic interaction of inner polymer segments also must be taken into account as well.

Investigating the behaviour of the mono-component constituents, one can find significant dissimilarities with adsorption onto PS-P2VP brush, considered above. Concerning the IEP of PAA (pH 3.2) one can expect a constantly increase of the charge densities along the chains. About 50 % growth in adsorbed amount by PAA brush, compared to PAA-P2VP one, was measured, as the adsorption behavior is similar. In more acidic medium (pH up to 4) the behavior of the binary brush and of its constituents separately, differs from each other obviously. Within this region PAA begins to dissociate. Over pH 3.2, a linear increase of adsorbed amount onto PAA is in progress, whilst PAA-P2VP (IEP at pH 4.9) and P2VP (IEP at pH 6.7) bear positive charges and allow repulsive forces to operate in the system. Pointing out this, one can find more similarities between PAA-P2VP and P2VP bushes adsorption behaviour, i.e. the P2VP component has stronger influence than PAA one on the binary brush activity-particularly at mentioned low pH conditions. Around pH 4.9 the components in the binary brush composition form a neutral complex, resulting in a non-charged surface. By such conditions hydrophobic interactions take place in polyampholyte deposition, as it was stated above. Above this point, the binary brush adsorption behaviour mimics obviously the PAA one, since the surface charge turns from a positive to a negative and the polyampholyte adsorbs mainly electrostatically. At relatively high (basic) pH, the mono-component PAA brush tends to become nearly fully dissociated, and hence, strongly stretches away from the substrate. Then the interface contact area increases significantly, and the adsorption curve is sharpening for PAA and PAA-P2VP. The larger adsorbed amount for PAA than for PAA-P2VP devotes to the higher grafting density of PAA chains in the mono-component brush, compared to the binary one. For PAA-P2VP, about half of the grafting sites per unit area are occupied by P2VP chains, which are not electrostatically active at alkali conditions, and therefore are located near the substrate.

On the AFM images (Figure10.4.), one can follow surface morphology as function of pH. At pH 2.2 and 4.9, one can recognize cluster-like brush morphology, with small amount of polyampholyte globules, randomly ordered on the surface. Revealing a poor adsorption at these points- a result, confirmed by ellipsometry as well, we were able to change the picture only by adjusting of the external conditions. A medium alkalisation leads to a maximum of adsorbed amount and in round shaped globular structures of PMAA-PDMAEMA (pH 7.7, 9.3 and 10), ordered on the brush surface. Compared to the PS-P2VP brush adsorption case, micelle shell structures of the polyampholyte overlap each other and form a continuous sub-film, which surrounds the cores, limited by inter micelles distance.
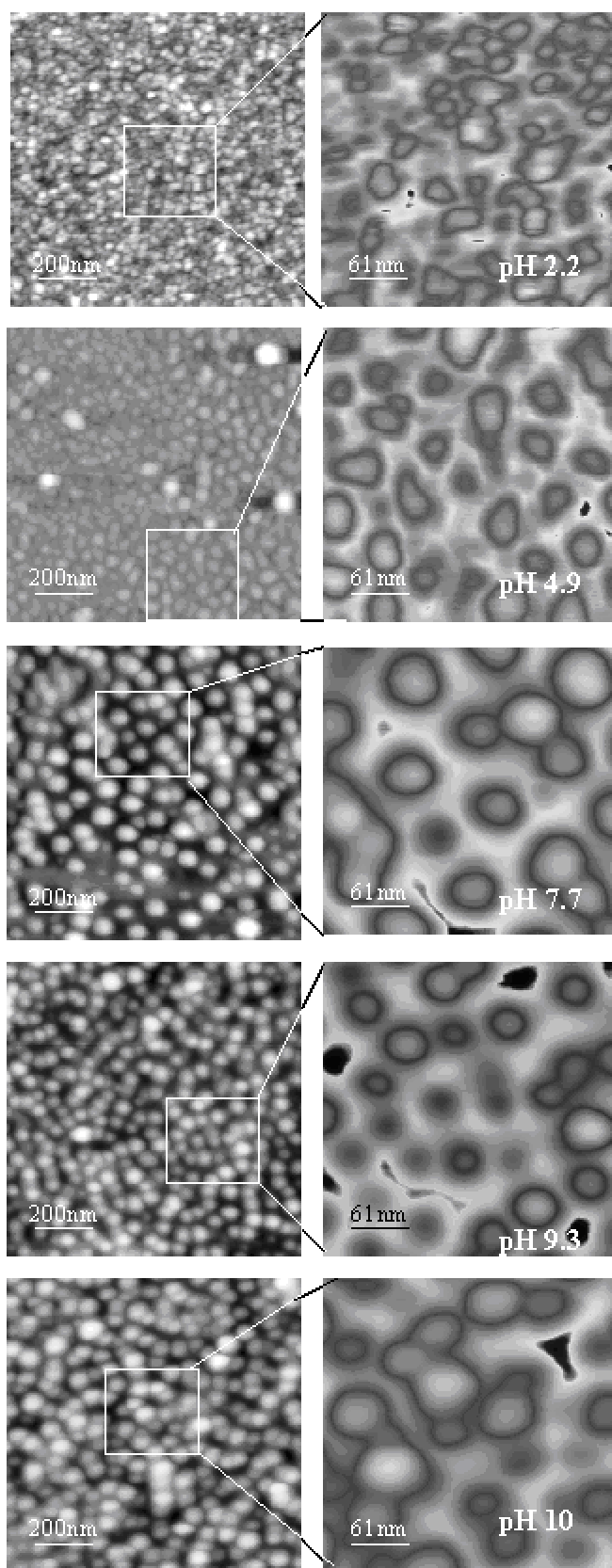
Figure 10.4. AFM images of adsorbed polyampholyte PMAA-b-PDMAEMA on PAA-P2VP polymer brush at step wisely pH increase.
Left images represent topography of the adsorbed polyampholyte dry layer, whilst the right ones are zoomed spots, treated by contrast tools at the AFM program. Poor adsorption is revealed at pH 2.2 and 4.9; favoured adsorption was measured at pH 7.7, 9.3 and 10. Cross-sections are given in Appendix 1.

Comparing the poor and good adsorption cases, one can distinguish between the brush structures (not uniform in shape-pH 2.2 and 4.9) and core-shell features (pH 7.7, 9.3, 10) getting close together, because of the dense package of the micelles.

10.5. Conclusions.

Adsorbed amount and morphological changes in the polyampholyte dry layers were investigated as a function of pH and substrate properties (surface charge, energetic state and compositional transformations) affected by external stimuli and components chemistry. Modelling the interactions within the system by switching brush phenomenon, a tuneable interfacial behaviour of the PMAA-PDMAEMA was found to influence the adsorbed amount and its conformational variances. The adsorption takes place mostly forced by electrostatic interactions between oppositely charged monomer units along the polymer chains. Adsorption in pH ranges, where the surface charge has the same sign as the net charge of the polyampholyte was observed as well. Interplay between electrostatic forces, hydrogen bonds and hydrophobic interactions in the formation of compact surface structures shows the brush switching to influence significantly the system behaviour. An attempt to show the closeness of structural organization of synthetic polyampholytes to natural ones is undertaken and described in the next three chapters.

Chapter 11

Regulation of Protein Adsorption by Switching of Surface Charge, Surface Energetic State and Chemical Composition of Binary Polymer Brushes

11.1. Abstract. In this chapter, we discuss the ability of grafted polymers to control the protein adsorbed quantity and the surface morphology by the switching layers phenomenon. We extensively investigate the adsorption of different proteins onto symmetrical amphiphilic and binary polyelectrolyte brushes by varying the pH within a limited range of buffer capacities. The ability of the brush to switch the surface component dominance upon external stimuli is shown to be a successful tool for designing the system properties, and particularly, the protein interfacial behavior.

11.2. Introduction.

As an amphiphilic substance, proteins exhibit a strong tendency to adsorb at interfaces [Gra04]. Investigation of protein adsorption on different solid substrates, and further exploring the interaction between the underlying substrate and protein molecules, opens a large field of applications in the biomedical science [Che97, Mah00, Bla98, Lee02].

Understanding the effect of solution variables, such as pH and ionic strength, and substrate composition/architecture on the protein adsorption, allows one to make a proper qualitative and quantitative evaluation of the interaction forces within many artificial and bio systems. The permission and prevention of protein adsorption onto different surfaces is one of the important requirements in the design of biocompatible materials. In recent years, it has been shown that grafting of polymer molecules to the surfaces may be a very effective instrument in regulation of many processes [Hub03, Har92, Ma01, Sukh99, Wal94, Pro03].

11.3. Experimental.

11.3.1. Substrates.

We synthesized two different types of polymer brushes, further used as substrates for protein adsorption. The synthetic route, covered by procedures, developed for "grafting to" method [Sid99, Min02] and consecutive analogous chemical reaction for converting the non-polar constituents to polar was applied [Hou03]. The procedure is described in Chapters 6 (6.2.2., 6.2.3.), 7 (7.3.1.) and 8 (8.3.1.) as well.

The first type polymer brush, polystyrene-poly(2-vinyl pyridine) (PS-P2VP), consists of the non-polar PS and polyelectrolyte P2VP. The second substrate, polyacrylic acid- poly(2-vinyl pyridine) (PAA-P2VP) binary polyelectrolyte brush, has the particularity to be composed of two polymers that are both polyelectrolytes- a weak base (P2VP) and a weak acid (PAA), and was synthesized from PBA and P2VP by converting the first one to polyelectrolyte (PAA). The characteristics of both brushes were calculated by 7.1, 7.2 and 7.3 and are summarized below.

Table 11.1. Characteristic of binary and mono-componentpolyelectrolyte brushes.

Composition	PS-P2VP	PS	P2VP	PBA-P2VP	PBA	P2VP
Thickness, d, nm	6.5	3.4	3.1	6.1	3.1	3.0
Grafted amount A, mg.m^{-2}	7.3	3.6	3.7	6.8	3.3	3.5
Grafting distance, d_g, nm	3.2	4.6	4.3	3.3	4.6	4.6
Grafting density, σ, nm^{-2}	0.10	0.05	0.05	0.1	0.05	0.05

11.3.2. Proteins.

Horse skeleton myoglobin, hen egg white lysozyme, human plasma fibrinogen and bovine serum albumin were purchased from Sigma. Fibrinogen was additionally purified by dialysis to obtain a certain value of substance purity. The properties of studied proteins are summarized in Table 11.2.

Bovine serum albumin (BSA) is a naturally occurring minor protein shaped as an ellipsoid.

Lysozyme is relatively hydrophobic and very basic protein (pKa 11).

Fibrinogen has a rod-like structure with approximately 10 nm width and the molecules may lie planar on the biomaterials interface.

Table 11.2. Properties of proteins under study [Arai90, Murp00].

Protein	Molecular mass, kg/mol	Dimensions, nm	Radius based on sphere, nm	Isoelectric point
Myoglobin	17.8	4.5 x 3.5 x 2.5	2.06	7.2
Lysozyme	14.4	4.5 x 3.0 x 3.0	1.6	11
BSA	66.7	4.0 x 4.0 x14.0	2.69	4.8
Fibrinogen	340	9.0 x 47.5 x 6.0	10.7	5.5

11.3.3. Adsorption procedure.

Under constant conditions (room temperature), the proteins were adsorbed after exposure of the brushes to protein solutions of concentration 0.25 mg/ml in phosphate buffered saline (PBS) - pH 7.4, containing 0.01 M sodium phosphate and 0.137 M sodium chloride, for 6 h. Not tightly adsorbed proteins were then removed by rinsing the samples in pure buffer, adjusted to the adsorption pH. The samples were then dried with N_2 and measured by null ellipsometry and Atomic Force Microscopy (AFM).

11.3.4. Ellipsometric measurements.

Null ellipsometry was applied to determine the thickness of chemisorbed GPS, grafted amount of the polymers after the grafting procedure and adsorbed amount of the proteins.

All the measurements were carried out using null-ellipsometer in a polarizer-compensator-sample-analyzer (Multiscope, Optrel Berlin) mode. As light source a He-Ne laser with $\lambda=$ 632.8 nm was applied and the angle of incident was set to 70^0. A multilayer model for homogeneous films covering the silicon substrate has been used for calculation the thickness of chemisorbed GPS and grafted polymer layers in air from the ellipsometric angles ψ and Δ. The refractive indexes used in the calculations were n= 3.8850 for the silicon substrate, n=1.4598 for GPS, n=1.59 for PS, n=1.466 for PBA and n=1.595 for P2VP. After the hydrolysis of PBA, a refractive index of 1.527 was used for the thickness evaluations of the PAA layer.

For the mixed brush we used three layer model, when SiO_2 and GPS layers were considered as one layer with effective n = 1.445. We found that this approach results in the error not larger than 5%. Refractive index for the proteins was averaged to n=1.5. All the measurements were carried out in dry state mode.

11.4. Results and Discussion.

The adsorption of proteins on hydrophobic surface can significantly differ from that, obtained on hydrophilic one. Within the following discussion, we will try to outline the main differences and their origin.

11.4.1. Effect of switching charge and wettability on protein deposition.

The adsorption was performed from PBS with relative high NaCl concentration (0.137 M), often inducing self-association, crystal nucleation and/or amorphous aggregation of proteins, showing the important role of electrostatic interactions. The proteins were deposited onto a

polymer brush, comprising chemically functionalized chains, exposed to interaction with the protein functionalities.

Evaluating the driving forces on a hydrophilic surface (when PAA or P2VP dominate at various top layer ratios, controlled by pH), one can define the electrostatic attraction between the charged surface and an oppositely charged protein molecule as an important force, coupling the protein to the surface. The amount adsorbed may then be partially determined by a balance between this electrostatic attraction and the electrostatic repulsion within the system. The contribution of the hydrophobic interactions as a further (or main) driving force for protein adsorption was found to operate in the system as well. The hydrophobic effect originates from entropic changes, associated with dehydration or a structural rearrangement of the protein- an effect that is not typical for synthetic polyampholytes, explored in Chapter 10. Considering BSA, the similarity of the electric charge, especially with PAA-P2VP brush ($IEP_{substrate} \sim IEP_{protein}$), leads to a system that excludes any electrostatic attraction. The adsorbed layer values oscillate around 7 nm thickness with a small rising at pH 4 and 8.6 (Figure 11.1.).
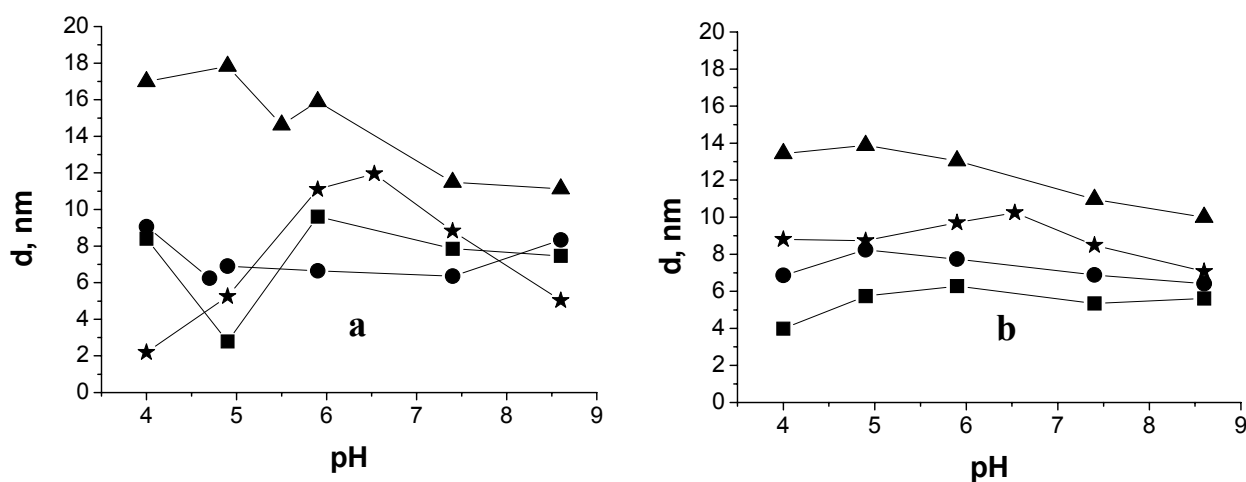

Figure 11.1. Adsorbed dry layer thickness, d, as function of the solution pH; a) PAA-P2VP substrate (IEP 4.9), b) PS-P2VP substrate (IEP 5.9); Proteins: lysosyme (squares), fibrinogen (triangles), BSA (circles), myoglobin (asterisk).

Since the IEPs of the brushes and the protein are equal, nearly no changes in the adsorbed amount occur. This information together with the molecular geometry of the native BSA (see Table 11.1) suggests that the protein adsorbs in double layer at its short axis, adopting a sideways-on conformation in the concentration studied (0.25 mg/ml).

However, the constant value adsorbed over the investigated pH region suggests a constant range of the electrostatic repulsion forces, which keeps the adsorbed amount similar among the different points. On the other hand, the protein adsorbs even despite the unfavourable

electrostatic conditions. That can mainly dedicate to the hydrophobic forces, not influential electrostatically and always operating by the proteins.

At pH 4 and 8.6, the brush layer adopts more extended conformations which increase the active surface (chain) area, available for the protein molecules to interact with. Regarding the high salt concentration (in respect to 0.137 M NaCl), PAA and P2VP are not sufficiently swollen to ensure a brush height 5-6 fold more than its original dry state thickness (Chapter 8, Figure 8.7). However, swelling effect is partially acting and results in an increase of adsorbed protein thickness at these particular points. The inhomogeneous charge distribution at a weak polyelectrolyte brush can be important as well. The effect is studied by serial numerical simulation [Berg97, Boruk00], and more recently, a generalization of the theory to the case of flexible chains has been given by Castelnovo et al. [Cast00]. Qualitatively it was found that a charge accumulation take place at the chain ends. The counterion distribution is significantly different from that around the inner part of the chain, hence, the mixed brush can locally adapt to protein.

Exchanging the brush composition by introducing PS instead of PAA, we prevent the ability of the substrate to complex at neutral and slightly acidic medium, as well as to swell in basic water. The adsorbed amount is approximately constant between pH 4 and 8.6 with a weak increase at pH 5. Near this value is the isoelectric point of the protein, which adsorbs easily on the weakly charged surface with partially present PS and P2VP. In spite of that hydrophobic adsorption does not have any influence from pH, the buffer medium and pH can affect the conformation of the conjugated protein, and therefore to contribute to the efficiency of the protein deposition.

11.4.2. Morphology variations of adsorbed protein layer, regulated by polymer brush chemistry and responsive properties.

AFM analysis is useful for probing the lateral distribution of the protein molecules within the monolayer and confirms indirectly the presence of the adsorbed protein on the surfaces.

AFM measurements of adsorbed BSA, indicates a layer, dominated by protein clusters and fragments of various size, controlled by the media quality and brush chemical composition, are shown inn Figure 11.2.

By the transition A-B, the chemical composition is constant (PAA-P2VP) and only the pH was adjusted from 8.6 to 4. A remarkable lamella-cluster conversion occurs. At pH 4, the P2VP component is only slightly protonated, and the protein is slightly charged as well, i.e. not significant electrostatic interactions take place. The protein aggregates on the surface in

small globular features. At pH 8.6, the surface is dominated by PAA (IEP 3.2), which is substantially dissociated, and repels electrostatically the equal charged protein. The lamellar protein structures can be assumed to originate from properties of the adsorbing charged surface, which does not allow the protein to coagulate due to increased surface tension on the hydrophilic brush surface.
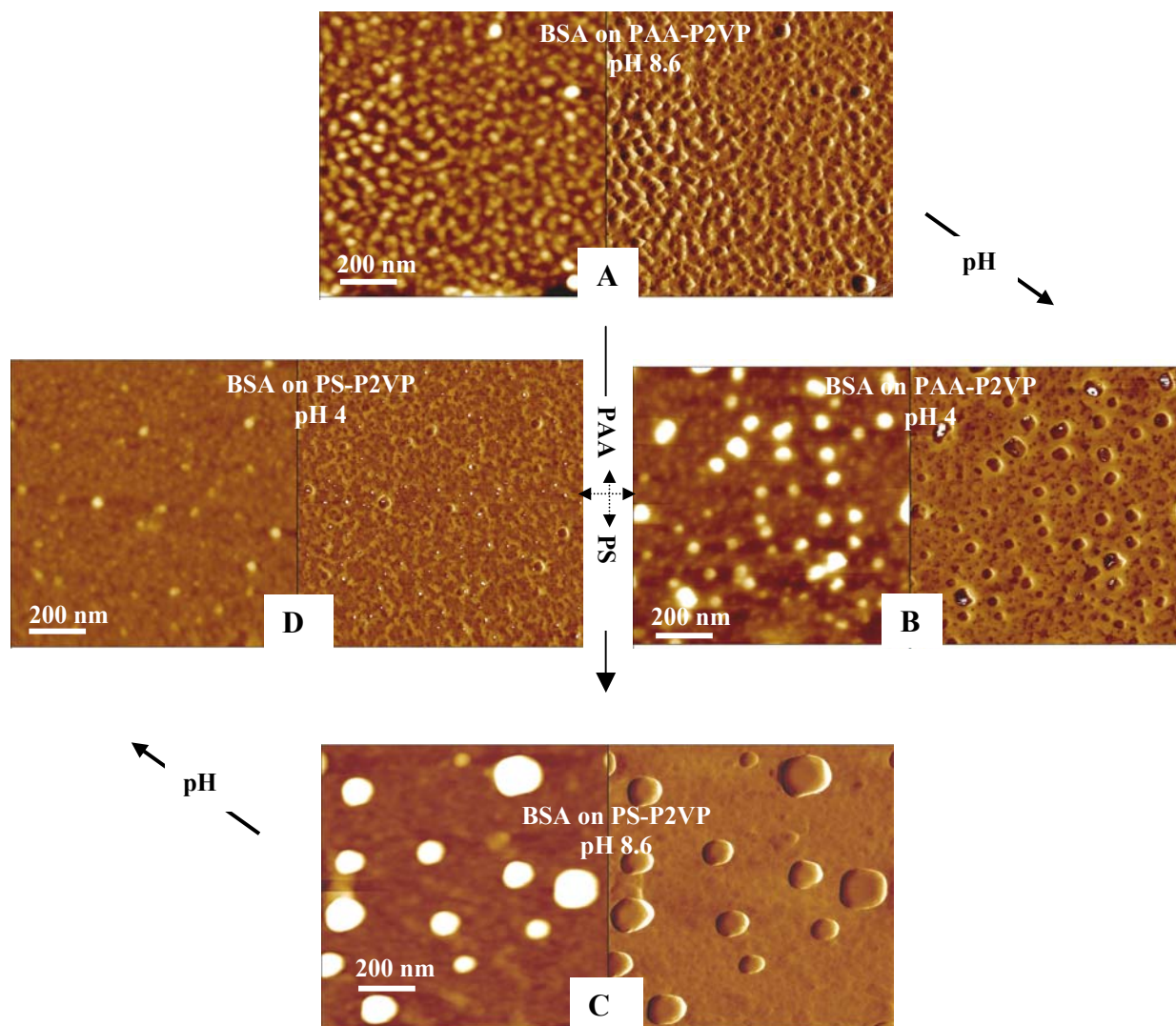
Figure 11.2. 1X1 µm AFM images (left, topography; right, phase) of BSA, adsorbed on: A) PAA-P2VP at pH 8.6, RMS 3.59 nm; B) PAA-P2VP at 4, RMS 5.74 nm; C) PS-P2VP at pH 8.6, RMS 9.8 nm; D) PS-P2VP at pH 4, RMS 1.97 nm.; Z range-A) 60 nm, B) 60 nm, C) 140 nm, D) 60 nm. The cross-sections, corresponding to the topography images, are presented in Appendix 2.

The hydrophobic residues at PS chains are exposed mainly in case C and partially in case D, and are available for contact with the hydrophobic parts of the adsorbing proteins,

resulting (as it is shown on AFM images by transitions A-C and D-C) in obvious surface aggregation. It is known that the hydrophobic surfaces promote aggregation of proteins due to rearrangement in protein structure by hydrophobic contact with water excluding non-polar macromolecules. By replacing PAA with PS, one generally amplifies the hydrophobicity of the brush, which is well seen at A-C differences. At pH 4 (case D), the presence of PS does not block P2VP in a complex, as it is in PAA-P2VP brush. Hence, the P2VP chains much more freely arise at the top surface. This effect is well pronounced, compared to image B. Changing pH to 8.6 (C-D), the chemical composition is the same, but the fraction of PS on the top is higher than at pH 4, because basic water is a poor solvent for both components (PS and P2VP). Considering these conditions, the surface gets hydrophobic, adapting the protein molecules in big globular aggregates (case C).

Fibrinogen has a molecular weight of 340 kg/mol, which is the highest one in our study. It has a rod-like structure with approximately 10 nm width and the molecules may lie planar on the reactive interface. It adsorbs stronger than the other proteins (Table 11.2.) on both PAA-P2VP and PS-P2VP brushes. This fact is mainly dedicated to its size and weight, having in mind that its IEP is of similar range of that as previously studied BSA. On both brushes, adsorption runs through a weak maximum at pH 4.9- a point near to the IEP of fibrinogen as well (Figure 11.1.). Here the similarity ends. PAA-P2VP brushes exhibit more pronounced response to the fibrinogen adsorption than PS-P2VP. Probably, the presence of two polyelectrolytes gives a better response to the aqueous media, i.e. throughout the entire pH range, a triple hydrophilic-hydrophobic-hydrophilic (acidic-neutral-basic media) transition is established, whilst by PS-P2VP only one direction (hydrophilic-hydrophobic) is present.

An interesting case is how the switching of surface charge of the binary polyelectrolyte brush PAA-P2VP influences the conformational changes of adsorbed protein layer with higher molecular weight, such as fibrinogen. In Figure 11.3, we show how the pH (electric charge, surface energetic state) affects the interaction among the system components, initiated by the switching phenomenon.

The first case, at pH 4.9 (brush IEP), represents charge exception interactions within the system (IEP of the protein is 5.5, i.e. nearly non-charged state). The morphology of adsorbed fibrinogen layer is much smoother than at pH 7.4 and 8.6. Practically, no pronounced features can be detected. The protein spreads out on the surface in a smooth layer, characterized by large lateral net-like continuous domains. The reason of such behavior could be found in a synergic action of slightly charged protein state, its higher molecular weight and uncharged brush polyelectrolyte complex state. The repulsion among the protein molecules is

insignificant, since its IEP is at pH 5.5. Fibrinogen is a big protein, with larger hydrophobic inner fragments, than the small proteins in this study. Discharged from intra- and inter-molecular repulsion, the protein hydrophobically coagulates in big aggregates, furthermore reacting with the underlying neutral brush complex, hydrophobic as well. The smooth wave-like (horizontal cross section and height analysis) layer then easily is formed, driven by the non-polar protein-protein, protein-brush interactions. Adjusting pH to 7.4, small clustered-lamellae features, forming intermittent necklace surface coverage, were detected.

At this point, the protein and the surface are already charged with the same sign, and protein-protein, protein-brush electrostatic repulsions do not favorize that smooth uniform coverage, found at the previous case.
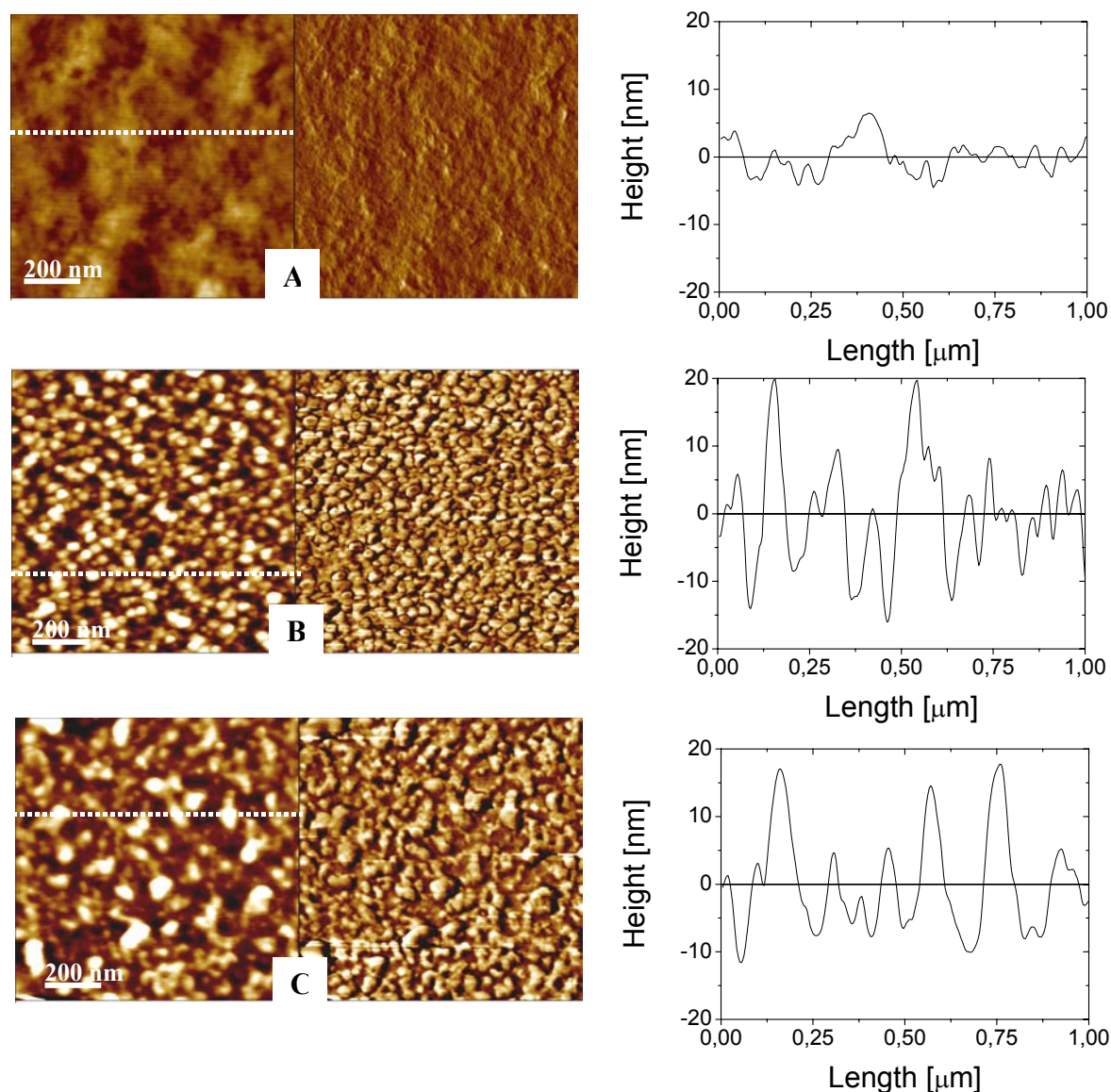

Figure 11.3. 1X1 μm AFM images (left, topography- Z range 40 nm; right, phase) and corresponding cross-sections of fibrinogen, adsorbed on PAA-P2VP brush at: A) pH 4.9, RMS 2.63 nm; B) pH 7.4, RMS 6.79 nm; C) pH 8.6, RMS 6.64 nm.

The cluster nucleation effect is significantly amplified at pH 8.6, where clusters convert more apparently to big lamellar fragments. PAA component dissociates to higher degree than at pH 7.4, and occupies the top layer easier. Then the protein tends to form the elongated structures at the hydrophilic surface, observed at these conditions for BSA as well.

The adsorption of lysozyme onto polymer brushes was monitored, as in the previous two cases, by ellipsometry and tapping mode AFM in air. Under the same constant conditions, lysozyme, adsorbed in different conformations, was imaged after exposure the brush to the solution. The results from ellipsometry obtained over pH 4.9 (Figure 11.1), reveal preferable electrostatic interaction between carboxyl groups of dissociated PAA and amino groups of the protein. The sharp increase in the lysozyme adsorbed amount, also in conjunction with the AFM images on Figure 11.4, shows stronger lysozyme adsorption, controlled by the charge of the both components.

On PS-P2VP brush, the adsorbed protein amount does not undergo significant changes with pH. It is devoted to the constant hydrophobic interaction (pH independent), amplified by the presence of PS in the top surface composition.

The most pronounced electrostatic effect is shown by choosing a protein with IEP that gives a possibility to investigate those pH boundaries, providing interaction between opposite charges on the one hand, and equal charges on the other. The IEP of myoglobin is at pH 7.2. Regarding the binary brushes IEPs (4.9 for PAA-P2VP and 5.9 for PS-P2VP) we have a narrow region to interplay with opposite charged components of the system. In case of PAA-P2VP, the sensitivity of the system to the electrostatic interactions is shown. The adsorbed amount increases between pH 4.9 and 7.2 (Figure 11.1). At such conditions, the protein and the polyelectrolyte brush bear opposite charges and the attractive electrostatic forces dominate over the others. By small shift away from the favorable electrostatic region, one can find a sharp decrease in amount of the deposited protein. Since the charges are equal, the electrostatic repulsion becomes the main reason for reduction of thickness in the protein layer. Nevertheless, the hydrophobic contribution is also a fact, keeping the adsorbed amount over pH 7.2 and below pH 4.9 far from zero. By PS-P2VP a similar effect was also observed, but the observed dissimilarities, exploring the different pH regions, were not that strong. At pH 6.5 one can see only a weak peak- an illustration of factors discussed above. By this type of binary polymer brush, the presence of PS makes the attractive electrostatic effect not that distinguished, and the adsorbed layer has a comparable thickness range in the most measured pH points.
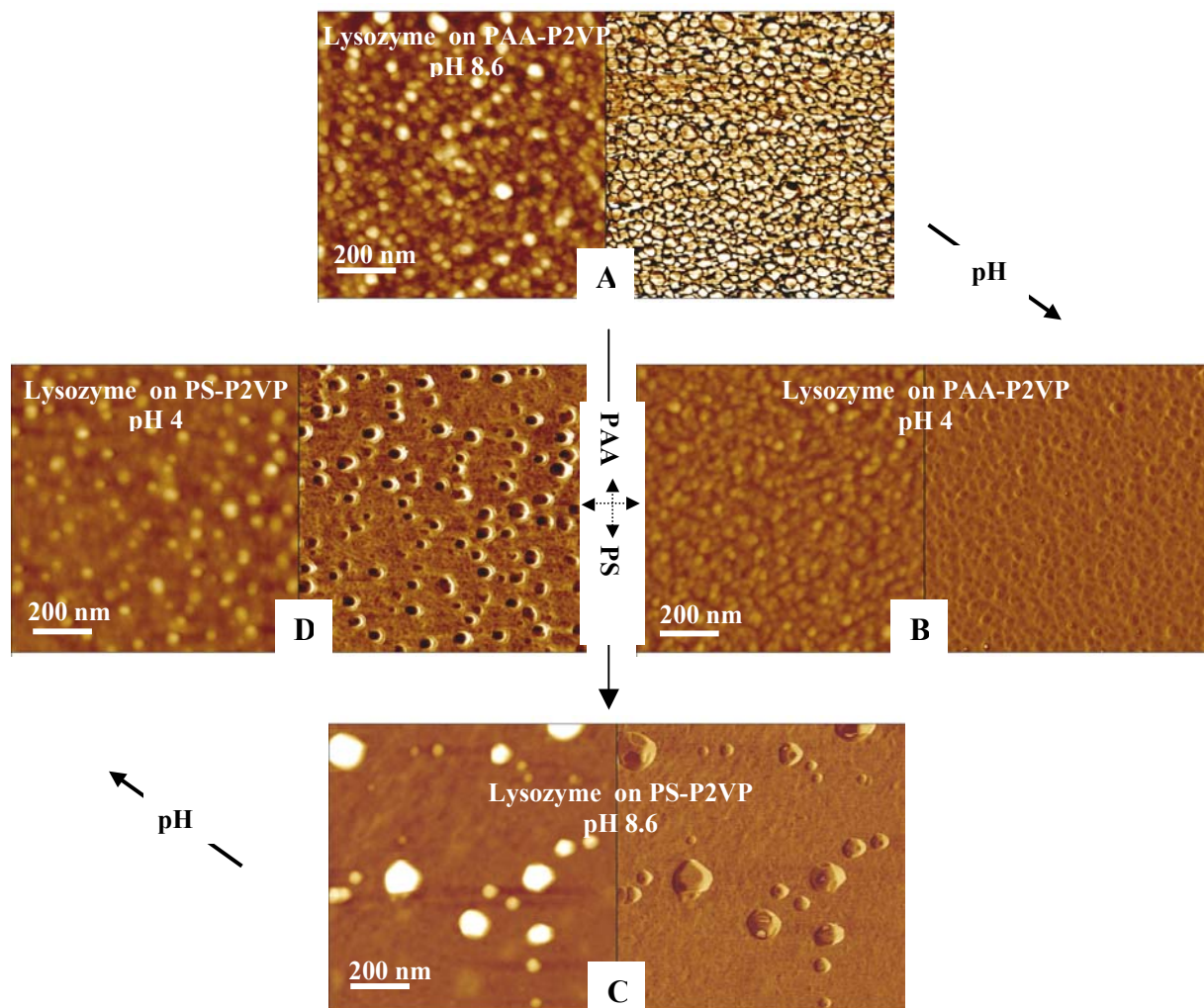
Figure 11.4. 1X1 μm AFM images (left, topography; right, phase) of lysozyme, adsorbed on: A) PAA-P2VP at pH 8.6 (Z range 60 nm, RMS 5.10 nm); B) PAA-P2VP at 4 (Z range 60 nm, RMS 2.04 nm); C) PS-P2VP at pH 8.6 (Z range 120 nm, RMS 8.63 nm); D) PS-P2VP at pH 4 (Z range 60 nm, RMS 3.44 nm). The cross-sections, corresponding to the topography images, are presented in Appendix 3.

Considering the ellipsometric results for all the proteins (Figure 11.1), in all cases we were able to detect adsorption "on the wrong side" of the protein and binary brush IEPs.

Each of these substances contains both positive and negative charges, activated at proper solvent conditions. Having in mind the well-known situation of adsorption of polyelectrolytes to a surface with net charge opposite to that of the polymer, we show that a polyelectrolyte (as the proteins generally are) can adsorb onto a surface with similar charge density and sign.

Counting the hydrophobic interactions that always operate at the protein adsorption, simultaneously we assume a possibility for an additional driving force to act in the system. In that sense, the spatial inhomogeneity of the surface charges, creating attractive regions with charge density different from the overall charge density of the surface, can contribute to the

adsorption as well. The spatial inhomogeneity of the surface charges also can lead to differences in the morphology of the adsorbed protein layers, well monitored with AFM imaging.

11.5. Conclusions.

Different molecular dimensions and effective charge of the four proteins throughout the experimental pH region, as well as the medium responsive behavior of the "smart" binary brushes, present a system with diverse possibilities to regulate the adsorption behavior. We found that the sharp environmental response of the adsorbent (the polymer brush) strongly influences the morphology of adsorbed protein layer, its thickness and properties. By keeping one of the variables in the system constant (brush composition, pH or protein type), we were able to determine to influence of the each factor separately.

A remarkable aggregation of protein molecules on the amphiphilic PS-P2VP brush occurred in basic media. The brush undergoes a hydrophilic/hydrophobic transition, caused by P2VP deprotonation and PS appearance within the top layer. Aggregates monitored on the surface overcome by size any molecular dimension of the proteins. We can assume that proteins diffuse on a time scale of minutes on the surface, to form clusters consisting of several molecules; effects, found to be well controlled by the brush switching phenomenon in hydrophilic-hydrophobic direction.

Comparing to PAA-P2VP brush, the stronger role of electrostatic forces by adsorbed layer formation was shown. The presence of two weak polyelectrolytes at the interrface gives an improved response to acid/base variations within the system. A hydrophilic state, shifting the conditions away from the neutral medium, continuously replaces the hydrophobic one.

Chapter 12

Protein Adsorption onto Binary Polymer Brushes: Effect of Electrolyte Concentration, Surface Chemistry, and Switching Layers Phenomenon.

12.1. Abstract. The preferential interactions of biomolecules with polyelectrolyte brushes and solvent components were examined in phosphate buffered saline (PBS) as a solvent media. The adsorption behavior of four model proteins was studied in 0.01 and 0.001 M solutions, and at pHs between 4 and 8.6. Varied surface compositions were imposed by chemistry and/or external stimulated switching of the adsorbing layers. The dependence of the equilibrium adsorbed amount on the ionic strength was investigated with the purpose to determine the screening effect of a monovalent salt on the variously charged proteins. The system becomes more complicated with the presence of binary polymer brushes as an adsorbing substrate. Environmental changes influence strongly not only the studied proteins. They also promote an equilibrium brush state transition to another one, in response to particularity of the media. The polymer brushes, chosen for the experiments consist of at least one weak polyelectrolyte, in the case of polystyrene-poly(2-vinyl pyridine) (PS-P2VP), or of two oppositely charged polyelectrolytes, in the case of polyacrylic acid-poly(2-vinyl pyridine) (PAA-P2VP). In the first case, the salt effect concerns mainly the behavior of P2VP. Monovalent salt ions screen inter and intra repulsions along the chain, as well as it is expected for the protein molecules. Introduction a second polyelectrolyte, PAA, instead of the non-polar PS, turns the substrate to be more influential on the electrolyte concentration in the solution. At higher buffer concentration (0.01 M PBS), the electrostatic interactions within and between the proteins molecules are screened, which leads to a globular protein conformation already in the solution. On the other hand the brush reduces partially its swollen thickness upon addition of salt as a salt screening effect is acting in the whole system. Diluting the buffer by factor of 10 (0.001M), causes more extended chain conformation by the protein and the polymer brushes, which results in different adsorption behavior at the interface.

12.2. Introduction.

Protein adsorption onto solid surfaces attracted much attention during last years, due to its scientific importance [Nor95, Hor95, Bra85] and its applications in bio-fouling [San91], biosensor development [Rech88] and construction of biocompatible materials [Hubb95].

An added salt at various concentrations is known to affect the conformation and charge densities of polyelectrolytes and biomolecules [Mar03, Nash91, Herr87, Yan97, McDon00, Lah03, Hub03]. The contribution of salts to the adsorption behavior of proteins on polymer brushes has not been extensively studied nor well. For protein molecules, salts with its molal surface tension increments stabilize native protein in solution and increase the adsorption when a surface is present. In addition, salt concentration gradients are correlated with the effects on swelling/deswelling order of the chargeable segment units.

A novel system, containing charged polymers, grafted onto a planar surface, simple salt, and solvent has been considered in the framework of its ability to guide protein binding and surface conformation. Optimizing the design of the protein adsorbing polymer brush for various applications, must be assisted by experimental arguments relating the many parameters involved [Hub03, Hu92, Jam91, Li95, Stahl92, Roth93, Roth96]. This chapter aims to extend the analysis on the topic as well as to obtain simple scaling relationships for the various design parameters, which control the adsorption of proteins on polymer brushes. This opens the possibly of exploring the advantages of selective adsorption by appropriate immobilization of specific molecules.

12.3. Experimental.

12.3.1. Substrates.

The amphiphilic PS-P2VP brush was synthesized according to S. Minko et al. [Min02a], described in details in Chapters 6 (6.2.2., 6.2.3.) and 7 (7.3.1).

The second substrate, PAA-P2VP binary polyelectrolyte brush, has the distinctiveness to be composed of two polymers that are both polyelectrolytes- a weak base (P2VP) and a weak acid (PAA), and was synthesized from poly(tert-butyl acrylate) (PBA) and P2VP by converting the first one to PAA. The convertion of PBA (a neutral polymer) to PAA (a polyelectrolyte) was performed in p-toluenesulfonic acid saturated benzene solution at 55 ^{0}C for 1 h, via acid catalyzed ester hydrolysis via $S_N1$mechanism ([Hou03], Chapters 6 and 8). Some important, for this study, properties of both kind of brushes are summarized in Table 11.1 (Chapter 11).

12.3.2. Protein adsorption measurements.

Lysozyme (IEP at pH 11), BSA (IEP at pH 4.7), myoglobin (IEP at pH 7.2) and fibrionogen (IEP at pH 5.5) were purchased from Sigma and obtained as lyophilised powders (Chapter 11, Table 11.2). Fibrinogen was additionally purified by dialysis against the experimental buffer. The buffer used in all protein adsorption experiments was PBS (pH 7.4), composed of 0.01 M sodium phosphate, 0.137 M sodium chloride. For low-salt concentration experiments the initial buffer solution was diluted to 0.001 M. The buffer pH was adjusted by 0.1 M NaOH and 0.1 M HCl. All adsorption experiments were performed from freshly prepared protein solutions with C=0.25 mg/mL, for 6 h. Afterwards, non-adsorbed protein was removed by PBS. The ellipsometric and morphology tests were performed in dry state.

12.4. Influence of salt concentration and polymer brush properties on the amount and morphology of adsorbed proteins.

The behavior of the proteins and polyelectrolyte brushes is influenced by salt concentration in the solution. The binary polyelectrolyte brush responds very strongly to the environmental changes. Being around IEP of the PAA-P2VP (pH 4.9) brush, both components are in equilibrium, non-charged state via charge compensation. The complex formed is not influenced by salt concentration at all, and the chains are only slightly swollen (pH 4-7). At pH 7.4, PAA-P2VP does not adopt a significantly different chain conformation at low and high salt concentration regimes. The reason is, that even in salt free media, this pH region does not provide conditions for proton association by pyridine rings of P2VP, or carboxylic groups dissociation at PAA (partially trapped in the polyelectrolyte complex). However, a weak increase of the layer thickness from 6 to 8 nm was measured in neutral water. In alkali medium the swelling from salt free solution to 0.001 M salted medium (C_{NaCl}= 0.0137 M) is between 18 nm and 23 nm, and for 0.01 M (C_{NaCl}= 0.137 M) decreases to 12 nm (see Figure 8.7, Chapter 8). The reason of such interesting behavior, at low salt concentration, concerning the maximum in the swollen thickness is discussed. In solution, the polyelectrolyte chains have stretched conformation and only a fraction of their charge is compensated by condensed counterions. Addition of salt to the solution induces collapse of the chains. A collapse occurs when the charge of the added salt is (almost) equal to the bare charge of the polymers. At low pH (protonated P2VP) and high pH (dissociated PAA) the swollen brush thickness reaches a maximum, which can be explained in terms of equalized concentrations of the salt and released ions within the brush.

Advanced contact angle in neutral water varies around 65 ^{0}, i.e., one observes relatively hydrophilic surface. When immersed in alkali medium over pH 8, the brush adopts extended conformation, with swelling degree by factor of 6 of its original dry state thickness. The contact angle approaches values below 50 ^{0}. The influence of monovalent electrolyte ions at all discussed circumstances is generalized below:

a) weak acidic medium- no influence registered.

b) neutral medium- the initial thickness increases from 6 to ca. 8 nm for both regimes.

c) alkali medium-salt free conditions provide ca. 18 nm swollen state, which reaches 20- 22 nm increase in 0.001 M buffer solution (0.0137 M in respect of NaCl) and decreases back to ca. 12 nm in 0.01 M PBS (0.137 M NaCl).

The other, amphiphilic, polymer brush gives a response to the pH and ionic strength only by P2VP, since PS is a hydrophobic, non-polar polymer, which contributes only to surface hydrophobicity.

Protein molecules exist as either native form or as a single unfolded protein species. The unfolded protein may be completely denatured or only partly unfolded. The globule density is governed by the added salt, and scales as the Debye screening length, k^{-1}, of electrostatic interactions, specified in Chapter 3, equation 3.3.

The screening is controlled by k^{-1}, and decays exponentially with the distance. It has an effect of lowering the potential surrounding any ion, which will lower the total free energy of the ionic solution, and cut back interactions between the ions.

In case of salt-free solution, polyelectrolytes like repulsions distort the shape of the collapsed protein globule at large length scales. Depending on the net charge of the chain (long range repulsions), on solvent quality and on charge asymmetry (short range attractions), cascade of transitions is expected between necklace conformations of various numbers of beads.

Both of the species (partially unfolded and globular) can be adsorbed on a heterogeneous surface. Hydrophobic interactions take a place in aqueous solvent conditions and changes in ionic strength reduce or amplify them. The protein typically binds in the native state via hydrophobic groups located on the surface of the protein. The native state is retained during lower salt conditions as well. This information together with the structure of the proteins enable one to assess the extent of structural deformation and, in some cases, unfolding, leading to a partial or complete loss of globular frame network (adsorption scheme in Figure 12.1 and 12.4). The proteins activities in salted solution and at a heterogeneous (brush-like architecture) interface are schematically shown below.
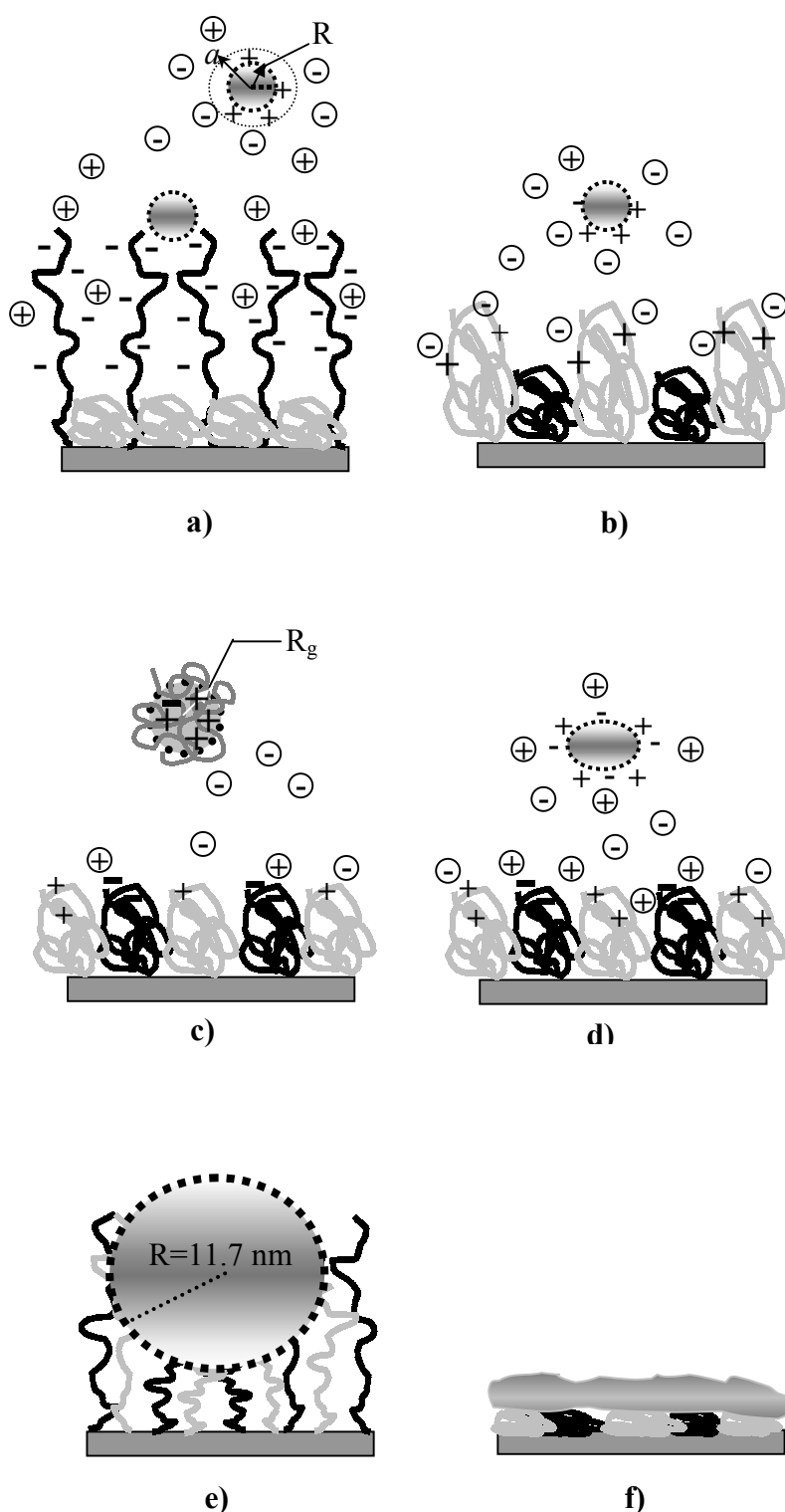
Scheme 12.1. Illustration of some adsorption regimes, performed with large and small proteins.
(a) A small protein (lysozyme) adsorption on swollen (highly charged) polyelectrolyte brush (PAA-P2VP) in a basic medium, and
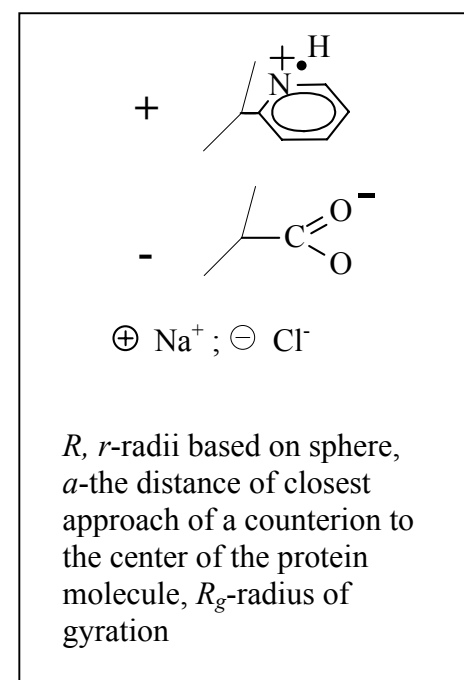(b) on slightly charged brush (PS-P2VP and PAA-P2VP) at mild acidic conditions.
(c) Partially unfolded protein at low ionic strength adsorbing onto non-stretched brush
(d) A middle-weight protein adsorbing on polymer brush with a similar IEP (BSA onto PAA-P2VP at the IEP).
(e) A large protein, which cannot enter the brush inner part and adsorbs at the outer top area.
(f) Adsorbed and structurally rearranged protein layer.

R, r-radii based on sphere, a-the distance of closest approach of a counterion to the center of the protein molecule, R_g-radius of gyration

The adsorption behavior of lysozyme, BSA, myoglobin and fibrinogen is shown in Figure12.1. Significant difference was observed concerning the adsorption of the proteins, varying their type, polymer brush nature and external conditions (pH and salt content). Regarding protein-protein, protein-solution, brush-brush, brush-solution and brush-protein
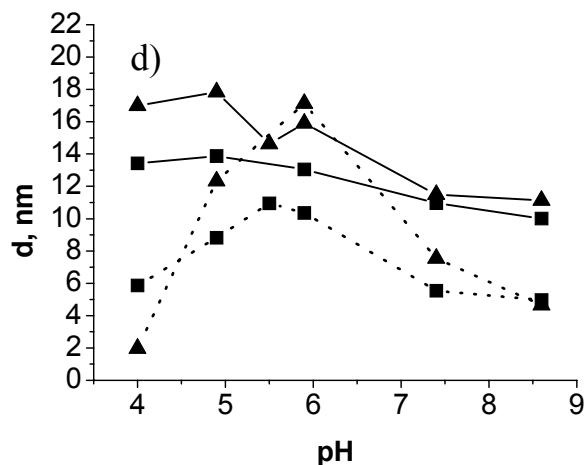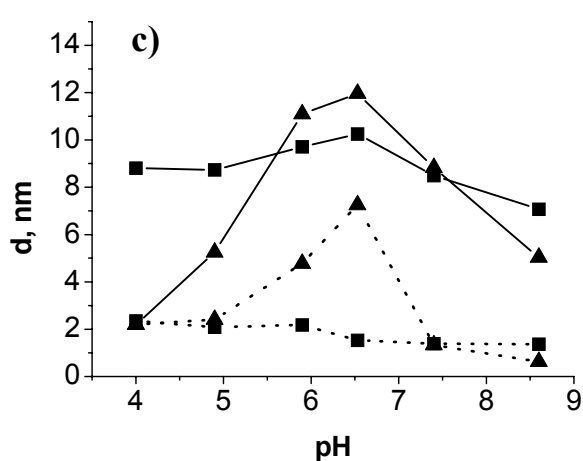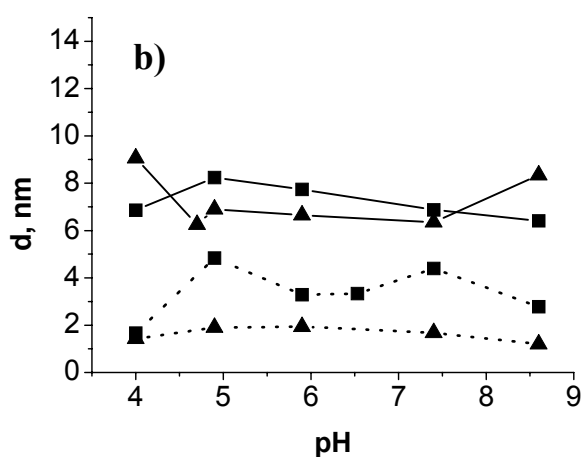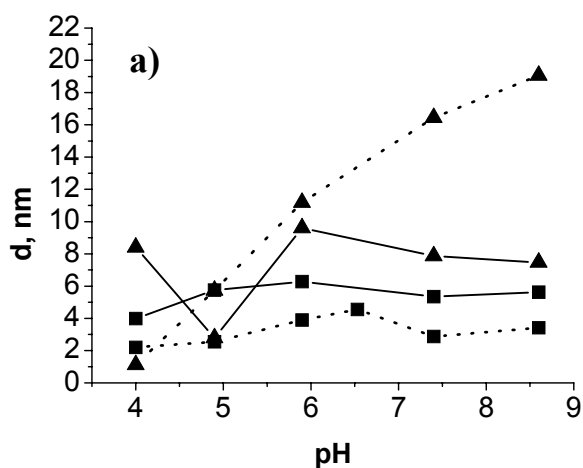
interactions, one observes several adsorption regimes, revealing a sharp environmental response of all system constituents.

Lysozyme is a small protein with isoelectric point fixed at pH 11, i.e., with prominent basic properties.

Figure 12.1. Adsorbed proteins dry layer thickness ((a) lysozyme, (b) BSA, (c) myoglobin, (d) fibrinogen) as a function of pH, polymer brush composition (PS-P2VP (squares), (PAA-P2VP (triangles)) and electrolyte concentration in PBS protein solutions (0.01 M PBS -solid lines, 0.001 M PBS-dotted lines).

The isoelectric points of the adsorbents are at pHs 5.9 and 4.9 for PS-P2VP and PAA-P2VP respectively. Regarding the IEP of lysozyme (pH 11), the difference allows the electrostatical attractive forces to operate between the adsorbent and adsorbate, clarifying the main driving force as a coulombic attraction.

At lower salt content (0.001 M PBS), the electrostatic interactions are favorized, because of the salt screening effect minimization, valid for all systems studied here. In case of amphiphilic polymer brush (PS-P2VP) as an adsorbent, the curve shape is similar at both salt concentrations. The presence of PS and only weakly charged P2VP (pH 4) makes the adsorption being contributed mainly by hydrophobic forces. In the case of higher salt concentration (0.01 M PBS), the globular conformation of protein molecules ensures a denser surface packing and an increase of conformational entropy (unlike to flexible polymers adsorption, Chapter 10), resulting in an adsorbed amount of lysozyme approximately two times higher than as it is by adsorption from 0.001 M PBS. The presence of relative high salt concentration, promotes denser protein sphere and, hence, results in more adsorbed mass per unit surface area, measured by ellipsometry (Figure 12.1), also seen in Figure 12.2, showing the adsorbed layer morphology at both salt regimes.
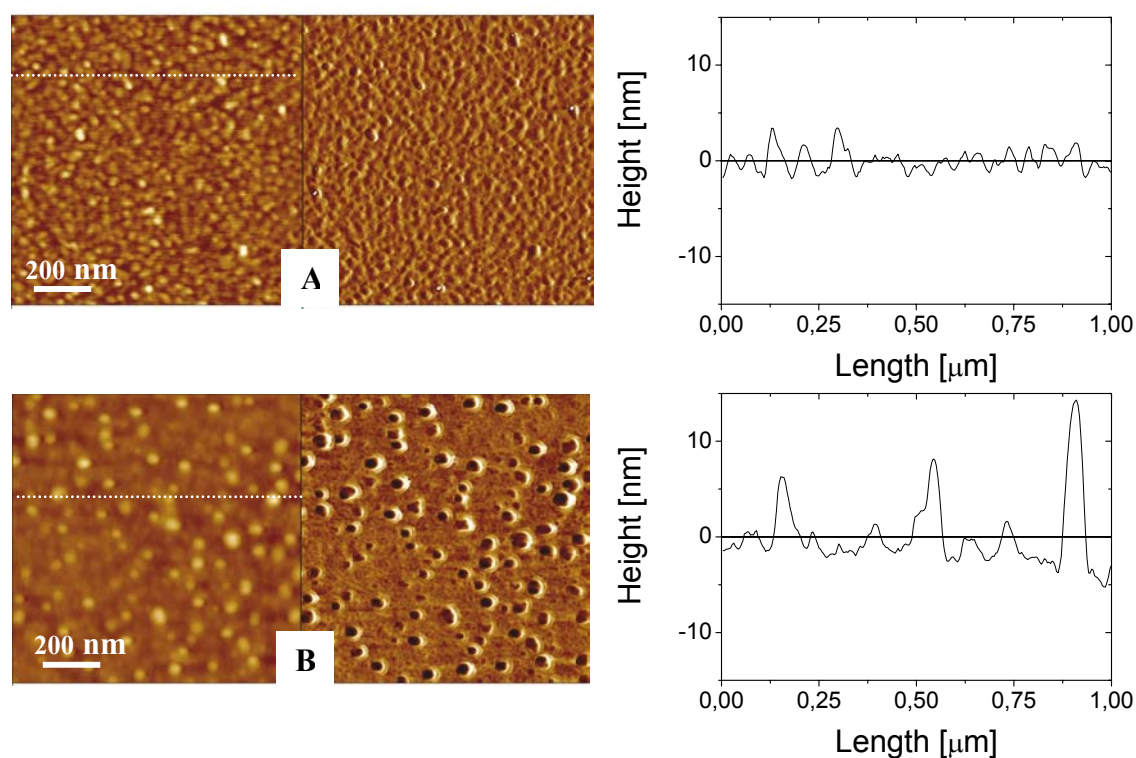

Figure 12.2. 1X1 μm AFM images (left, topography, Z range 30 nm; right, phase) and corresponding cross-sections, representing morphology transition in adsorbed onto PS-P2VP lysozyme layer at pH 4 and varied ionic strength: A) 0.001 M PBS, RMS 1.15 nm, B) 0.01 M PBS, RMS 2.44 nm.

An interesting salt effect was observed by adsorption of lysozyme onto the binary polyelectrolyte brush. Exchanging PS-P2VP with PAA-P2VP, a precondition for a sharper response to the ionic strength changes in the solution occurs. At lower salt content (0.001M), the electrostatic interactions are facilitated. As it is seen in the Figure 12.1a, between both

isoelectric points (pH 4.9-11), a continuously increase of the adsorbed protein amount is in progress. This fact correlates mainly with the switched brushes surface, enriched with dissociated carboxyl groups, and hence, PAA chains swell. The free energy of the system is minimized by charge compensation during the adsorption of opposite charges. In this case, adsorbed protein mass at higher salt concentration is less than that, obtained for lower one. This result can be considered as unexpected, and finds its explanation in the specific nature of the binary polyelectrolyte brush. At lower electrolyte content, the screening of electrostatic attraction between charged species (-COO $^-$) along the brush chains and amino groups of the protein molecules decreases as well. This effect is minimized, when the buffer concentration is increased by factor of ten.

The morphological changes in the adsorbed lysozyme layer are shown on Figure 12.3. It is well seen, that allowing the electrostatic interactions to operate at lower ionic strength, the protein adsorbs in a more extended state than it would at an increased salt concentration, and hence, this corresponds to decreasing the Debye screening length. This effect is visualized by lysozyme adsorption onto PAA-P2VP brush. The pH was kept constant (7.4), for reason to clarify influence of the salt and the brush constituents as well. Adsorbing from 0.001 M PBS, the protein spreads the surface, forming much smoother layer (see RMS values) than from 0.01 M PBS. At the higher ionic strength buffer adsorption, well defined globular-shaped features dominantly occupy the surface, confirming the aggregation and screening effects at the interface.
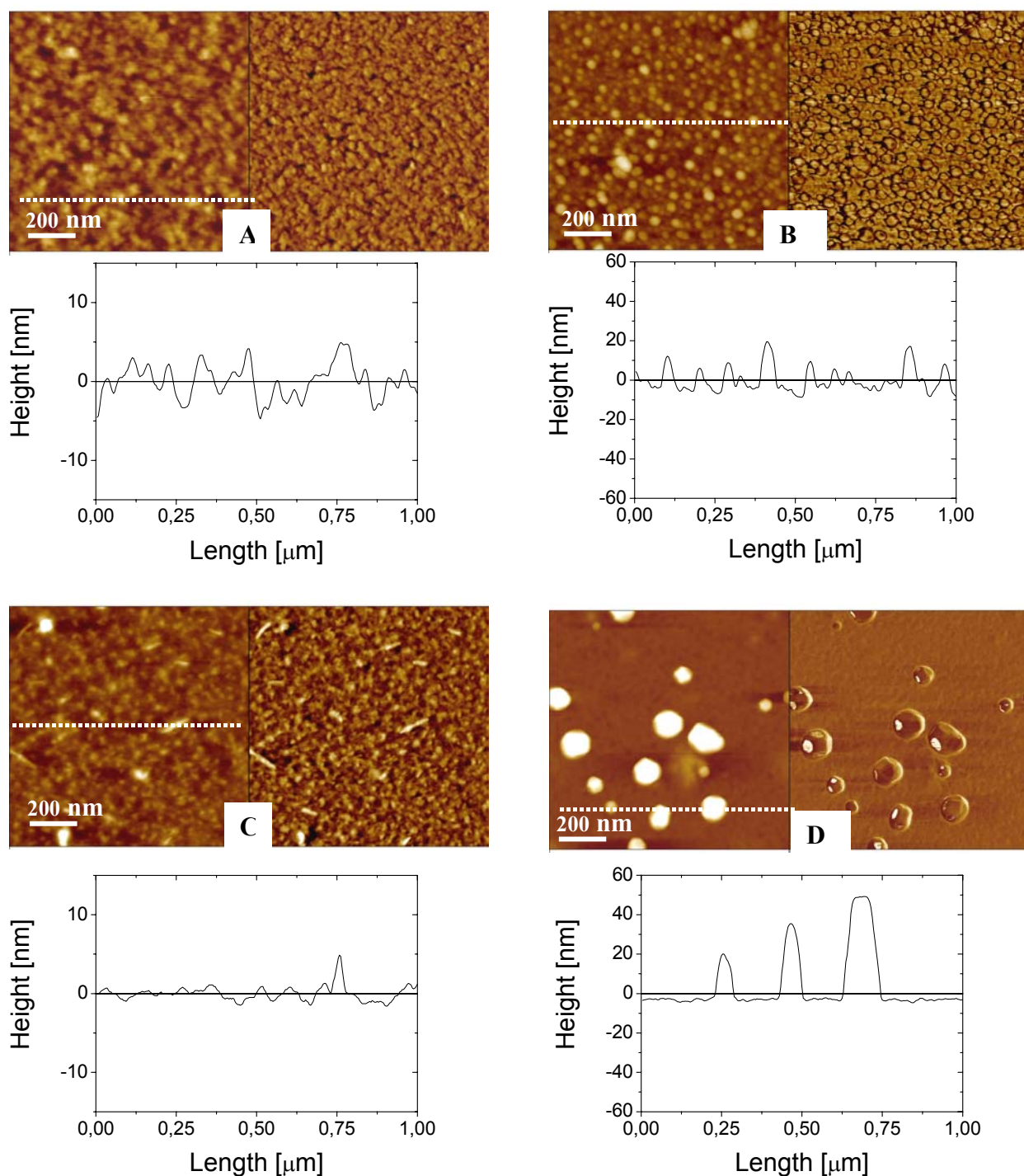
Figure.12.3. 1X1 μm AFM images (left, topography; right, phase) and corresponding cross-sections, representing morphology of adsorbed onto different substrates, at **pH 7.4** and varied ionic strength, lysozyme layer: A) PAA-P2VP, 0.001 M PBS (Z range 30 nm, RMS 1.85 nm) , B) PAA-P2VP, 0.01 M PBS (Z range 120 nm, RMS 5.35 nm), C) PS-P2VP, 0.001 M PBS (Z range 30 nm, RMS 1.24 nm), D) PS-P2VP, 0.01 M PBS (Z range 120 nm, RMS 10.86 nm).

Monitoring the adsorption of BSA onto both brushes and at both ionic strengths, one can observe different adsorption regimes, compared to lysozyme adsorption. The isoelectric points of the substrates are similar to the non-charged state of BSA- at pH 4.7. It imposes likely charged components within the entire range of pH, i.e., overall electrostatic repulsion operates in the system, originating from equal charged adsorbent and adsorbate molecules. This system is appropriate to demonstrate an adsorption against electrostatic repulsive, unfavorable regime.

At buffer concentration of 0.001 M, BSA adsorbs onto PS-P2VP (IEP at pH 5.9) with a weak maximum at pH 4.9- near the protein IEP. The maximum reproduces itself at C_{PBS}=0.01 M as well, confirming the relative inertness of this substrate to the external stimuli. Concerning the adsorbed layer thickness, BSA (likely to lysozyme) adsorbs onto PS-P2VP stronger from 0.01 M PBS medium, than from the dilute one.

The IEP of PAA-P2VP is at 4.9 on the acid/base pH scale. This value repeats the IEP of the protein; hence, the electrostatic repulsive forces remain of the same magnitude over all experimental points. Nevertheless, the adsorption from 0.01 M PBS takes place, even against an unfavorable electric potential and the layer thickness approaches values of around 8 nm. It can be explained in terms of the Gibbs energy of adsorption. From thermodynamic point of view, protein adsorption at constant temperature and pressure is determined by the change in Gibbs energy, which depends on the enthalpy and the entropy of adsorption [Nor00]. In the case of studied proteins, changes in the enthalpy involve repulsive Coulombic interactions and attractive van der Waals forces between protein and interface. Entropic contributions to the Gibbs energy of adsorption originate from hydrophobic dehydration (i.e., displacement of the highly ordered water molecules from hydrophobic surfaces upon adsorption), which make the adsorption possible, even when the protein molecules are repelled by the similarly charged surface. Hence, polyelectrolytes (the surface) and the protein (the adsorbate- a polyelectrolyte as well) can interact even at unfavorable charge signs via non-polar parts of the molecules. Many proteins are able to expose such groups on their surface and this exclusion from solvent provides the basis of the binding energy, i.e. the hydrophobic effect.

Considering the dilute buffer regime, one observes a very poor adsorption over the entire experimental pH scale. The values do not exceed 2 nm and remain constant in this range. At such low ionic strength, both protein-protein and brush-protein repulsions result in a strong expansion of chains in solution, leading to such low surface coverage. A weak adsorption increase can be measured within the neutral pH region, corresponding to non- or slightly charged system components.

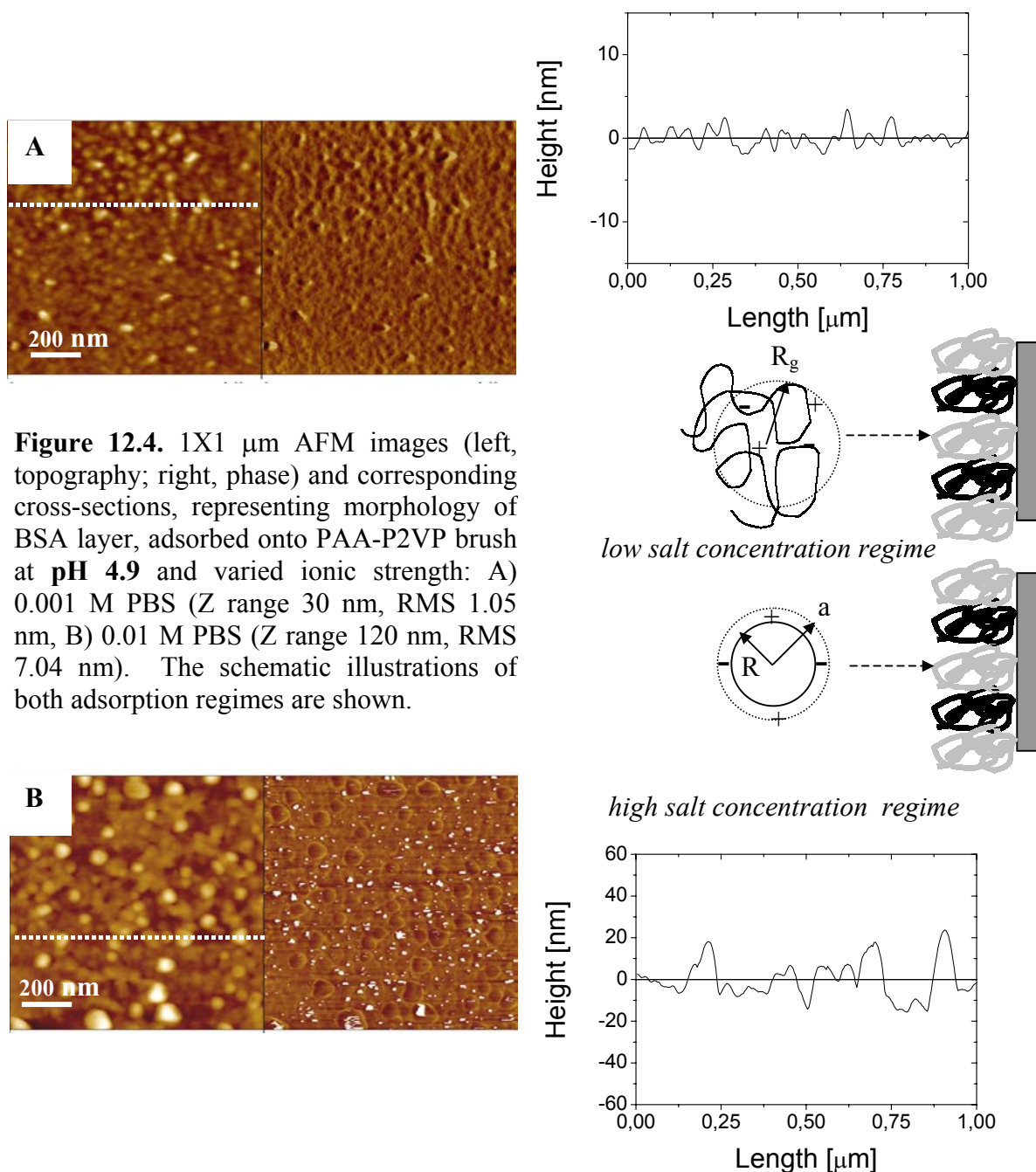Below an example for different interface interactions by surface deposition of BSA is presented.

Figure 12.4. 1X1 μm AFM images (left, topography; right, phase) and corresponding cross-sections, representing morphology of BSA layer, adsorbed onto PAA-P2VP brush at **pH 4.9** and varied ionic strength: A) 0.001 M PBS (Z range 30 nm, RMS 1.05 nm, B) 0.01 M PBS (Z range 120 nm, RMS 7.04 nm). The schematic illustrations of both adsorption regimes are shown.

The next protein under investigation is myoglobin, with IEP at pH 7.2. The PS-P2VP binary brush does not give a remarkable response to myoglobin molecules from 0.001 PBS solutions as it is seen in Figure 12.1c. Adsorbed layer thickness is ca. 2 nm at lower pH and tends to zero, by approaching pH 8.6. At this condition, the reactive protein groups cause an expansion of the protein chains, and do not allow a sufficient access of hydrophobic hydrocarbon part of

the protein molecules to the brush surface. As it was evaluated by the previous experiments (with lysozyme and BSA), by increasing the salt concentration, the adsorbed layer jumped sharply to value of ca. 10 nm at pH 6.5. This point lies in the region, where the surface and the protein are oppositely charged, which results in such maximum.

By replacing again the PS with PAA, the situation changes obviously in respect to the adsorption behavior in the system. Between pH 4.9 and 7.2 the brush carries a negative charge (dominance of dissociated (–COO⁻) groups), whilst the protein is still positively charged, hence, preconditions for electrostatic adsorption are present. As it was shown with both proteins investigated above, the ionic strength and the medium pH strongly affect the adsorption process on such a particular material, as a binary polyelectrolyte brush. At pH 4 (at both ionic strenghts) the layer thickness does not exceed 2 nm, attesting for poorly adsorbed myoglobin, being rejected from the brush surface. A further basification of the medium results in sharp increase in adsorbed layer thickness, reaching a maximum value of 6.6 nm for 0.001 M PBS and 12 nm for 0.01 M PBS, measured at pH 6.5. Between pH 6.5 and 8.6, the adsorbed amount decreases to 1.5 nm for diluted buffer and to 5 nm for the concentrated, 0.01 M PBS, one. The shapes of both curves almost repeat each other, differing only in thickness of deposited protein layer. This obviously defines the influence of salt screening effect in adsorption of proteins, and outlines its quantitative dimensions.

Fibrinogen is a large protein with an IEP at pH 5.5. Intriguing system behavior was observed in Fig. 12.1d, with respect to polymer brush/salt effect on fibrinogen adsorption regime. It occurred that the main qualitative difference is caused by the salt concentration, instead of the substrate type. Diluting the buffer to 0.001 M, the protein follows a similar adsorption performance on PS-P2VP and PAA-P2VP brush substrates. The reason can be the large size of protein molecules (Table 11.2, Chapter 11). At C_{PBS}=0.001 M, the adsorption pattern and the pH effects (i.e. charge of the protein) are in agreement with that of polyampholyte: the adsorbed mass generally is at a maximum around the IEP of the protein/surface complex. At these conditions the charges on the protein and the surface compensate each other. Maxima were measured around pH 6 (17.5 nm for PAA-P2VP and 11 nm for PS-P2VP), where the repulsive Coulombic force regime does not take a part or is sufficiently minimized. A pH adjustment to the acidic or the basic scale drops the adsorption down, and values measured were 2 nm (pH 4) and 4.5 nm (pH 8.6) for PAA-P2VP and 6 nm (pH 4) and 4.5nm (pH 8.6) for PS-P2VP.

Screening the electrostatic interactions by 0.01 M PBS, one turns the driving force to be dominantly hydrophobic for this particular system. The adsorbed amount appeared to be not

that influential by pH variations- evidence for a hydrophobic effect, operating in the system. For PS-P2VP substrate the highest adsorbed layer value was 14 nm at pH 4.9 and drops to 11 nm at pH 8.6. Fibrinogen adsorbs onto PAA-P2VP in a similar way, but the interactions have more pronounced electrostatic contribution. The presence of dissociated PAA in alkali part of the pH scale, results in an unfavorable electrostatic potential, originating from stronger Coulombic repulsion between negatively charged PAA chains and protein molecules. Due to this potential, the hydrophobic surface coupling is not that effective as it was on PS-P2VP brush surface, where no any active to an alkali medium weak polyelectrolyte is presented. Additionally, it is necessary to take into the account the size of the protein molecules, which cannot penetrate trough the inner brush matrix. Since the grafting density of both brushes does not exceed 0.1 nm^{-2}, the grafting distance between two sites on the surface is ca. 3 nm. The sphere based radius of fibrinogen is 10.7 nm, which results in an adsorption only at the upper part of the brush top line. The effect can be illustrated as a "smashing" of the brush chains by the protein sphere (Scheme 12.1d).

12.5. Conclusions.

Tuning the surface performance of a substrate by binary polymer brushes, responsive to media stimuli, was shown to be a powerful and applicable tool for controlling the protein adsorption. The synergic and antagonistic effects by the polymer brush-protein system with variable electrolyte content were investigated. With changing the polarity of the substrate by varying its composition, surface top dominance (by pH), and solution ionic strength one can regulate the adsorption process, qualitatively and quantitatively. At lower salt content, the adsorption dropped approximately by factor of 2 for BSA and myoglobin. Qualitatively, the curves shapes (couple PS-P2VP and couple PAA-P2VP curves) follow similar pH/thickness dependences- a remark for the brush alternative activity, regulating the quantity of deposited proteins by ionic strength variations. Shifting the IEP (myoglobin as an adsorbate) to a neutral water range, a favorable electrostatic potential between substrate IEP and protein IEP occurred and reflected in a well pronounced maximum of protein surface coverage.

Increasing ionic strength enhanced the hydrophobic interactions, such that proteins may bind under high salt and elute under low salt conditions, which allows a strong adsorption behavior even against an electrostatic potential at the "wrong side" of the IEP.

The hydrophobic surfaces and high salt concentration resulted in protein conformational changes and a collapse protein extended structure, as the AFM investigation confirmed. Interaction with hydrophilic water-swollen surfaces at low ionic strengths has small effect on

the secondary structure of investigated proteins, and adsorption proceeds without obvious surface aggregation. The role of polymer brush switching between hydrophilic and hydrophobic state is essential, concerning the interplay of electrostatic, electrodynamic (van der Waals), hydrogen bonds or hydrophobic interactions. In addition, it is a basis for highly specific interactions, depending on geometric factors, conformational state, and environment.

Chapter 13

Control of Protein Adsorption via Compositional Gradients on Polymer Brush Surfaces.

13.1. Introduction.

Polymer brushes composed of two polymers grafted to the same substrate can be manipulated in order to switch the surface dominance by one of the constituents, and on this manner to tune the system properties in an aimed direction. The lateral phase segregation within the grafted layer, as well as perpendicular reorganization of the polymer chains, incompatible in their nature, is the precondition for the switching of the surface properties from hydrophilic to hydrophobic [Sid99, Min03a, Ion03, Min02] and even for a closed hydrophilic-hydrophobic–hydrophilic cycle transition, implied by components specificity (for instance two weak polyelectrolytes) [Hou03]. The segregation is forced by exposure of the mixed polymer brushes to a solvent, selective for one of the polymers [Min03b]. The mixed polyelectrolyte brushes offer possibilities for surface manipulation, since the conformation of tethered polyelectrolyte chains depends strongly on external environment- ionic strength, valence of counterions, pH, and composition.

The behavior becomes more multifaceted, if one is able to create two-dimensional gradients onto a single surface. First dimension (direction) is compositional gradient, whilst the second one may be the thickness, variable between both ends of the substrate. Such a substrate offers wide range possibilities to investigate adsorption of different substances (proteins, particles, synthetic polymers, etc.), using a limited number of samples. The reason is that all possible variations of properties are available on the same substrate, only changing the external conditions. The capability of mixed polystyrene-polyacrylic acid (PS-PAA) gradient polymer brush for switching of wetting behavior and surface charge density, upon change of the pH, was used to control the protein adsorption by the local composition at particular points on the material.

In this chapter, a combinatorial approach for investigating protein adsorption is discussed.

13.2. Experimental.

Synthesis of the substrate is described in details elsewhere [Ion04, Min02]. Gradient brushes consisting of two incompatible polymers, PS and PAA, were prepared via two-step grafting procedure onto thin layer of polyglycidyl methacrylate (PGMA), used as an anchoring agent.

Silicon (Si) wafers (100) with ca. 1.5 nm native SiO_2 layer thickness were obtained from Wacker-Chemitronics. The Si wafers were rinsed several times in dichloromethane in an ultrasonic bath and afterwards placed in cleaning solution of NH_4OH and H_2O_2 for 2 h at 60 °C.

PGMA (M_n=84 000 g/mol) was synthesized by free radical polymerization of glycidyl methacrylate (Aldrich) [Iy03]. The polymerisation was carried out in methyl ethyl ketone (MEK) at 60 °C. Azobisisobutyronitrile (AIBN-Aldrich) was used as an initiator. The obtained polymer was purified by multiple precipitations from MEK solution in diethyl ether.

A thin layer of PGMA (1.5±0.1 nm) was deposited by spin-coating from 0.01% solution in MEK. Afterward, a film of poly(tert-butyl acrylate) (PBA-COOH, M_n =42 000, M_w= 47 000 g/mol) was spin-coated from 2% solution in toluene and annealed for 1 h on a specially designed stage with a 1D gradient of temperature, so that the temperature of the stage changed gradually from 90 °C on the left-hand side of the stage to 130 °C on the right-hand side. The temperature gradient was measured using thermocouples built into the stage. Upon heating, the esterification reaction results in the formation of a grafted PBA layer with a gradient of grafting density caused by a temperature dependence of the grafting kinetics. Epoxy groups of the PGMA anchoring layer react with the end carboxyl groups of the polymer, yielding a layer of tethered chains. The ungrafted polymer was removed using Soxhlet extraction in toluene for 3 h. In the second step, a film of PS-COOH (M_n = 45 900, M_w = 48 400 g/mol) was spin-coated on the top of the gradient PBA brush from 1% solution in toluene. The film was annealed at 150 °C for 8 h to graft PS-COOH. Afterward the ungrafted polymer was removed by Soxhlet extraction in toluene for 4 h. After grafting, PBA was hydrolyzed upon treatment in benzene solution of *p*-toluenesulfonic acid monohydrate at 55 °C for 1 h [Hou03, Chapters 7, 9] to yield polyacrylic acid. The thickness of the mixed brush along the *X*-axis has changed from 2 to about 6 nm (dry film), whilst along the *Y*-axis the layer thickness varied between 2 an 8 nm (Figure 13.1). The region on the sample surface with equal amount of PS and PAA corresponds to a grafting density of ca. 0.1 chains/nm^2.

Bovine serum albumin (BSA-isoelectric point at pH 4.8, Molecular mass 66 700 kg/mol (Table 11.2, Chapter 11)) was chosen for adsorbing protein, because of its medial molecular

size and isoelectric point, near to the IEP of the substrates (~pH 4 at a symmetrical ratio between the components in the brush).

13.3. Results and Discussion.

On the surface section, where the brush is symmetrical, swollen PAA chains preferentially cover the top of the layer at pH 7.4 (experimental condition provided by the phosphate buffered saline (PBS) solution properties). The brush adopts hydrophilic state, committed to the nature of the weak polyelectrolyte PAA, dissociable over pH 3.2 [Hou03]. If the brush is nonsymmetric, i.e., exploring areas far from the sample centre, one observes different switching behavior. Approaching a composition, where the number of grafted PAA chains overcome that of PS, the hydrophilicity is amplifying till the point of fully absence of PS, providing a surface with a contact angle of ca. 45 ^{0} (Figure 8.5a, Chapter 8). The inverse scenario takes place, increasing the amount of the hydrophobic PS. Water is a bad solvent for PS, because of the absence of ionisable groups among its chains. The pure PS brush substrate exhibits approximately constant contact angle value of 87-90 ^{0} (Table 7.2, Chapter 7), not affected by pH. The compositional diagrams and gradient directions, as well as the adsorbed protein map are shown in Figure 13.1.

Regarding the brush composition gradient role in the adsorption process, one can clearly outline three regions of different adsorption regimes. The first one (I), is area with ca. 11 nm adsorbed protein layer, i.e., favourite adsorption conditions, comparing to other two regions (discussed latter). On the compositional maps, one can distinguish, that in this region, PS is the main component composing the brush, as at very end points it is in fact the only one presented. The driving forces then are evaluated to be hydrophobic, because of the absence of ionisable groups at the brush chains. Contrary to an unfavourable electrostatic potential (IEPs at pH 4.3 and 4.7 for PS and BSA respectively), the adsorption takes place, as the adsorbed amount of the protein reveals multi-layered surface packing. This finding confirms investigation of number of researchers, that a protein binds more successively to a hydrophobic surface, than to hydrophilic one, even against an electrostatic repulsive regime, operating in the system [Yoo96].   The second region (II) is nearly symmetric, regarding the ratio between the PS and PAA. The adsorbed protein layer thickness decreases to 7-9 nm, following the decrease of PS fraction within the top surface composition. The PAA chains partially take a control on the surface properties of the brush layer, which results in a hydrophilic surface, repulsing the equally charged protein molecules effectively, vice versa

comparing to the PS component. Despite the antagonistic effect of two oppositely directed forces (diminishing and enabling the protein deposition), adsorption takes place in the system.
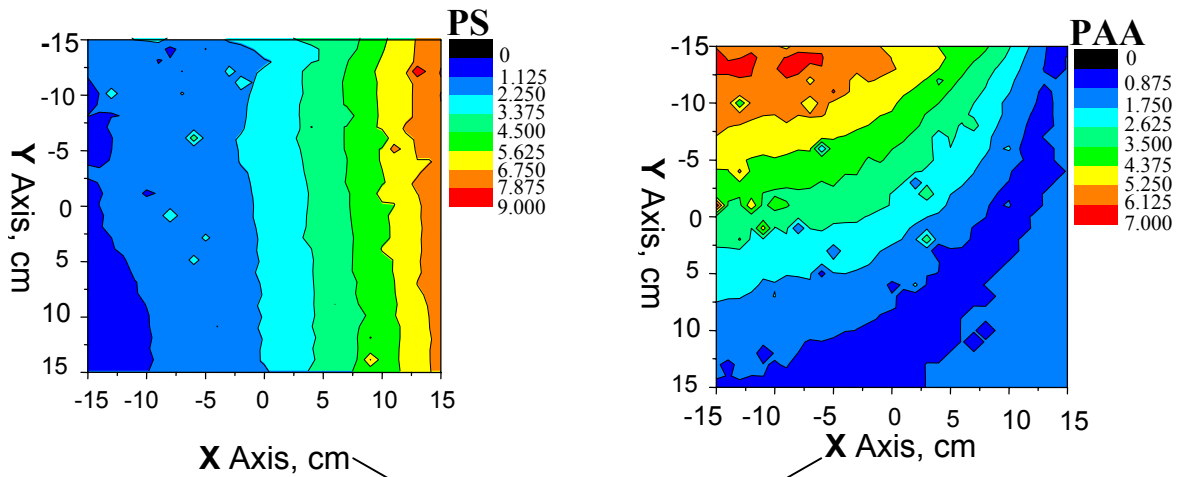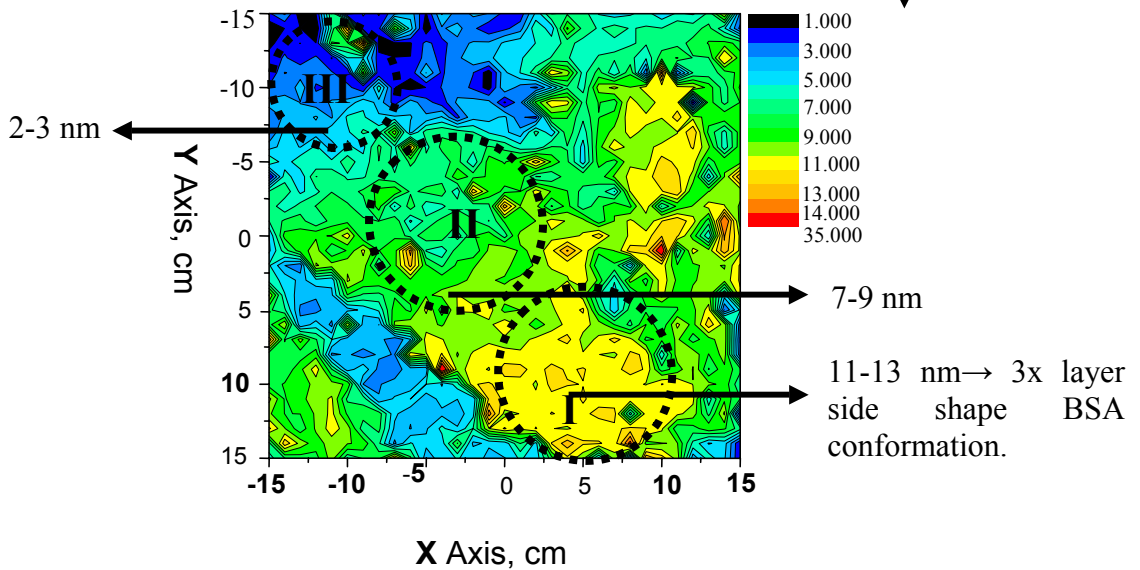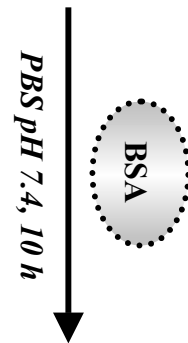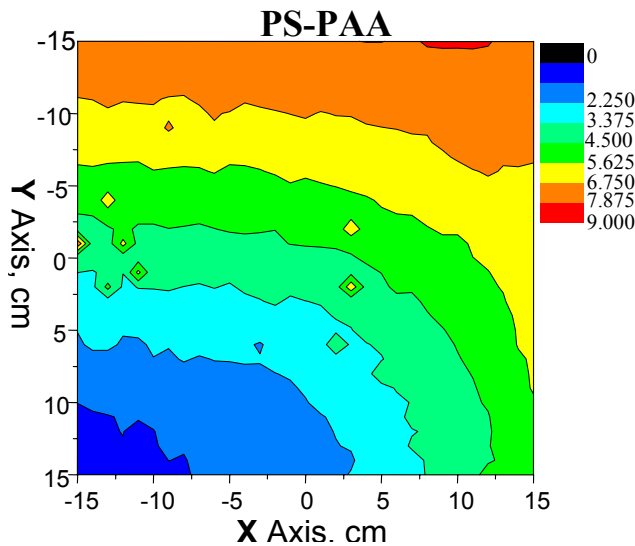
Figure 13.1. Ellipsometric maps of the protein (down) adsorbed onto PS-PAA mixed gradient brush (up). Different colored scales reveal the grafted polymer (PS-PAA) and adsorbed protein layers thicknesses. Numbers I, II and III define different adsorption regimes, and find visualization on microscopic scale in Figure 13.2.

Third region (III) consist of solely PAA component, hence, regarding all results obtained, the surface is repulsive for the approaching protein molecules. IEP of PAA was measured to be at pH 3.2, i.e., at pH 7.4 the brush is sufficiently charged from the dissociated carboxyl groups at the outer part. The repulsive regime brings the system to poor adsorption conditions, leading to an adsorbed layer of 2-3 nm in thickness.

Ellipsometry explorations were supported by AFM visualization of the morphological features, forming the protein layer, deposited onto different brush profiles. Figure 13.2 shows the architecture of adsorbed layers, governed by the brush composition.

The area of strong adsorption (I) represents large cluster-like features, interconnected in continuous lamellar network, almost fully covered the surface. The structures are of larger size than adsorbed on the images II and III. The underlying adsorbent in this case is PS brush (or PS brush with a small amount of PAA). The surface is hydrophobic, which means low surface tension values. The protein molecules, arriving to such a surface, do not change sufficiently their conformation, as they aggregate in large clusters and lamellas. The interaction forces, operating in the system, do not allow the protein to spread out the surface, and to loose its secondary structure. The presence of big aggregates (overcoming the size of the natural BSA molecule) fits to the results, obtained for the same protein, as it adsorbs onto hydrophobic surface at neutral and basic aqueous media (Figure 11.2, Chapter 11; Figure 12.4B, Chapter 12).

In the AFM image II the clusters increase their number at expense of the size. Both phases are presented, namely, round-shaped features and lamellas. This morphology we depict as a transitional between the two limiting cases of solely presented PS or PAA substrates. Since the external conditions (pH 7.4) are not favorable for a complete dissociation of the carboxylic groups at the PAA chains (see Chapter 8), one can assume a hydrophobic contribution to the adsorption, resulting in 7-9 nm adsorbed protein layer.

On the third image, mostly clusters are seen, with a radius differing in some magnitudes of that measured on I and II images. The poor adsorption conditions (strong repulsive electrostatic regime) does not allow the protein molecules to bind to the surface successfully, so they form a thin protein layer, ca. 2 nm, of small globular structures, randomly adsorbed onto the PAA surface. The transition is from large clusters and lamellas (hydrophobic interaction between PS chains and the protein) through medium size protein aggregates, mainly clusters (hydrophobic interaction, electrostatic repulsion) to poorly adsorbed protein molecules, weakly aggregated in small clusters (electrostatic repulsion, weak hydrophobic binding).
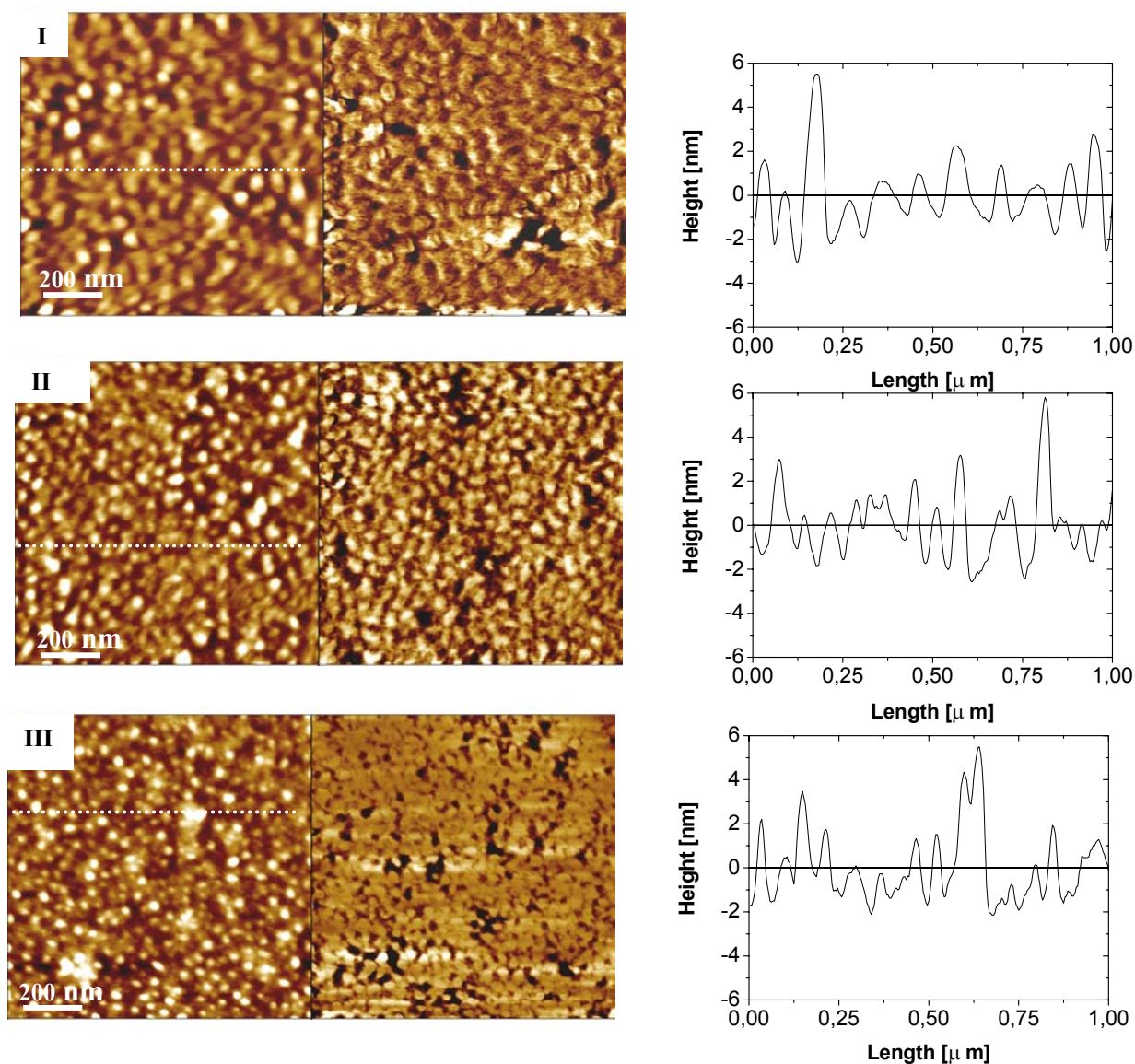
Figure 13.2. AFM images of BSA, adsorbed onto PS-PAA mixed gradient brush. Numbers I, II and III mark the different colored regions (thickness) in the mapping plot 13.1. Left image presents the protein layer topography, whilst the right one is the phase contrast. Graphics on the right side are the cross sections through the height images: RMS; I) 1.3 nm, II) 1.2 nm, III) 1.1 nm.

13.4. Conclusions.

The combinatorial approach for studying protein adsorption was applied to show the advantages, regarding the simplification of the experiment in respect of consumed time and materials. Binary polymer brush was shown to be an appropriate model surface, concerning its ability to switch the surface charge and energetic state. At particular pH point 7.4, we explored the interaction types, responsible for the protein adsorption at different brush components ratio.

Summary

The aim of this thesis is fabrication of materials, which responsive to external stimuli behavior can find application in fields where a fine tuning of interfaces is required. Thin films composed of two polymers grafted by one end to a solid substrate, forming binary polymer brushes, are a very proper candidate for this objective. Their behavior can be easily modeled and interpreted as a function of environmental changes, which is important for a better control of surface and interfacial characteristics of the materials.

Mixed amphiphilic polystyrene-poly(2-vynil pyridine) (PS-P2VP) brushes are an example for responsive class of smart materials, which can switch between hydrophilic and hydrophobic energetic state upon changes in the quality of surrounding media. This material exhibited homogeneity at the macroscopic level, phase segregation ability at the nanoscopic level, and sharp switching capacity as a function of surrounding conditions. Grafting of two incompatible polymers via "grafting to" and "grafting from" the surface approaches, prevented segregation on the macroscopic level.

The switching of wettability was found to operate in a broad range and was selectively controlled in organic solvents, and most importantly, in aqueous solutions, which is as a new aspect of investigation of this material. Film morphology reversibly switches from dimples (perpendicular segregation) in acidic media, when the hydrophilic P2VP occupies the surface, to ripples in neutral and basic media, when the polymers segregate laterally due to the poor solvent conditions for both of them.

Another example for an adaptive/switching behavior is addressed to a polymer brush with a remarkable response to the pH and the ionic strength variations of the aqueous solutions. We succeeded to synthesize for first time a binary polyelectrolyte brush using "grating to" approach, starting from composition of two incompatible polymers, poly(tert-butyl acrylate)-poly(2-vynil pyridine) (PBA-P2VP), and consecutive conversion of the non-polar PBA to polar polyacrylic acid (PAA). Combination of weak polyacid, PAA, and weak polybase, P2VP, in the anchored layer allowed one with a small shift of the pH, to obtain a significant effect on the surface and the interfacial properties of the material. The reversible switching between PAA and P2VP resulted in change of the surface charge, as at particular pH-isoelectric point, the brush formed a collapsed polyelectrolyte complex with zero charge. The switching operates by a preferential swelling of one of the components and results in hydrophilic surface either in acidic and basic media.

The binary polyelectrolyte brush was examined in salted aqueous media, since these are the typical conditions for adsorption of charged polymers and biomolecules. In acidic and basic

aqueous media, the effect of added salt was more obvious, concerning the higher initial swollen state of the brush. The influence of the added salt on the swollen layer thickness was found to be non-monotonic, as a maximum was detected at low salt concentrations.

Different morphologies, generated by solvent quality variation were measured. In poor solvent conditions (neutral and slightly acidic) toroidal structures rising from the tendency of the polymer to exclude the solvent molecules and that way to minimize the surface area, as well as from the collapse of the slightly swollen P2VP chains during the drying. In good solvent conditions for one of the components, acidic or basic water, we measured clustered surface features, typical for perpendicular segregated layers.

Both type of polymer brushes were examined as adsorbing materials for nanoparticles and charged synthetic- and bio-macromolecules. Their adaptive properties were successively linked to the results of the adsorption experiments.

The simplest case was adsorption of nano-particles, functionalised with strong ionic groups, onto binary, PAA-P2VP, polyelectrolyte brushes. Maintaining a constant charge density of the adsorbing component (strong polyelectrolyte effect), allows one to cause and manipulate a privileged swelling of one of the weak polyelectrolyte brush layers (PAA or P2VP), without affecting the adsorbate properties. The adsorption strength increased significantly in that part of the pH scale, where the surface and the particles bear an opposite charge, i.e. the electrostatic interactions were classified as the main driving force in the system. Via switching charge effect, we were able to regulate the thickness of adsorbed layer from zero to an approximately double layer value (in respect to particles diameter), only by the pH signal.

In the case of adsorption of macromolecules with tuneable electrical charge, the system became more complicated, regarding their environmentally responsive properties, similar to that exhibited by the polymer brushes. The driving forces were regulated by the switching performance of the brush, simply by adjusting the pH and/or ionic strength conditions.

The adsorbed amount and morphological changes of polyampholyte dry layers were investigated as function of pH and was performed on mixed amphiphilic and binary polyelectrolyte brushes. The surface charge, energetic state and compositional transformations, affected by the external stimuli and components chemistry, were the major variables of the polymer brushes, used for modelling the interactions within the system. It was found, that between the isoelectric points of the brush substrates and the polyampholyte, the adsorption takes place mostly forced by electrostatic interactions between oppositely charged monomer units along the polymer chains. In most cases maximum was reached near to the

IEP of the polyampholyte. Weak adsorption at pH values where the surface charge has the same sign as the net charge of the polyampholyte was observed as well. Interplay between coulombic and hydrophobic forces in the formation of compact surface structures showed the brush switching to influence significantly the system behavior. A nearly linear increase of the adsorbed amount on PAA-P2VP after its IEP we devote to the swelling of PAA, caused by an increase of charge densities along the chains. This effect was not observed on PS-P2VP amphiphilic brush, since PS is a hydrophobic polymer and P2VP do not swell in alkali medium.

The closeness and the divergence between the structural reorganization of synthetic polyampholytes and proteins at an adsorbing polymer brush interface were investigated in the final part of this thesis. An emphasis was set on the binary brush capability to take the control over the interfacial performance of attaching proteins. It was found, that the sharp environmental response of the adsorbent (the polymer brush) strongly influences the morphology of adsorbed protein layers, their thickness and properties. Keeping one of the variables in the system (brush composition, pH or protein type) constant, we determined the influence of each factor separately. Changing the polarity of the substrate allowed one to regulate the adsorption processes qualitatively and quantitatively. The significant aggregation of protein molecules on PS-P2VP brush in alkali media and their disassembly on PAA-P2VP brush at the same solvent conditions, we devote to the hydrophobic-hydrophilic transition, occurred at the surface by replacing PS with PAA. The protein aggregates, monitored on the surface of PS-P2VP, sufficiently decrease their size, when switching the brush energetic state from hydrophobic to hydrophilic by adjusting the pH of the media. This effect was found to be well controlled by the brush switching phenomenon in hydrophilic-hydrophobic direction and vice versa.

The electrolyte concentration in the buffer solutions was found to play very important role at the brushes-protein interactions as well. The effect was measured to be more pronounced for PAA-P2VP polyelectrolyte brush, since both constituents are weak polyelectrolytes, and hence, influential by the solution ionic strength.

Increasing the ionic strength enhanced the hydrophobic interaction, so that proteins may bind under high salt and elute under low salt concentration conditions. A strong adsorption behavior against an unfavorable electrostatic potential was measured and explained by hydrophobic interaction and surface rearrangement at the interface, as well as inhomogeneous charge distribution at the weak polyelectrolyte chains. The hydrophobic surfaces and high salt concentration resulted generaly in protein conformational changes and aggregation.

Interaction with hydrophilic, water-swollen surfaces at low ionic strengths was measured to have a small effect on the secondary structure of investigated proteins, and adsorption proceeds without obvious surface aggregation.

Further a combinatorial approach for studying protein adsorption was applied to show the advantages, regarding the simplification of the experiment in respect to consumed time and materials. The tendencies observed for symmetrical polymer brushes were confirmed for the gradient brush as well.

In conclusion, we showed how the structural reorganization in thin polymer brush layers of different type might dramatically affect their surface properties. The adaptive behavior in response of external stimuli was found to be a basis for highly specific interactions, depending on geometric factors, conformational state, and environment.

References

[Aks96] Aksay, A.; Trau, M.; Manne, S.; Honma, I.; Yao, N.; Zhou, L.; Fenter, P.; Eisenberger, P.; M.; Gruner, S. M. *Science* **1996**, *273*, 892- 894.

[Ale77] Alexander S. J. *J. Phys (Paris)* **1977**, *38*, 983-987.

[Arai90] Arai, T., Norde, W. *Colloid Surf.*, **1990**, *51*,1.

[Atk90] Atkins, P. W. *Physikalische Chemie*,VCH-Verlag, Weinheim, 2. Aufl., **1990**.

[Azz79] Azzam, R. M. A; Bashara, N. M. *Ellipsometry and Polarized Light*, **1979,** North-Holland Publishing Company, Amsterdam.

[Bar00] Bar, G.; Ganter, M.; Brandsch, R.; Delineau, L. *Langmuir* **2000**, *16*, 5702-5711.

[Barr95] Barrat, J.-L.; Joanny, J.-F. *Adv. Chem. Phys.*, **1995**, *94*, 1.

[Berg97] Berghold, G., van der Schoot, Pm, Seidel, C. *J. Chem. Phys.* **1997**, *107*, 8083.

[Ber98] Berman, A.; Steinberg, S.; Campbell, S.; Ulman, A.; Israelachvili, J. N. *Tribol. Lett.* **1998**, *4*, 43-48.

[Bert00] Bertrand, P.; Jonas, A.; Laschewsky, A.; Legras, R. *Macromol. Rapid Commun.* **2000**, *21*, 319.

[Bie99a] Biesalski, M. ; Rühe, J. *Langmuir,* **1999**, 16, 1943.

[Bie99b] Biesalski, M.; Rühe, J. *Macromolecules* **1999**, 32(7), 2309.

[Bie99c] Biesalski, M.; Rühe, J.; Johannsmann, D. *J. Chem. Phys.* **1999**, 111(15), 7029.

[Bie99d] Biesalski, M.; Johannsmann, D.; Rühe, J. *Macromol. Symp.* **1999**, 145, 113.

[Bie00] Biesalski M.; Rühe J.; *Langmuir*, **2000**, 16:1943.

[Bie02a] Biesalski, M.; Rühe, J. *Macromolecules* **2002**, *35*, 499-507.

[Bie02b] Biesalski, M.; Rühe, J.; Kügler, R.; Knoll, W. Polyelectrolytes at Solid Surfaces. In *Handbook of Polyelectrolytes and Their Applications*; Tripathy, S. K., Kumar, J., Nalwa, H. S., Eds.; *American Scientific Publishers*: San Diego, **2002**; Chapter 2, p 39.

[Bie02c] Biesalski M., Rühe J. *Macromolecules*, **2002**, 3:2309.

[Bie02d] Biesalski M.; Johannsmann, D.; Rühe, J. *J. Chem. Phys.*, **2002**, *117*, 10, 4988.

[Bir00] Birstein, T. M.; Amoskov, V. M. *Polymer Sci.*, **2000**, *C42*, 172.

[Binn86] Binnig, G.; Quate, C. F.; Gerber, Ch. *Phys. Rev. Lett.*, **1986**, *56*, 930.

[Boruk00] Borukhov, I., Andelman, D., Borrega, R., Cloitre, M., Leibler, L., Orland, H. *J. Phys. Chem. B*, **2000**, *104*, 11027 .

[Bli98] Bliznik, V. N.; Everson, M. P.; Tsukruk, V. V. *J. Tribology*, **1998**, *120*, 489.

[Born85] Born, M. *Optik*, **1985,** Springer-Verlag, Berlin.

[Böhm97] Böhm N. and Kulicke W.-M. Colloid Polym. Sci., **1997**, *275*, 73.

[Blaw98] Blawas, A. S.; Reichert, W. M. *Biomaterials* **1998**, *19*, 595-609.

[Bra85] Brash J. D., Protein Adsorption:, *Surface and Interfacial Aspects of Biomedical Polymers*, Vol. 2, Plenum, New York, NY, **1985**.

[Bro94] Brown, G.; Chakrabarti, A.; Marko, J. F. *Europhys. Lett.* **1994**, *25*, 239-244.

[Bru97] Bruening, M. L.; Zhou, Y.; Aguilar, G.; Agee, R.; Bergbreiter, D. E.; Crooks, R. M. *Langmuir* **1997**, *13*, 770.

[Cag01] Cage R. A.; Currie, E. P. K.; Cohen Stuart, M. A. *Macromolecules,* **2001**, *34*, 5078.

[Cast00] Castelnovo, M., Sens, P., Joanny, J.-F. *Eur. Phys. J. E 1*, **2000**, 115.

[Caz87] Cazabat, A.-M., How does a droplet spread ?, *Contemp. Phys.*, **1987**,28, 347-367.

[Che97] Chen, C. S.; Mrksich, M.; Huang, S.; Whitesides, G. M.; Ingber, D. G. *Science (Washington, D.C.)* **1997**, *276*, 1425-1428.

[Coh91] Cohen Stuart, M. A.; Fleer, G. J.; Lyklema, J.; Norde, W.; Scheutjens, J. M. H. M;. *Adv. Coll. Interf. Sci.*, **1991**, *34*, 477.

[Court94] Courtney, J. M.,; Lambda, N. M. K.; Sundaram, S; Forbes, C. D. *Biomaterials*, **1994**, *15*, 737.

[Creu97a] Creutz S., Teyssie P., Jerome R., **1997**, *Macromolecules*, 30, 6.

[Creu97b] Creutz S., Stam J., Antoun S., De Schryver F. C., Jerome R., **1997** , *Macromolecules*, 30, 4078.

[Dau94] Dautzenberg H., Jaeger W., Kötz, Philipp B., Siedel C., Stscherbina D. *Polyelectrolytes*, Hanser Publishers, Münich, **1994**.

[Daw99] Dawson, K. A.; Timoshenko, E. G. and Y. A. Kuznetsov, *Physica A* 236, 58 (1997).

[Di99] Digital instruments, Veeco Metrology Group, *Training Notebook*, **1999**, rev. 3.0.

[Dub99] Dubas, S. T.; Schlenoff, J. B. *Macromolecules* **1999**, *32*, 8153.

[Ebe93] Ebert, G. *Biopolymere*, **1993**, Teubner, Stuttgart.

[Elb96] Elbert, D. L.; Hubbell, J. A. *Annu. Rev. Mater. Sci.* **1996**, *26*, 365.

[Eir77] Eirich, F. R. *J. Coll. Interf. Sci.*, **1977**, *58*, 423.

[Erb93] Erb, V. Reaktionen von Polystyrolanionen an Siliziumdioxid- und silanisierten Siliziumdioxidoberflächen, Diplomarbeit, , **1993,** Universität Mainz.

[Erb97] Erb, V. *Filmbildung von endfunktionalisierten Gruppen,* Dissertation, **1997,** Universität Mainz.

[Eve86] Evers, O. A.; Fleer, Scheutjens, G. J.; J. M. H. M.; Lyklema, J. *J. Coll. Interf. Sci.*, **1986**, 111, 446.

[Fahr61] Fahrenfort, J. *Spectrochim. Acta*, **1961**, *17*, 698.

[Fen95] Feng, L.; Andrade, J. D. In *Proteins at Interfaces II, Fundamentals and Applications*; Horbett, T. A., Brash, J. L., Eds.; American Chemical Society: Washington D.C., **1995**; Vol. 602 ACS Symposium Series; pp 66.

[Fish99] Fisher, P.; Laschewsky, A.; Wischerhoff, E.; Arys, X.; Jonas, A.; Legras, R. *Macromol. Symp*. **1999**, *137*, 1.

[Fle93] Fleer, G.J.; Cohen Stuart, M.A.; Scheutjens, J.M.H.M.; Cosgrove, T.; Vincent, B. *Polymers at Interfaces,* **1993**, (Chapman & Hall, London, Glasgow, New York, Tokyo, Melbourne, Madras).

[Flo81] Flory, P. J. Principles of polymer chemistry. Ithaka, Ny: Cornell University press, **1981**.

[För95] Förster, S.; Schmidt, M. *Adv. Polym. Sci.*, **1995**, 120, 133.

[From92] Frommer, J. *Angew. Chem*., **1992**, *104*, 1325.

[Gen76] de Gennes, P. G. *J. Phys. (Paris)* **1976**, *37*, 1445.

[Gen80] de Gennes, P. J. *Macromolecules* **1980**, *13*, 1069-1075.

[Gen85a] de Gennes, P. G., Wetting: Statics and Dynamics, *Reviews of Modern Physics*, **1985**, 57, 827-863.

[Gen85b] de Gennes, P. G. *J. Phys. Lett*. **1985,** 46, 639.

[Gert93] Gerthsen, C. ; Vogel, H. *Physik*, **1993** Springer-Verlag, Berlin.

[Göp94] Göpel, W.; Ziegler, C. *Struktur der Materie: Grundlagen, Mikroskopie und Spektroskopie*, Teubner Verlag, Stuttgart, **1994.**

[Goe94] von Goeler, F.; Muthukumar, M. *Macromolecules* **1994**, *27*, 7085.

[Grah48] Grahame, D. C. *J. Chem. Phys.*, **1948**, 16, 1117

[Grau99]Graul, W. G.; Li, M.; Schlenoff, J. B.*J. Phys*. *Chem*. *B* **1999**, *103*, 2718.

[Gray04] Gray, J. J. *Current Opinion in Structural Biology*, **2004**, *14*,110–115.

[Gru01] Grundke., K: *Handbook of Applied Surface and Colloid Chemistry (K. Holmberg, Ed.)*, **2001**, Vol. 2, Chapter 7: Wetting, Spreading and Penetration, pp. 119-142.

[Guo99] Guo, X.; Weiss, A.; Ballauff, M. *Macromolecules* **1999**, *32*, 6043- 6046.

[Hab99] Habicht, J.; Schmidt, M.; Rühe, J.; Johannsmann, D. *Langmuir* **1999**, *15*, 2460-2465.

[Halp92] Halperin, A.; Tirrell, M.; Lodge, T. P. *Adv. Polym. Sci.* **1992**, *100*, 31-71.

[Halp99] Halperin, A. *Langmuir* **1999,** *15,* 2525-2533

[Halp00] Halperin, A. and Goldbart, P. *Phys. Rev. E*. **2000** 61, 565.

[Harr92] Harris, J.M., editor Poly(ethyleneglycol) chemistry: *Biotechnical and Biomedical*

Applications, **1992**, Plenum Press, NY.

[Hart92] Hartmann, U. *Ultramicroscopy*, **1992**, *59*, 42 – 44.

[Herr87] Herren, B. J.; Shafer, S. G.; Alstine, J. van; Harris, J. M. and Snyder, R. S. *J. Colloid Interface Sci.* **1987**, 115, 46-55.

[Hess91] M. Hesse, H. Meier, B. Zeeh, *Spektroskopische Methoden in der organischen Chemie*, Thieme Verlag, Stuttgart, 4. Aufl., **1991**

[Hol98] Holm, C.; Kremer, K.; Vilgis, T. A. *Phys. Bl.*, **1998**, *54*, 1013.

[Hoo96] Hoogeveen, N. G.; Cohen Stuart, M. A.; Fleer, G. J. *J. Colloid Interface Sci.*, **1996**, *182*, 146

[Hor95] Horbett T. A., Brash J. L., Proteins at Interfaces: *Physicochemical and Biochemical Studies: ACS Symp. Ser.* **1995**, 602, 1.

[Hou03] Houbenov, N; Mnko, S.; Stamm, M. *Macromolecules*, **2003,** *36,* 5897-5901.

[Hu92] Hu, S.-G., Do D.D. and Hossain Md.M., *J. Chrom.* **1992**, 605, 175.

[Hubb95] Hubbell, J. A. *Bio-Technol.* **1995**, 13, 565.

[Hub03] Huber, D. L.; Manginell, R. P.; Samara, B.-I. Kim, and Bunker, B. C. *Science*, **2003,** *301*.

[Huss00]Husseman, M.; Benoit, D. G.; Frommer, J.; Mate, M.; Hinsberg, W. D.; Hendrick, J. L.; Hawker, C. J. *J. Am. Chem. Soc.* **2000**, *122*, 1844-1845.

[Ion03] Ionov, L.; Minko, S.; Stamm M.; Gohy, J.-F.; Jérôme, R.; Scholl, A. *J. Am. Chem. Soc.* **2003**, *125*, 8302 – 8306.

[Ion04] Ionov, L.; Zdyrko, B.; Sidorenko, A.; Minko, S.; Klep, V.; Luzinov I.; Stamm, M. *Macromol. Rapid Comm.* **2004**, *25*, 360 - 365.

[Isra94] Israels, R.; Leermakers, F.A.M.; Fleer, G.J. *Macromolecules* **1994**, *27*, 3087.

[Iy03] Iyer, K. S.; Zdyrko, B.; Malz, H.; Pionteck, J.; Luzinov, I. *Macromolecules* **2003**, *36*, 6519-6526.

[Jac84] Jacobasch, H.-J. *Oberflächenchemie faserbildender Polymerer*, **1984**, Akamedie-Verlag, Berlin.

[Jac96] Jacobasch, H.-J.; Simon, F.; Werner, C.; Bellmann, C. *Technisches Messen*, **1996**, *63*, 447

[Jeo91a] Jeon, S. I; Lee, J. H.; Andrade, J. D.; de Gennes, P-G *J. Colloid Interface Sci.,* **1991,***142,* 149.

[Jeo91b]Jeon, S. I; Lee, J. H.; Andrade, J. D. *J. Colloid Interface Sci.,* **1991,** *142***,** 159.

[Jon49] Jones, R. C. *J. Opt. Soc. Am.*, **1949**, *16*, 488.

[Kat47] Katchalsky, A. Spitnik, P. *J. Polym. Sci.* **1947**, 2, 432.

[Kle94] Klein, J.; Kumacheva, E.; Mahalu, D.; Perahia, D.; Fetters, L. J. *Nature* **1994**, *370*, 634-636.

[Kno01] Knoll, A.; Magerle, R.; Krausch, G. *Macromolecules* **2001**, *34*, 4159-4165.

[Kopp00] Kopp-Marsaudon, S.; Leclère, P.; Dubourg, F.; Lazzaroni, R.; Aime, J. P. *Langmuir* **2000**, *16*, 8432-8437.

[Kot98] Kotov, N. A.; Magonov, S.; Tropsha, E. *Chem. Mater.* **1998**, *10*, 886.

[Kud99] Kudaibergenov S. E. Adv. Polym. Sci., **1999**, *144*, 115.

[Lah03] Lahann J., *Science*, **2003,** 299, 371.

[Lai92] Lai, P.-Y.; Binder, K. *J. Chem. Phys.* **1992**, *97*, 586-595.

[Lai94] Lai, P.-Y. *J. Chem. Phys.* **1994**, *100*, 3351-3357.

[Las93] Lasic, D. D. *Liposomes: From Physics to Applications*; Elsevier: Amsterdam, **1993**.

[Las96] Lasic, D. D.; Papahadjopoulos, D. *Curr. Opin. Solid State Interface Sci.* **1996**, *1*, 392.

[Lee95] Lee, J. H.; Lee, H. B.; Andrade, J. D. *Prog. Polym. Sci.* **1995**, *20*, 1043.

[Lee02] Lee, K.-B.; Park, S.-J.; Mirkin, C. A.; Smith, J. C.; Mrksich, M. *Science (Washington, D.C.)* **2002**, *295*, 1702-1705.

[Leg92] Leger, L., Joanny, J.-F., Liquid Spreading, *Rep. Prog. Phys.*, **1992** 55, 431-486.

[Lem03] Lemieux, M.; Usov, D.; S. Minko, , M. Stamm, H. Shulha, and Tsukruk, V. V. *Macromolecules* **2003,** *36,* 7244-7255.

[Li95] Li, Y. and Pinto N.G., *J. Chrom.*, **1995**, A 702, 113.

[Ley64] Leyte, J. C.; Mandel, M. *J. Polym. Sci. A*, **1964**, *2*, 1879.

[Luz04] Luzinov, I.; Minko, S.; Tsukruk, V. V. *Prog. Polym. Sci.* **2004**, *29*, 635-698.

[Ma01] Ma H., Hyun J., Nath N., Chilkoti A. *European Cells and Materials*, *6*, Suppl. 1, **2001**, 16

[Mag97] Magonov, S. N.; Cleveland, J.; Elings, V. *Surf. Sci.* **1997**, *389 (Nov 6)*, 201-211.

[Mah00] Maheshwari; G.; Brown, G.; Lauffenburger, D. A.; Wells, A.; Griffith, L. G. *J. Cell Sci.* **2000**, *113*, 1677-1686.

[Mahl99] Mahltig B. Walter H., Harrats Ch., Müller-Buschbaum P., Jerome R., Stamm M. *Phys. Chem. Chem. Phys.*, **1999**, *1*, 3853

[Mahl00] Mahltig B., Gohy J.-F., Jerome R., Bellmann C., Stamm M. *Colloid Polym. Sci.* **2000**, 278, 502.

[Mahl01a] Mahltig B., Gohy J.-F., Jerome R., Stamm M. *J. Polym. Sci. B: Polym. Physics*, **2001**, *39*, 709.

[Mahl01b]Mahltig B., Müller-Buschbaum P., Wolkenhauer M., Wunicke O., Wiegand S., Gohy J.-F., Jerome R., Stamm M. *J. Colloid Int. Sci.*, **2001**, *242*, 36.

[Malm99] Malmsten, M. In *Biopolymers at Interfaces*; Malmsten, M., Ed.; Surfactant Science Series; Marcel Dekker: New York, **1999**.

[Man70] Mandel, M. *Europ. Polym. J.*, **1970**, *6*, 807.

[Man88] Mandel, M. in *Encyclopedia of Polymer Science and Engineering*, **1988**, edited by Mark, H.F.; Bikales, N.; Overberger, C.G.; Menges, G.; Kroschwitz, J.I. 2nd edition, Vol. 11 (J. Wiley, New York,) p. 739.

[Mans97] Mansky, P.; Liu, Y.; Huang, E.; Russell, T. P.; Hawker, C. J. *Science* **1997**, *275*, 1458-1460.

[Mar91] Marko, J. F.; Witten, T. A. *Phys. Rev. Lett.* **1991**, *66*(11), 1541-1544.

[Mart03] Martins M.C.L, Wang D., Jia J., Feng L., Barbosa M.A., *Biomaterials*, 24, **2003**, 2067-2076.

[Mat94] Matsen, M. W.; Schick, M. *Phys. Rev. Lett.* **1994**, *72*, 2660-2663.

[McDon00] McDonald J. C., *Electrophoresis*, **2000**, 21, 27.

[McPher98] McPherson, T.; Kidane, A.; Szleifer, I.; Park, K. *Langmuir* **1998**, *14*, 176-186.

[Mil88] Milner, S. T.; Witten, T. A.; Cates, M. E. *Macromolecules* **1988**, *21*, 2610-2619.

[Mil89] Milner, S. T.; Witten, T. A.; Cates, M. E. *Macromolecules* **1989**, *22*, 853-861.

[Mil91] Milner, S. T. *Science* **1991**, *251*, 905

[Min99] Minko, S.; Gafijchuk, G.; Sydorenko, A.; Voronov, S. *Macromolecules* **1999**, 32, 4225.

[Min00a] Minko, S.; Sidorenko, A.; Goreshnik, E.; Usov, D.; Stamm, M. *Amer. Chem. Soc. Polym. Mater. Sci. Eng.* **2000**, *83*, 448-449.

[Min00b] Minko, S.; Stamm, M ; Goreshnik, E.; Usov, D.; Sidorenko, A. *Amer. Chem. Soc. Polym. Mater. Sci. Eng.* **2000**, *83*, 533-534.

[Min01] Minko, S.; Usov, D.; Goreshnik, E.; Stamm, M. *Macromol. Rapid Commun.* **2001**, *22*, 206.

[Min02a] Minko, S.; Patil, S.; Datsyuk, V.; Simon, F.; Eichhorn, K.-J.; Motornov, M.; Usov, D.; Tokarev, I.; Stamm, M. *Langmuir* **2002**, *18*, 289.

[Min02b] Minko, S.; Müller, M.; Usov, D.; Scholl, A.; Froeck, C.; Stamm, M. *Phys.Rev.Lett.* **2002**, *88*, 035502-1 -035502-4.

[Min03a] Minko, S.; Müller, M.; Motornov, M.; Nitschke, M.; Grundke, K.; Stamm, M. *J. Am. Chem. Soc.* **2003**, *125*, 3896.

[Min03b] Minko, S.; Usov, D.; Luchnikov, V.; Müller, M.; Ionov, L.; Scholl, A.; Pfütze, G.; Stamm, M. *Polymer Preprints* **2003**, *44*(1), 478.

[Min03c] Minko, S., Luzinov, I., Luchnikov, V., Marcus, M., Patil, S., and Stamm, M. *Macromolecules* **2003,** *36,* 7268-7279.

[Mir95] Mir Y., Auroy P Auvray. L., *Phys. Rev. Lett.* **1995**, 75:2863.

[Mis89] Misra, S.; Varanasi, S.; Varanasi, P. P. *Macromolecules* **1989**, *22*, 4173.

[Mots] Motschmann, H. *Aufbau eines Ellipsometers zum Studium von Monoschichten an der Wasser Luft-Grenzfläche und Adsorptionsprozesse aus Lösung von Blockcopolymeren,* Dissertation, **1991**, Universität Mainz.

[Mül93] Müller, M.;*Grenzen und Möglichkeiten der Infrarotspektroskopie bei der Sekundärstrukturanalyse von Proteinen und Peptiden,*Dissertation, **1993** ETH Zürich.

[Mül96] Müller, M.; Werner, C.; Grundke, K.; Eichhorn, K. J.; Jacobasch, H.-J. *Macromol. Symp.*, **1996**, *103*, 55.

[Mül97] Müller, M. ; Schmitt, F.-J. *Macromol. Symp.*, **1997**, *119*, 269.

[Mül02] Müller, M. *Phys. Rev. E.* **2002**, *65*, 030802(R).

[Murp00] Murphy, E. F., Lu, J. R., Lewis A. L., Brewer J., Russell, J., Stratford, P. Macromolecules, **2000**, *33*, 4545.

[Nash91] Nashabeh, W. and Rassi, Z. E. *J. of Chrom.* **1991**, 559, 367-383.

[Nor95] Norde W., *Cell Mater.* **1995**, 5, 97.

[Nor00] Norde, W. *Phys. Chem. Bio. Inter.* **2000** , 115-135, Marcel Dekker, NewYork.

[Niu98] Niu, Q. J.; Frechet, J. M. *Angew. Chem., Int. Ed. Engl.* **1998**, *37*, 667-670.

[Odi78] Odijk, T.; Houwaart, A. C. *J. Polym. Sci.: Polym. Phys. Ed.*, **1978**, *16*, 627.

[Ohl96] Ohlemacher A., Candau F., Munch J. P., Candau S. J., J. Polym. Sci., **1996,** *34*, 2747

[Pin91] Pincus, P. *Macromolecules* **1991**, *24*, 2912.

[Prokh03] Prokhorova, S. A., Ramakrishnan, A., Zhang H., Rühe, J. *Nanotechnology* 14 (October **2003**) 1098-1108.

[Pru98] Prucker, O; Rühe, J *Macromolecules*, **1998**, 31, 602.

[Raph90] Raphael, E.; Joanny, J.-F. *Europhys. Lett*. **1990**, 13, 623.

[Raph92] Raphael, E.; de Gennes, P. G. *J. Phys. Chem.* **1992**, *96*, 4002- 4007.

[Rech88] Rechnitz G. A., *Chem. Eng. News* **1988**, 66(36), 24.

[Röm94] Römer, H. *Theoretische Optik*, **1994,** VCH-Verlag, Weinheim

[Ross92] Ross, R. S.; Pincus, P. *Macromolecules* **1992**, *25*, 2177.

[Roth93] Roth, C.M. andLenhoff A.M., *Langmuir* 9, **1993**, 962

[Roth96] Roth, C.M., Unger K.K. and Lenhoff A.M., *J. Chrom. A*, **1996**, 726, 45.

[Row82] Rowlinson, J., Widom*, B*, Molecular Theory of Capillarity, Oxford University Press, Oxford, **1982**.

[Russ02] Russell, T. P. *Science* **2002**, *297*, 964-967.

[Ruth00] Ruths, M.; Johannsmann, D.; Rühe, J.; Knoll, W. *Macromolecules*, **2000**, *33*, 3860-3870.

[Rüh00] Rühe J., Knoll W. (Ciferri A.) Supramolecular Polymers. **2000** Dekker New York

[Sak02] Sakaue, T. and Yoshikawa, K. *J. Chem. Phys* **2002**, 117(13):6323-6330.

[San91] Sandu C., Singh R. K., *Food Technol.* **1991**, 45, 84.

[Schle01] Schlenoff, J. B.; Dubas, S. T. *Macromolecules* **2001**, *34*, 592.

[Scho97] van der Schoot, P. Langmuir **1997**, 13, 4926.

[Schnu00] Schnurr, B.; Mackintosh, F. C. and Williams, D. R. M. *Europhys. Lett.* **2000**, 51(3):279-285.

[Schnu02] Schnurr, B. Gittes, F. and MacKintosh, F. C. *Phys. Rev. E.* **2002**, 65*, 061904*

[Sem75] Semenov, A. N. *Sov. Phys. JETP*, **1975**, 61, 733.

[Sev96] Sevick, E. M. *Macromolecules* **1996,** *29,* 6952-6958

[Shu01a] Shusharina, N. P.; Linse, P. *Eur. Phys. J. E* **2001**, *6*, 147.

[Shu01b] Shusharina, N. P.; Linse, P. *Eur. Phys. J. E* **2001**, *4*, 399.

[Sko77] Skolnick, J.; Fixman, M. *Macromolecules*, **1977**, *10*, 944.

[Sog96] Soga, K. G.; Zuckermann, M. J.; Guo, H. *Macromolecules* **1996**, *29,* 1998-2005.

[Sof98] Sofia, S. J.; Premnath, V.; Merrill, W. *Macromolecules*, **1998**, *31*, 5059

[Stahl92] Ståhlberg, J., Jönsson, B. and Horváth, C., **1992**, *Anal. Chem.* 64, 3118.

[Stam92] Stamm, M. *Adv. Polym. Sci.*, **1992**, *100*, 357

[Stry91] Stryer, L.*Biochemie*, **1991**, Spektrum Verlag, Heidelberg, 4. Aufl.

[Styr] Styrkas, D.A.; Bütün, V;Lu, J.R.; Keddie, J.L.; Armes, S.P. *Langmuir*, **2000**,16, 5980.

[Sukhish99] Sukhishvili S., Granick S. *Journal of Chemical Physics*, *110* (20), **1999,** 10155.

[Sukhor96] Sukhorukov, G. B.; Mohwald, H.; Decher, G.; Lvov, Y. M. *Thin Solid Films* **1996**, *284-285*, 220.

[Syd99] Sydorenko, A.; Minko, S.; Schenk-Meuser, K.; Duschner, H.; Stamm, M. *Langmuir*, **1999**, 15, 8349-8355.

[Szle96] Szleifer, I.; Carignano, M. A. *Adv. Chem. Phys.* **1996**, *94*, 165.

[Tam96] Tamayo, J.; García, R. *Langmuir*, **1996**, *12*, 4430.

[Tha00] Thao, B.; Brittain, W. J. *Prog. Polym. Sci.* **2000***, 25*, 677-710.

[Tran99a] Tran Y Auroy P Lee LT *Macromolecules* **1999**, 32:8952.

[Tran99b] Tran Y, Auroy P, Lee LT, Stamm M *Phy.s Rev. E.* **1999**, 60:6984

[Tran01] Tran Y, Auroy P *J. Am. Chem. Soc.* **2001**, 123:3644

[Tomp93] Tompkins, H. G. *A User´s Guide to Ellipsometry*, **1993,** Academic Press, San Diego.

[Tsuk97] Tsukruk, V. V. *Rubber Chemistry and Technology,* **1998**, *14*, 446.

[Tsuk98] Tsukruk, V. V.; Bliznyuk, V. N. *Langmuir*, **1996**, *12*, 4430.

[Tsuk00] Tsukruk, V. V.; Wahl, K. Microstructure and Microtribology of Polymer Surfaces, ACS Symposium Series, **2000**, v 741.

[Urb93] Urban, M. W. Vibrational spectroscopy of molecules and macromolecules on surfaces,

1993,Wiley, New York.

[Uso02] Usov, D.; Stamm, M.; Minko, S.; Froeck, C.; Scholl, A.; Müller, M. *Nanostructured Interfaces*, R2.5., Editors: G. Duscher, J.M. Plitzko, Y. Zhu, H. Ichinose. *MRS Proceedings* **2002**, v. 727.

[Wan88] Wang, L.; Yu, H. *Macromolecules*, **1988**, *21*, 3498.

[Wal94] Walsh G., Headon, D. *Protein Biotechnology* (Wiley, New York, **1994**), 73.

[Zaj95] Zajac R., Chakrabarti A., *Phys. Rev. E.* **1995**, 52:6536.

[Zer94] Zerushalmi-Royen, R.; Klein, J.; Fetters, L. *Science* **1994**, *263*, 793-795.

[Zha00] Zhao, B.; Brittain, W. J. *Prog. Polym. Sci.* **2000**, *25*, 677.

[Zhu95] Zhulina, E.B.;. Birshtein, T.M; Borisov, O.V. *Macromolecules* **1995**, 28, 1491.

[Zhu96a] Zhulina, E.; Balazs, A. C. *Macromolecules* **1996**, *29*, 2667.

[Zhu96b] Zhulina, E. B.; Singh, C.; Balazs, A. C. *Macromolecules* **1996**, *29*, 6338.

[Zhu96c] Zhulina, E. B.; Singh, C.; Balazs, A. C. *Macromolecules* **1996**, *29*, 8254.

[Zhu97] Zhulina, E. B. and Borisov, O. V. *J. Chem. Phys.*, **1997***,*107, 5952.

[Zit02] Zito, T.; Seidel, C.; Eur. Phys. J. E, **2002**, 8, 339–346.

[Yan97] Yang Z. and Yu H., *Adv. Mater.* **1997**, 9, 426-429 James, E.A. and Do D.D., *J. Chrom.*, **1991**, 542, 19.
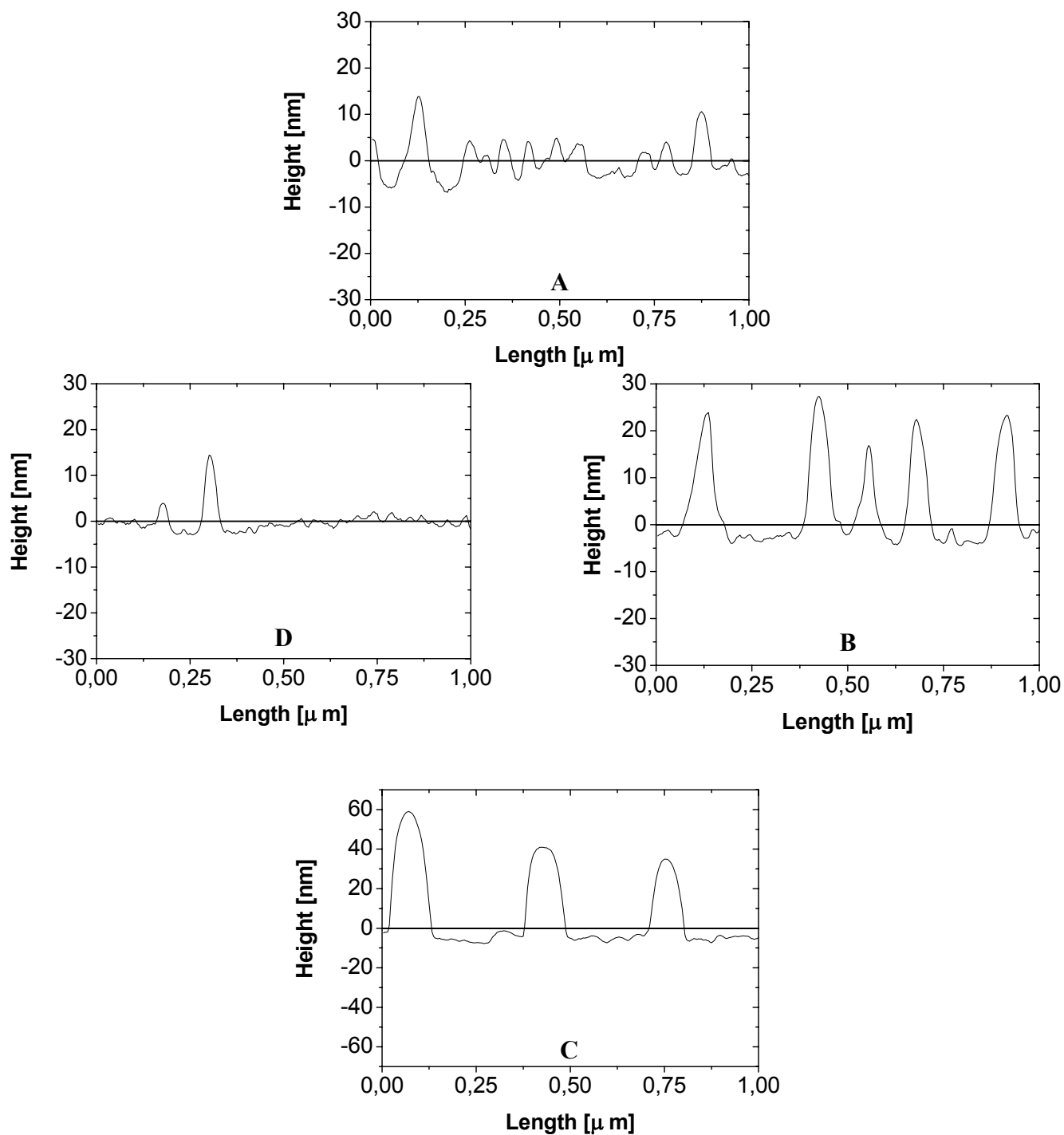
[Yoo96] Yoon, J.Y.; Park Y.H., Kim, J.H., and Kim, W.S. *J. Coll. Int. Sci.*, **1996**, 177, 613.

Appendix 1

pH 2.7

pH 4.9

pH 9.3

pH 10
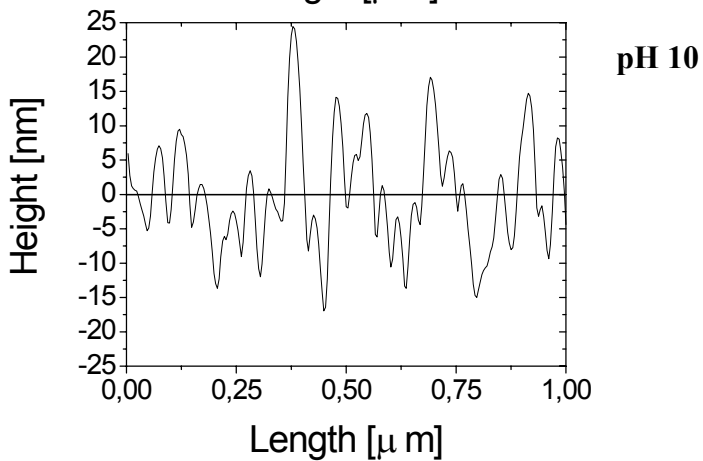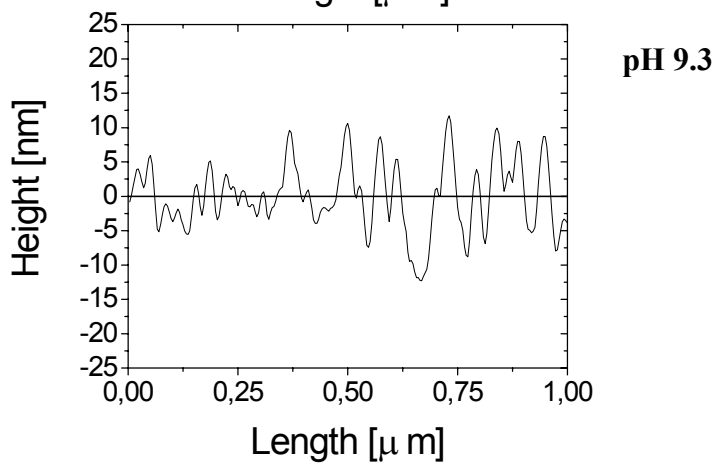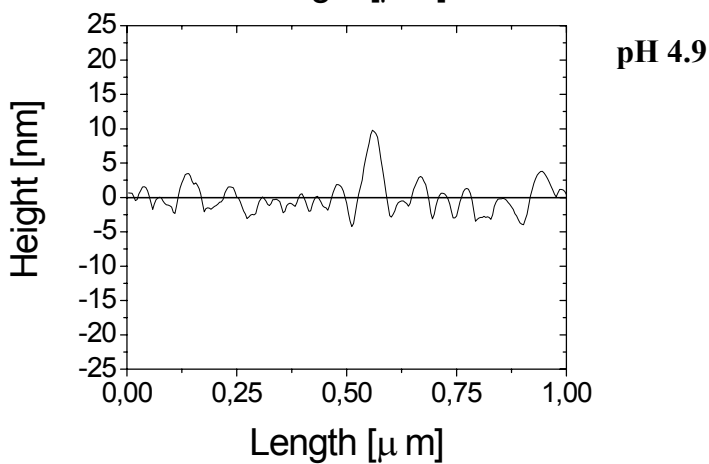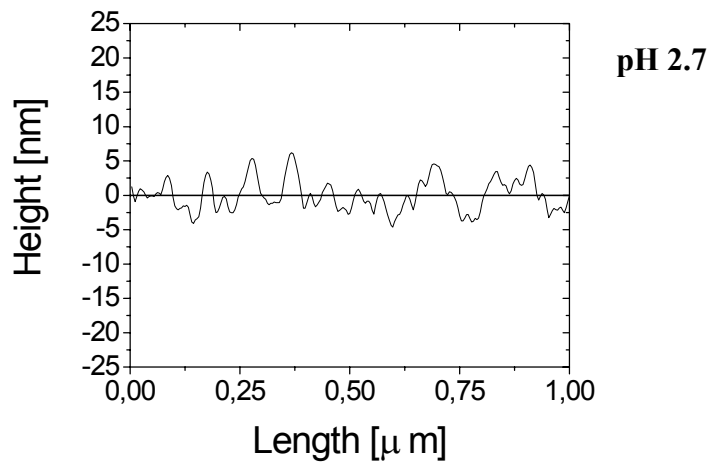
Cross-section analysis of adsorbed polyampholyte, PMAA-b-PDMAEMA, on PAA-P2VP polyelectrolyte brush at different pHs. The cuts are extracted from the topography images in Figure 10.4.

Appendix 2

Cross-section analysis of BSA, adsorbed onto: A) PAA-P2VP at pH 8.6, RMS 3.59 nm; B) PAA-P2VP at 4, RMS 5.74 nm; C) PS-P2VP at pH 8.6; D) PS-P2VP at pH 4.
 Z range-A) 60 nm, B) 60 nm, C) 140 nm, D) 60 nm. The cuts are extracted from the topography images in Figure 11.2.

Appendix 3
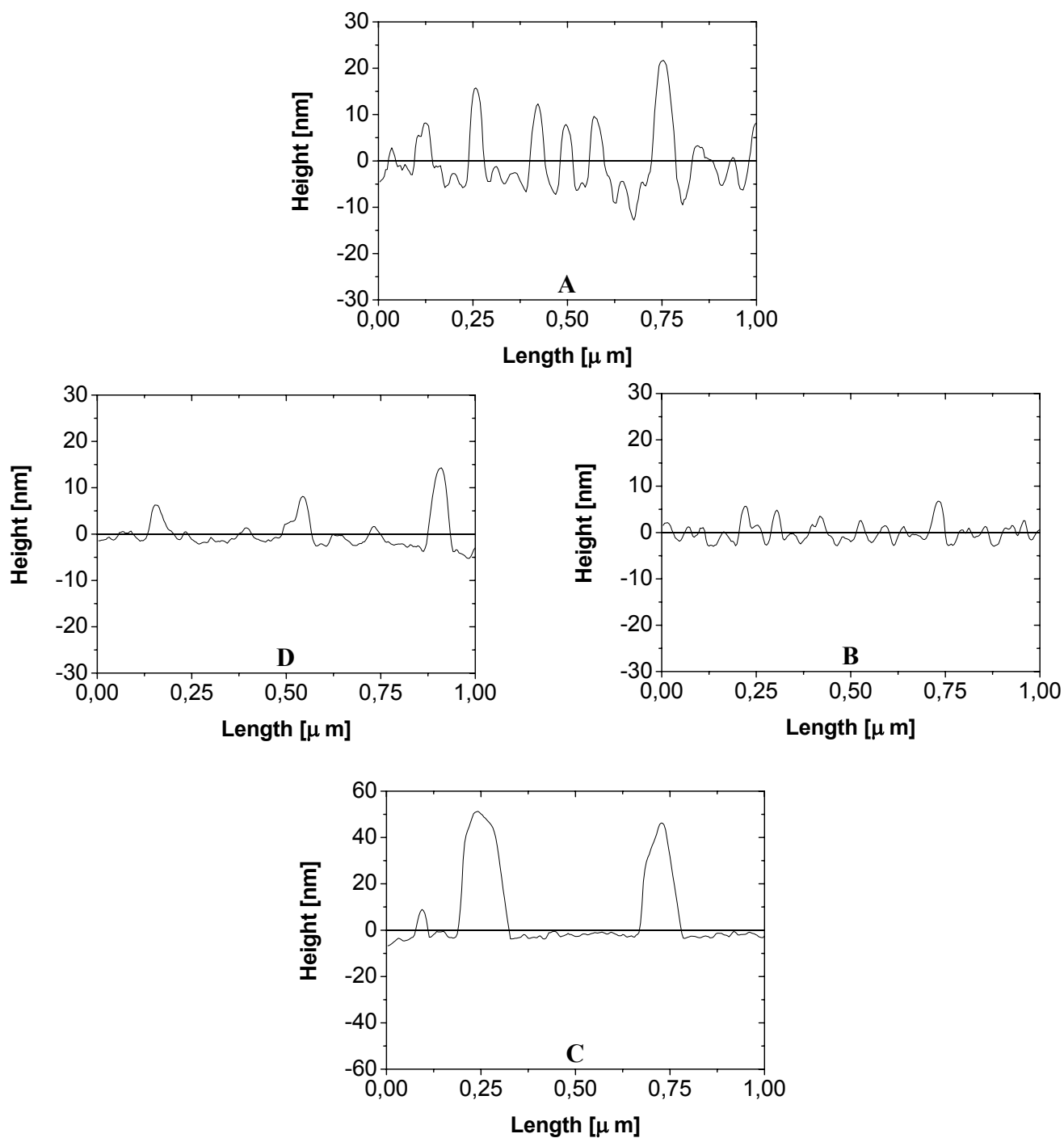
Cross-section analysis of lysozyme, adsorbed on: A) PAA-P2VP at pH 8.6, Z range 60 nm, RMS 5.10 nm; B) PAA-P2VP at 4, Z range 60 nm, RMS 2.04 nm; C) PS-P2VP at pH 8.6, Z range 120 nm, RMS 8.63 nm; D) PS-P2VP at pH 4, Z range 60 nm, RMS 3.44 nm. The cuts are extracted from the topography images in Figure 11.4.

Acknowlededement

List of Publications

<u>N. Houbenov</u>, N. Hermsdorf, I. Tokarev, A. Sidorenko, S. Minko, M. Stamm, R. Gehrke, S. Cunis, P. Müller-Buschbaum, "AFM and GISAX investigation of gold nanoparticles adsorbed onto thin polymer brush" *Jahresbericht HASYLAB*, **2002.**

<u>Houbenov, N</u>; Minko, S; Stamm, M, "Mixed Polyelectrolyte Brush from Oppositely Charged Polymers for Switching of Surface Charge and Composition in Aqueous Environment." *Macromolecules,* **2003,** *36,* 5897-5901.

Ruehe, J.; Ballauff, M.; Biesalski, M.; Dziezok, P.; Groehn, F.; Johannsmann, D.; <u>Houbenov, N.</u>; Hugenberg, N.; Konradi, R.; Minko, S.; Motornov, M.; Netz, R. R.; Schmidt, M.; Seidel, C.; Stamm, M.; Stephan, T.; Usov, D.; Zhang, H. Polyelectrolyte Brushes. In Polyelectrolytes with Defined Molecular Architecture I; Shmidt, M., Ed.; *Adv. polym. Sci.*, Springer: NY, **2004**; Vol. 165, 79-150

Ionov, L; <u>Houbenov, N</u>; Sidorenko, A.; Minko, S; Stamm "Gradient Mixed Polyelectrolyte Brushes" *Polymeric Materials: Science & Engineering* **2004,** *90,*104.

Leonid Ionov, <u>Nikolay Houbenov</u>, Alexander Sidorenko, Manfred Stamm, Igor Luzinov, and Sergiy Minko "Inverse and reversible switching gradient surfaces from mixed polyelectrolyte brushes", *Langmuir*, **2004**, published on web: 13-Oct-2004; DOI: 10.1021/1a048158a.

Uhlmann, P., <u>Houbenov, N.</u>, Ionov, L., Minko, S., Stamm, M.: "The Concept of Smart Binary Polymer Brushes to Tune Physical-Chemical Surface Characteristics at Biointerfaces", *Proceedings XXVII. FATIPEC Congress, Aix-en-Provence, France*, 19.-21.04., **2004**, pp. 875-883.

<u>Nikolay Houbenov</u>, Leonid Ionov, Sergiy Minko, Manfred Stamm "Control of Protein Adsorption via Adaptive Polymer Surfaces" *Polymer Preprints,* **2005**, submitted.

Contributions to Academic Conferences

<u>Houbenov, N</u>; Minko, S; Stamm, M "Development of a novel polymer system containing grafted polyelectrolytes with opposite electrical charges." Workshop in Trest within the frame of the 2nd European Graduate College *"Advanced Polymeric Materials"* - 23rd September to 4th October **2002**, Prague, Czech Republic.

<u>N. Houbenov</u>, S. Minko, M. Stamm, "Polymer Brush Composed of Oppositely Charged Polyelectrolytes" 5th IPF Colloquium „THEORY AND EXPERIMENT", November 14 and 15, **2002**, Dresden, Germany.

<u>N. Houbenov</u>, S. Minko, M. Stamm, "Synthesis of Polyelectrolyte Brushes and Nanoparticles Adsorption" 27.02.-01.03. **2003**, *EUROREGIONALE*, Dresden, Germany.

<u>N. Houbenov</u>, S. Minko, M. Stamm "Adsorption of charged nanoparticles onto thin polyelectrolyte brush composed of oppositely charged polymers" European Graduate College "Stimuli Sensitive Polymers", 30.06-05.07 **2003**, Gliwice, Poland.

<u>Houbenov, N</u>; Minko, S; Stamm, M "Switchable polymer surfaces for nanocolloidal adsorption." *European Graduate College* "Stimuli Sensitive Polymers"*, 30.06. -05.07., 2003, Gliwice, Poland.*

<u>N. Houbenov</u>, S. Minko, M. Stamm, "Properties of a Binary Polyelectrolyte Brush. Nanoparticles Adsorption" 9th Dresden Polymer Discussion: „*POLYELECTROLYTES*", 16-19.03, **2003**, Meißen, Germany.

<u>N. Houbenov</u>, S. Minko, M.Stamm, "Adsorption of Nanoparticles onto Thin Polymer Brushes" Verhandlungen der Deutschen Physikalischen Gesselschaft: AKF-Frühjahrstagung, 24-28.03, **2003**, Dresden, Germany.

<u>Houbenov, N</u>; Minko, S; Stamm, M *"Mixed Polyelectrolyte Brushes: Adaptive and Responsive Polymer Surfaces"* 05.04. **2004,** **BASF**-*Ludwigshafen, Germany.*

Lebenslauf

Name:	Nikolay Houbenov
Geboren am:	02.04.1971 in Sofia, Bulgarien
Familienstand:	ledig

Schulausbildung

1978-1989	Grundschule, Gesamtschule, Gymnasium in Sofia, Bulgarien

Hochschulausbildung

09/1989-02/1991	Techologische Univerität, Sofia
09/1991-04/1997	Universität Sofia „Saint Kliment Ochridsky" Chemische Fakultät, mit dem Schwerpunkt der Analytische und Physikalische Chemie
03-08/1996	Universität „Jaime I" Castellon de la Plana, Spanien Fakultät Organische und Einorganische Chemie Diplom Arbeit

Beruflicher Werdegang

01/1997-12/2000	Bulgarische Wissenschaftliche Akademie Institut für Katalyse

Promotion

seit 05/2001	Leibnitz Institut für Polymerforschung in Dresden **Arbeitsgruppe von Herr Prof. Dr. Manfred Stamm**

Versicherung

Hiermit versichere ich, dass ich die vorliegende Arbeit ohne unzulässige Hilfe Dritter und ohne Benutzung anderer als der angegebenen Hilfsmittel angefertigt habe; die aus fremden Quellen direkt oder indirekt übernommenen Gedanken sind als solche kenntlich gemacht. Die Arbeit wurde bisher weder im Inland noch im Ausland in gleicher oder ähnlicher Form einer anderen Prüfungsbehörde vorgelegt.

Die vorliegende Arbeit wurde unter der wissenschaftlichen Betreuung von Prof. Dr. Manfred Stamm und Prof. Dr. Sergiy Minko an dem Leibniz-Institut für Polymerforschung Dresden angefertigt.

Keine frühere erfolglose Promotionsverfahren statt gefunden haben.

Die Promotionsordnung der Technischen Universität Dresden der Fakultät Mathematik und Naturwissenschaft erkenne ich an.

Nikolay Houbenov

Dresden, 27.01.05